공학박사학위논문

Optimization of Metal Foam Cathode in Li Secondary Battery

리튬 이차 전지의 메탈 폼 양극 최적화에 관한 연구

2018 년 2 월

서울대학교 대학원
재료공학부
송 경 엽

Optimization of Metal Foam Cathode in Li Secondary Battery

Kyung Yup Song

Under supervision of Prof. Seung Ki Joo

A dissertation submitted to the Faculty of Seoul National University in partial fulfillment of the requirements for the degree of Doctor of Philosophy

February 2018

School of Materials Science and Engineering
Graduate School
Seoul National University

Optimization of Metal Foam Cathode in Li Secondary Battery

리튬 이차 전지의 메탈 폼 양극 최적화에 관한 연구

지도교수: 주 승 기

이 논문을 공학박사 학위논문으로 제출함

2018 년 2 월

서울대학교 대학원
재료공학부
송 경 엽

송 경 엽의 박사학위 논문을 인준함

2017 년 12 월

위원장	김 진 영	(인)
부위원장	주 승 기	(인)
위 원	임 인 곤	(인)
위 원	이 헌	(인)
위 원	배 병 성	(인)

ABSTRACT

Optimization of Metal Foam Cathode in Li Secondary Battery

Kyung Yup Song
Department of Materials Science and Engineering
The Graduate School
Seoul National University

Li secondary batteries are used widely batteries in portable devices, electrical vehicles (EVs), and laptops, owing to their very high energy density, high operating voltage (about 3.6 V), small size, and lightweight compared to other secondary batteries.

The commercialized batteries are to fabricate by coating the active material on the metal foil as a current collector to a thickness of about 40 ~ 100 μm. However, if the active material coated to a thickness of several hundred micrometers in order to manufacture a high capacity battery using a metal foil, peeling easily occurs between the active material and the metal foil, and the internal resistance of the electrode is increased. That is, since the active material has to be widened in area of the electrode coated with a thin active materials thickness, a large amount of separator and current collector are required regardless of the capacity, and the weight and volume of the battery are increased.

In this paper, three-dimensional (3D) metal alloy foam was used as a current collector for battery instead of the conventional metal foil. The advantages of using

metal foam are the much larger surface area, due to the many triple point (junctions of active material, metal frame, and liquid electrolyte) existing inside the electrode and shorter Li-ion diffusion length, therefore improving the electrical conductivity. In addition, metal foam as a current collector was enhanced the cycle-life due to the rough surface of metal frame enhanced adhesion properties and prevented separation of the active materials from the metal frames during the charge-discharge process.

The electrochemical performances were compared for the carbon black content in metal foam cathode. The metal foam cathode with increased carbon black loadings enhanced the electrochemical performances and significantly decreased the charge transfer resistance. This is due to the large effective contact area between the conductive carbon material and the active material. However, high carbon black loading resulted in low cell capacity (mAh) at low current density, due to decreased amount of active materials. That is, high-capacity batteries used in low current are advantageous in reducing the content of carbon black, while high-power batteries are advantageous in increasing the content of carbon black in metal foam cathode.

The electrochemical performances were also compared for the metal foam cathodes using different pore size of metal foam. In a case where the carbon black content was 15wt.%, the metal foam cathode of 450 μm-pore size showed the highest specific capacity and the lowest over-potential. This is because the small pore size has a short Li-ion diffusion length and provides a wide surface area for the oxidation/reduction reaction due to an increase in the triple point. However, in the case where carbon black content was 25 wt.%, 450 and 3000 μm-pore sizes showed similar specific capacity and over-potential. This is because a large pore size of metal foam cathode is greatly affected by carbon black. That is, light-weight and high capacity batteries are

most efficient when fabricated by adding 15 wt.%-carbon black to a metal foam of 3000 μm-pore size.

To improve the electrochemical performance of Li secondary batteries, it is important to optimize the electrode thickness and mass loading of active material. Thick electrodes exhibit higher cell capacity (mAh) and specific capacity (mAh g^{-1}) compared to thin electrodes. This is due to the increase in the amount of active materials and longer time of Li redox reaction. However, to obtain the high-power performance at high current, it is advisable to stack of a thin metal foam cathode, due to the wide reaction surface area and the short Li-ion diffusion length.

The electrochemical performances were compared to the electrode porosity in metal foam cathode. According to charge-discharge test and cyclic voltammetry analysis, metal foam cathodes with high intensity pressed after firing process lead to poor electrochemical and kinetic performances. This can be attributed to the reduced area of redox reaction. This means that the increases in the active material density caused a reduction in the efficiency of the battery because electrode porosity decreases and the diffusion limitation of Li-ion increases. This shows that the formation of the third pores into which the electrolyte can enter is very important factor when a battery is manufactured using the metal foam current collector. Therefore, the third pores should be maintained through a no press, pre-annealing process, and slightly press process. In addition, the large proportion of the metal frame enhanced the kinetic performance and decreased the charge transfer resistance due to the short diffusion length of Li-ion and large effective contact area between the metal frame and the $LiFePO_4$/C particles.

Recently, bendable Li secondary batteries have been studied due to the rapid development unique devices such as wearable, roll-up display and curved devices. However, bendable batteries have many limitations, including low electrochemical

performances and low areal capacity (mAh cm^{-2}). Therefore, we bendable batteries are fabricated using nickel-chromium (NiCr) alloy metal foam as the current collector of positive electrodes. As a result, we demonstrate the use of bendable lithium secondary batteries with a high areal capacity of about 3.5 mAh cm^{-2} at C-rate of 0.2, a high capacity retention rate in cycle life behavior, and a greatly low charge transfer resistance of around 6–8 Ω. Moreover, our bendable pouch batteries can be repeatedly bent to radii of 12.5 and 2.5 mm for several hundred times without fractures in the electrode and capacity fading.

As described in this study, the three-dimensional metal alloy foam is the most promising current collector because possible to fabricate a high capacity and high power Li secondary battery compared to the foil-type current collector.

Keywords: Li secondary battery, Metal foam cathode, Current collector, High capacity battery, High power battery, Curved battery

Student Number: 2013-30938

Table of Contents

LIST OF TABLES

LIST OF FIGURES

CHAPTER 1

Introduction

Energy storage will be more important in the future than at any time in the past. The various rechargeable batteries such as Nickel Cadmium (Ni-Cd), Nickel-Metal hydride (Ni-MH), lead-acid, and Li-ion batteries are available in commercial market [1]. The comparison of commonly used rechargeable batteries is briefly shown in Table 1.1.1. Li-ion batteries have been widely used as the most important element in many portable devices and in electric vehicle applications owing to the very high energy density (energy per unit volume), high specific energy (energy per unit weight), small size, and lightweight [2-7].

Table 1.1 Characteristics of commonly used rechargeable batteries.

	Ni-Cd	**Ni-MH**	**Lead Acid**	**Li-ion**
Gravimetric Energy Density (Wh/kg)	45-80	60-120	30-50	110-160
Volumetric Energy Density (Wh/L)	130	200	50	320
Cell Voltage (v)	1.25	1.25	2	3.6
Commercial use since	1970	1990	1940	1990~

Olivine lithium iron phosphate ($LiFePO_4$) has been extensively and intensively used as a cathode material [8]. $LiFePO_4$ belongs to the olivine family in the space group P*nma*, and the structure consists of Fe atoms occupying octahedral (4c) sites, and P

atoms occupying tetrahedral (4c) sites, while the Li ions occupy octahedral (4a) sites [9-15]. $LiFePO_4$ is relevant for high rate application such as EVs due to its limited energy density. The main benefits of $LiFePO_4$ are its high theoretical capacity (~160 mAh g^{-1}), high plateau region of voltage, low material cost, excellent cyclic performance, operational safety, abundant material supply, and superior environmental compatibility compared to other cathode materials [11-19]. Moreover, the structure of $LiFePO_4$ is more thermally stable than layered oxide cathode materials, because the oxygen atoms are strongly bonded by both Fe and P atoms [7, 15]. The disadvantages of $LiFePO_4$ include its relatively low density, poor electronic conductivity (~10^{-9} cm S^{-1}), and low ionic diffusivity (10^{-13} to 10^{-16} cm^2 S^{-1}), due to the strong covalent oxygen bonds [13-25]. In order to improve the electrochemical performance of $LiFePO_4$-based batteries, the electric conductivity is enhanced by coating with electronically conductive materials (carbon, Ag, conducting polymer, etc.) on the particle surface [15-23], or by doping with other elements, such as Cr, Mg, Ni, and Nb [24-28], and minimizing the particle size of $LiFePO_4$ [29, 30].

The electrochemical properties significantly change with active material, as well as the structure of the current collector. Generally, active materials are coated on the surface of a two-dimensional (2D) metallic foil current collector, such as Al, Ni, and Ti [31, 32]. However, in the case of metallic foil, thicker electrode rapidly increases the cell impedance, thereby decreasing the cell efficiency. Therefore, instead of the conventional foil-type for Li-ion batteries, a three-dimensional (3D) metal foam was used as a current collector, in order to improve the electrochemical and power performances. The advantages of using 3D metal foam as a current collector are the much larger surface area owing to its unique metal framework structure, and shorter Li-ion diffusion length due to the many triple points (junctions of active material,

metal frame, and electrolyte) existing inside the electrode, therefore improving the electrical conductivity [33-39]. Moreover, it can be loaded with higher mass of the active material, which makes it possible to reduce the mass and the volume of inactive materials, such as the current collector and separator [33, 35]. Thus, it can produce high power, high energy density, and smaller and lighter batteries. The pure Ni foam exhibits an increasing current above around 3.5～4.0 V, due to corrosion reaction [34, 36]. For this reason, Ni foam is used for Li-ion batteries in the current collector of negative electrode [40, 41] or Ni/MH batteries [42-45]. In order to prepare a positive electrode for high performance, Yao et al. [34] examined a Ni-35 wt.% Cr alloy foam, while Wang et al. [36] introduced an Al electroplated Ni foam to prevent the corrosion of Ni foam. Additionally, Yang et al. [35, 37] studied a 77 wt.% Ni - 15 wt.% Cr - 8 wt.% Al alloy metal foam for Li-ion batteries.

In addition, flexible LIBs have been studied due to the rapid development unique devices such as wearables, rollup displays, and conformable health-monitoring electronic skin [46-54]. It is critical for flexible LIBs to have lightweight, good flexibility, high energy density and cycling stability. The utilized materials for the current collector, active layer, and packaging determine the flexibility of batteries [51-54]. Recently, flexible LIBs are mostly fabricated using a thin-film active layer and a solid-state electrolyte on top of a polymer substrate in order to improve the flexibility and safety of batteries [55-63]. However, thin film flexible batteries show some disadvantages such as, significantly low electronic conductivity due to solid-state electrolyte and low areal capacity because of low mass of the active materials. Therefore, ongoing researches aim to improve the areal capacity and energy density by developing flexible batteries using graphene with three-dimensional (3D) structures [64-67], CNTs [68-74], textiles [75-79] or cellulose [80-82]. In this paper, we describe

a positive electrode fabricated using a 3D structured nickel-chromium (NiCr) alloy metal foam as the current collector for use in bendable pouch LIBs. The NiCr alloy metal foam current collector of the positive electrode resulted in stable charge-discharge performance due to the excellent resistance against corrosion [34].

To date, high power and specific energy are needed for a Li-ion battery to be used in various applications. To accomplish this, various experiments have tested active material density, electrode porosity, metal frame proportion in metal alloy foams, cell sizes, and electrode thicknesses.

CHAPTER 2

Experimental

2.1 Preparation of metal foam cathodes

The 3D NiCrAl alloy metal foam was obtained from foam-type polyurethane. First, Ni foam was prepared by nickel plating onto polyurethane, and the polyurethane was then removed by heat treatment. After that, NiCrAl alloy powder was adsorbed onto the Ni foam. The substrate was reheated to obtain the NiCrAl alloy foam (Figure 2.1.1). The metal alloy foam was consisted of 1st pore-large size and 2nd pore-small size like as soccer ball (Figure 2.1.2). This manufacturing process has been reported by Yao et al., [34] and by Yang et al [37]. The weight ratio of Ni, Cr, and Al was 77: 15: 8. The NiCrAl alloy metal foam was supplied by Alantum Corporation (Korea). The 1st pore sizes of metal foam as a current collector were 450, 800, 1200, and 3000 μm (Figure 2.1.3).

The slurry for the positive electrode was prepared by mixing $LiFePO_4$/C as the cathode material, carbon black as the conductive material, and polyvinylidene fluoride (PVDF) as the binder with *N*-methyl-2-pyrrolidone (NMP). The prepared slurry filled in the pore space of alloy metal foam, and was annealed in vacuum at 140 ◦C for 8 h (Figure 2.1.4).

2.2 Fabrication of pouch cells

The Li pouch cells were fabricated in a dry box filled with pure Ar gas. Cells were prepared with lithium metal as anode, and celgard (polypropylene) as the separator; these were placed in a polymer-aluminum-polymer laminated pouch bag containing 1 M $LiPF_6$ in ethylene carbonate (EC): diethyl carbonate (DEC) (1: 1 v/v) as the electrolyte (Figure 2.2.1). Li metal were placed single side or both sides of metal foam cathode. 4 mm width aluminum tab and copper tab were attached to the NiCrAl metal foam as positive electrode and a Li metal, respectively, to connect the battery cycler system. The stacked electrode was put in a pouch bag and 3 sides of pouch was sealed using heat sealer [83]. In order to seal between pouch and tabs (Al and Cu), sulfurized polymer resin materials (3 layers lamination) adhesive/sealant, which melts at high temperature, was used. After that, liquid electrolyte was filled by dropping pipet to the one side of opened edge and sealed. One formation of charge and discharge at 0.2 C were applied. Then, the surplus electrolyte and generated gas during formation in the pouch cell were removed by drilling holes using needle and sealed pouch again.

2.3 Measurement of electrochemical performances

The charge and discharge cut-off voltage were set at 4.0 V and 2.5 V for $LiFePO_4$/C. The cyclic voltammetry (CV) curves were recorded at a scan rate of 0.1 mV s^{-1}, and voltage range from 2.5 to 4.3 V. Both the charge/discharge test and the cyclic voltammetry curves were carried out by a WBCS 3000 battery cycler system at room temperature. Electrochemical impedance spectroscopy (EIS) measurements of the cells were tested with a CHI608A electrochemical analyzer at room temperature. The applied amplitude of the AC signal was 5 mV, and after the cells were discharged using the potentiostatic method in 2.5 V, the frequency ranged from 100 kHz to 0.01 Hz.

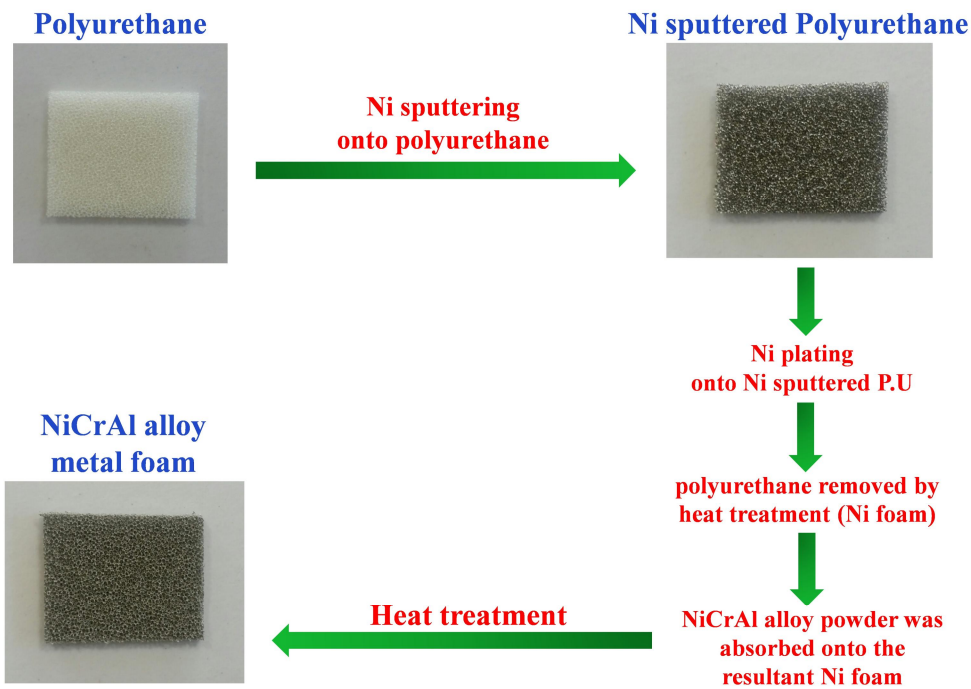

Figure 2.1.1 Fabrication of NiCrAl metal alloy foam

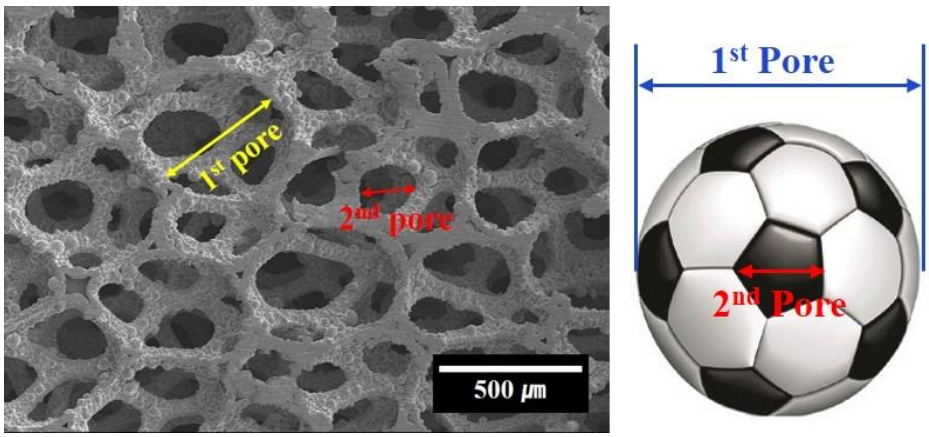

Figure 2.1.2 The morphology of metal alloy foam.

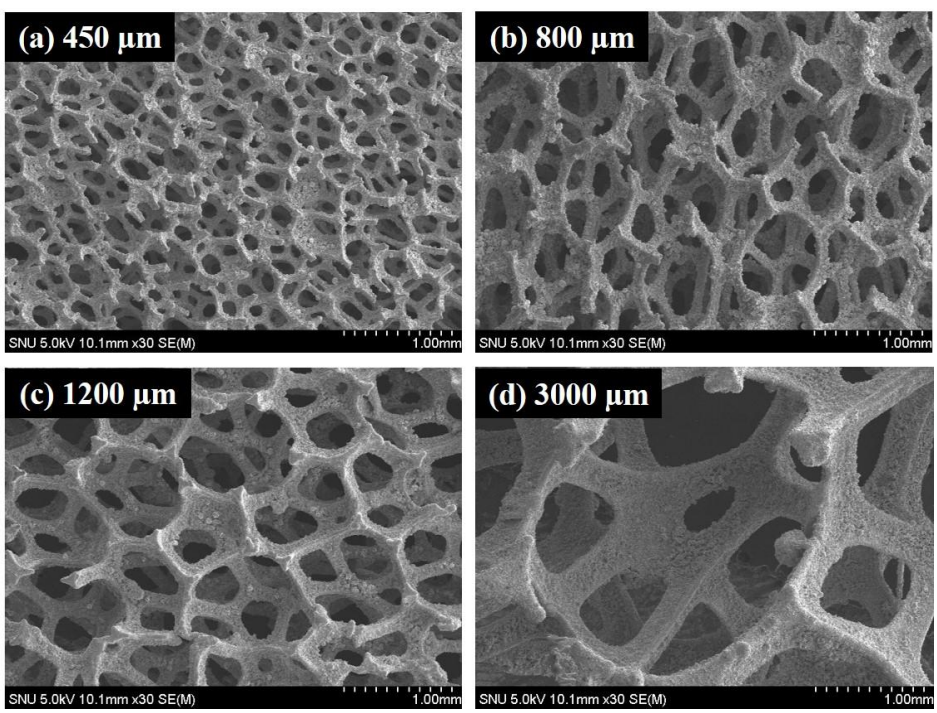

Figure 2.1.3 SEM images of NiCrAl metal alloy foam (a) pore size of 450 μm, (b) 800 μm, (c) 1200 μm, and (d) 3000 μm.

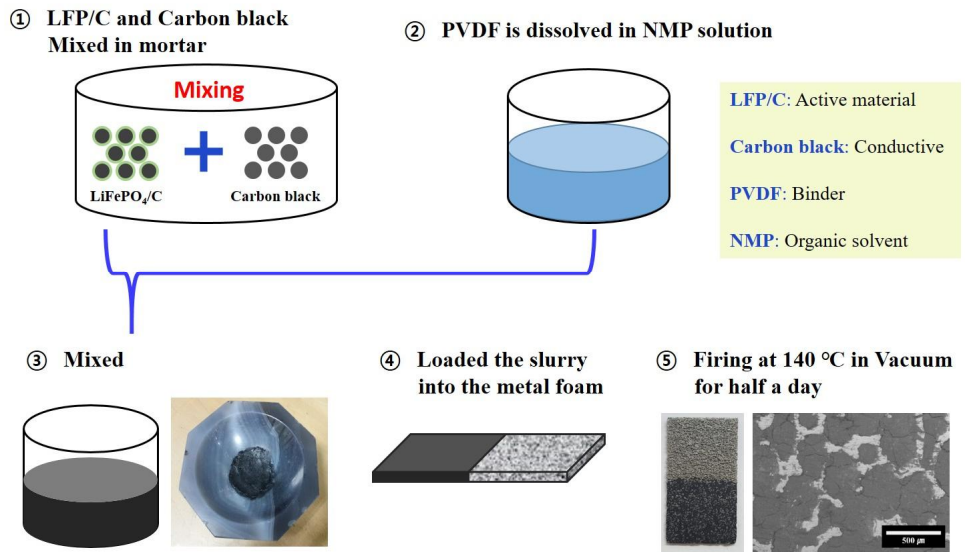

Figure 2.1.4 Fabrication of metal foam cathode.

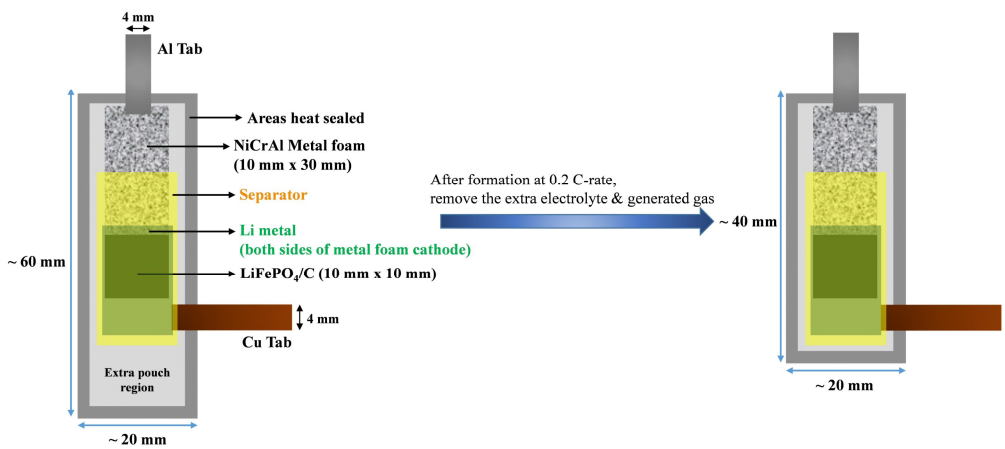

Figure 2.2.1 Schematic of the fabrication of pouch cell using polymer-aluminum-polymer pouch container.

CHAPTER 3

Results and Discussion

3.1 Effect of Carbon Black Content

The conductive carbon content significantly affected the electrochemical performance of the Li-ion batteries, due to the improvement in electronic contact between the active material particles and the electronic conductor [84-86, 90]. In this section, our study focuses on the optimized conductive carbon content using a 3D foam-type metal current collector to improve the electrochemical properties and stability of Li secondary batteries [90]. The first experiment, 450 μm-pore size and 1000 μm-thickness of metal foam current collectors were used for the metal foam cathodes. The mass of NiCrAl metal alloy foam was around 65 mg cm^{-2}. The amount of carbon black was varied as 0, 5, 10, 15, and 20 wt.%, respectively. The amount of PVDF was fixed to 10 wt.%. The mass of $LiFePO_4$/C loaded into each of the electrodes was 91, 77, 62, 48, and 38 mg cm^{-2}, respectively. The detail analytical data of the metal foam cathodes was listed as shown in Table 3.1.1.

Table 3.1.1 Analytical data of metal foam cathodes with different content of carbon black. (Metal foam cathode: 450 μm-pore size and 1000 μm-thickness)

Pore size (μm)	Electrode thickness (μm)	Content of PVDF (wt.%)	Content of Carbon black (wt.%)	Content of $LiFePO_4$/C (wt.%)	Amount of $LiFePO_4$/C (mg cm^{-2})
450	1000	10	0	90	91
			5	85	77
			10	80	62
			15	75	48
			20	70	38

Figure 3.1.1(a) shows the discharge specific capacity (mAh g^{-1}) obtained from the various discharge current densities (mA cm^{-2}). High carbon black content indicated high specific capacity and capacity retention rates between 2 and 8 mA cm^{-2}. In addition, capacity retention rates were 66, 83, 86, and 92 % for the metal foam cathodes of 5, 10, 15, and 20 wt.%-carbon black, respectively. In the case of no addition carbon black electrode, there was no indication of a discharge capacity at current density of 8 mA cm^{-2}. Capacity retention rate of less added conductive carbon electrodes were reduced, due to the high transport limitations of Li-ion and high charge transfer resistance (R_{ct}) as shown in Figure 3.1.8. Moreover, the effect of a large R_{ct} can be neglected at a low current rate, but the R_{ct} is mainly responsible for the voltage drop causing a sudden decrease in the electrochemical performance with increases current rate. On the other hand, Figure 3.1.1(b) shows that as the carbon black content of the electrodes decreased, the cell capacity (mAh) increased, except for the 0 wt.%-carbon black at current densities from 2 to 6 mA cm^{-2}. The cell capacities were 10.4, 8.7, 7.1, and 5.7 mAh cm^{-2} for the 5, 10, 15, and 20 wt.%-carbon black, respectively, at the current density of 2 mA cm^{-2}. The reason was that decreasing the carbon black content increases the amount of active material. That is, higher carbon black loading generally enhances the rate performance and reduces the internal resistance, but decreases the active material density of the cells.

Figure 3.1.2(a) and (b) show discharge curves at current densities of 2 and 8 mA cm^{-2}, respectively. In spite of the same current density, the current rates of metal foam cathodes differed according to the carbon black content, due to different active material loadings. For example, at current density of 2 mA cm^{-2}, the current rates of 0, 5, 10, 15, and 20 wt.%-carbon black were 0.15, 0.17, 0.22, 0.28, and 0.36 C, respectively. As a result, metal foam cathodes of increased carbon black content

increased the current rate, due to relative decrease of the active material loadings. According to the result of the discharge curves at current density of 2 mA cm^{-2} (Figure 3.1.2(a)), 15 and 20 wt.%-carbon black exhibited the same highest discharge capacity (150 mAh g^{-1}) and power performance by reducing the charge transfer resistance and enhancing the electrochemical performance, despite the relatively high current rate. As shown in the result for 8 mA cm^{-2} (Figure 3.1.2(b)), 20 wt.%-carbon black still had the highest specific capacity (137 mAh g^{-1}) and high power performance, due to superior electrochemical performances. Even though, the specific capacity of 15 wt.%-carbon black (127 mAh g^{-1}) was still higher than that of 10 wt.%-carbon black (118 mAh g^{-1}). However, the electrode polarization was higher than that of 10 wt.%-carbon black. It is because, 15 wt.%-carbon black has higher over-potential by the higher current rate with lower mass of active material. The current rates of the electrodes were 0.86 and 1.12 C for 10 and 15 wt.%-carbon black, respectively. As the results show that increasing the current rate increased the over-potential.

Additionally, the 0 wt.%-carbon black cell voltage significantly dropped to around 2.95 V simultaneously with the discharge process at 2 mA cm^{-2}, because of the large IR drop due to severely low electronic conductivity. After that, the cell voltage slightly increased to 3.06 V, because of the faster diffusion rate of Li-ion from the metal foam cathode surface to the inside of the metal foam cathode (D_2) by Li concentration gradient, than the insertion rate of Li-ion from anode (Li metal) to the metal foam cathode surface (D_1) by discharge current rate of 0.2 C, as Fig. 3.1.3 shows. However, when the discharge rate of 8 mA cm^{-2} (Figure 3.1.2(b)), no discharge capacity was observed, resulting from the electrochemical reaction mostly taking place at the metal foam cathode surface, because the rate of D_1 was much faster than the rate of D_2, and the large gradient of Li ion concentration for the $LiFePO_4$/C particle during the

discharge process. As a result, the cell voltage of metal foam cathode dropped greatly to the discharge cut-off voltage.

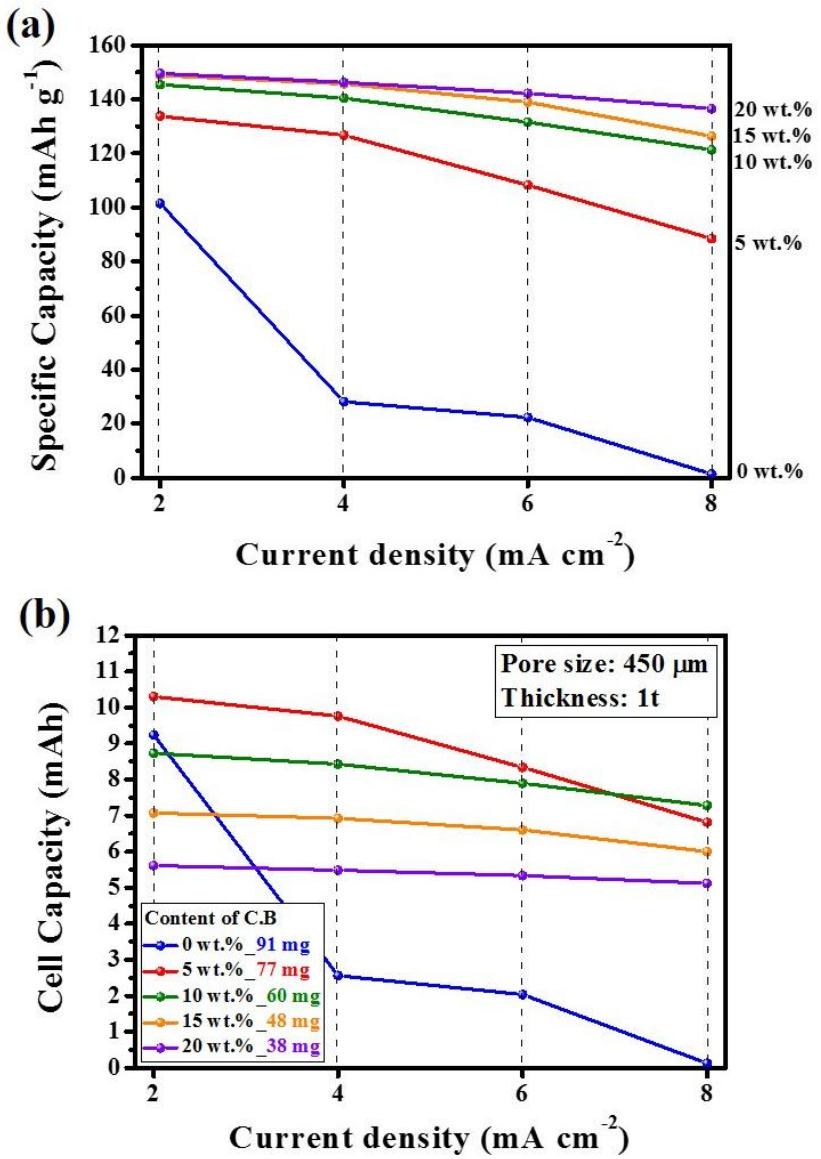

Figure 3.1.1 Comparison of the (a) specific capacity (mAh g^{-1}) and (b) cell capacity (mAh) with an increased in current density. (Metal foam cathode: 450 μm-pore size and 1000 μm-thickness)

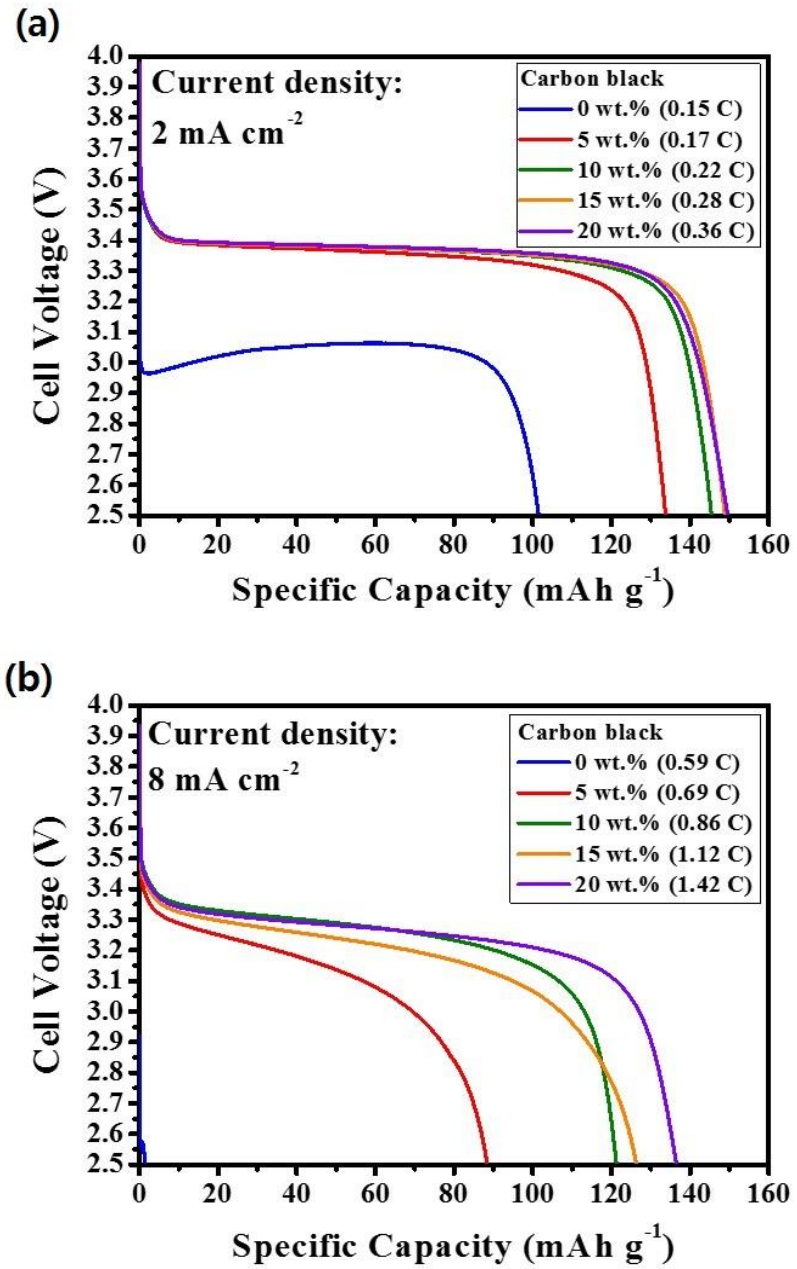

Figure 3.1.2 Comparison of the discharge curves at current density of (a) 2 mA cm^{-2} and (b) 8 mA cm^{-2}.

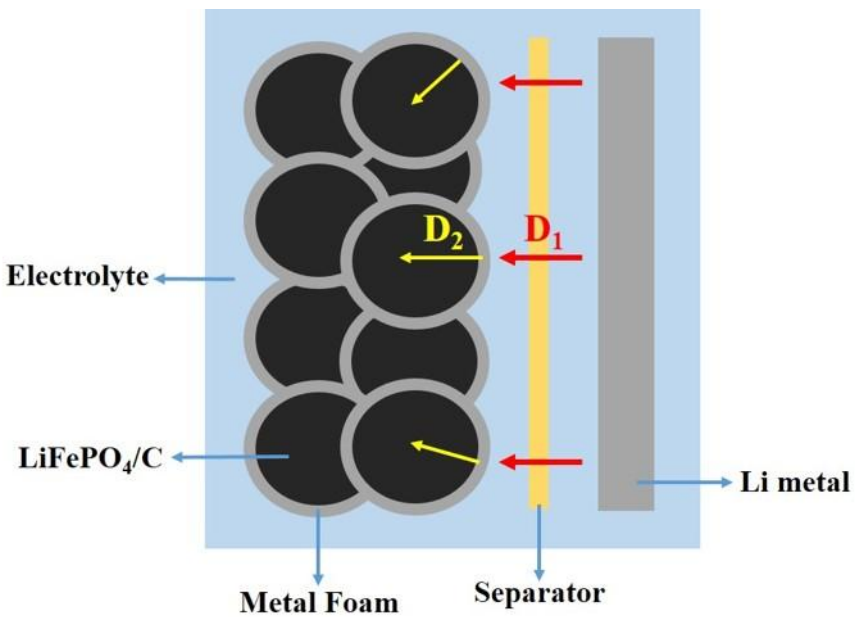

Figure 3.1.3 Schematic of insertion (D_1) and diffusion (D_2) rate of Li-ions during the discharge process.

Figure 3.1.4(a) shows the discharge curves of different carbon black content at a discharge current rate of 0.2 C. In the case of the 15 and 20 wt.%-carbon black, there was almost no difference in specific capacity (about 150 mAh g^{-1}) and voltage drop in the plateau region, because there were almost similar diffusion limitations of Li-ion. Higher carbon black content generally improves the rate performance by decreasing the charge transfer resistance, and enhancing the kinetic behavior [84]. The plateau region is attributed to the coexistence of the two phases ($LiFePO_4$ and $FePO_4$) with no change in the voltage. Deviating from the plateau region changed the composition from two phases to single phase, causing the voltage to rapidly increase or decrease. However, carbon black with less than 15 wt.%-carbon black exhibited relatively lower specific capacity (the specific capacities of 0, 5, and 10 wt.%-carbon black indicated 62, 135, and 141 mAh g^{-1}, respectively) and higher over-potential in the plateau region. Figure 3.1.4(b) shows the discharge curves at a current rate of 1 C. As shown in the graph, 20 wt.%-carbon black still had the highest specific capacity (143 mAh g^{-1}) and high power performance. And 5, 10, and 15 wt.%-carbon black showed 71, 109, and 132 mAh g^{-1}. In the case of the 0 wt.%-carbon black, the discharge capacity did not observe. Figure 3.1.5(a) shows the discharge specific capacity obtained from the various discharge current rates. Capacity-retention rates between 0.2 and 3 C of the electrodes were 33, 47, and 77 % for the 10, 15, and 20 wt.%-carbon black, respectively. In the case of 5 wt.%-carbon black, there was no indication of a discharge capacity from the current rate of 2 C. The capacity-retention rate of less added conductive carbon electrodes were reduced, due to the high transport limitations of Li-ion and high charge transfer resistance (R_{ct}) as shown in Figure 3.1.8. While, Figure 3.1.5(b) shows that as the carbon black content of the metal foam cathodes decreased, the cell capacity (mAh) increased, except for the 0 wt.%-carbon black at

current rates of 0.2 and 0.5 C. The cell capacities were 10.4, 8.7, 7, and 5.7 mAh cm^{-2} for the 5, 10, 15, and 20 wt.%-carbon black, respectively, at the current rate of 0.2 C. The reason was that decreasing the carbon black content increases the amount of active material. That is, higher carbon black loading generally enhances the rate performance and reduces the internal resistance, but decreases the active material density of the cells [84]. The active material densities were 1.34, 1.13, 0.91, 0.7, and 0.55 g cm^{-3} for the 0, 5, 10, 15, and 20 wt.%-carbon black, respectively. As a result, to manufacture a high-energy (capacity) density battery that uses a low current rate, electrode of lower carbon black content offers more advantage. However, as the current rate increases, the 5 and 10 wt.%-carbon black exhibited dramatic drops of cell capacity. The 5 wt.%-carbon black showed the lowest cell capacity (4.05 mAh cm^{-2}), while 10, 15, and 20 wt.%-carbon black exhibited similar cell capacities (the 10 wt.%-carbon black was 5.5 mAh cm^{-2}, the 15 wt.%-carbon black was 5.1 mAh cm^{-2}, and the 20 wt.%-carbon black was 5.2 mAh cm^{-2}) at the current rate of 1.5 C. Moreover, 20 wt.%-carbon black exhibited the highest cell capacity from 2 C and 3 C, respectively. This is because a lower carbon black loading generally yields a poor rate capacity by increasing the charge transfer resistance. That is, the conductive carbon loadings should be varied according to the intended use.

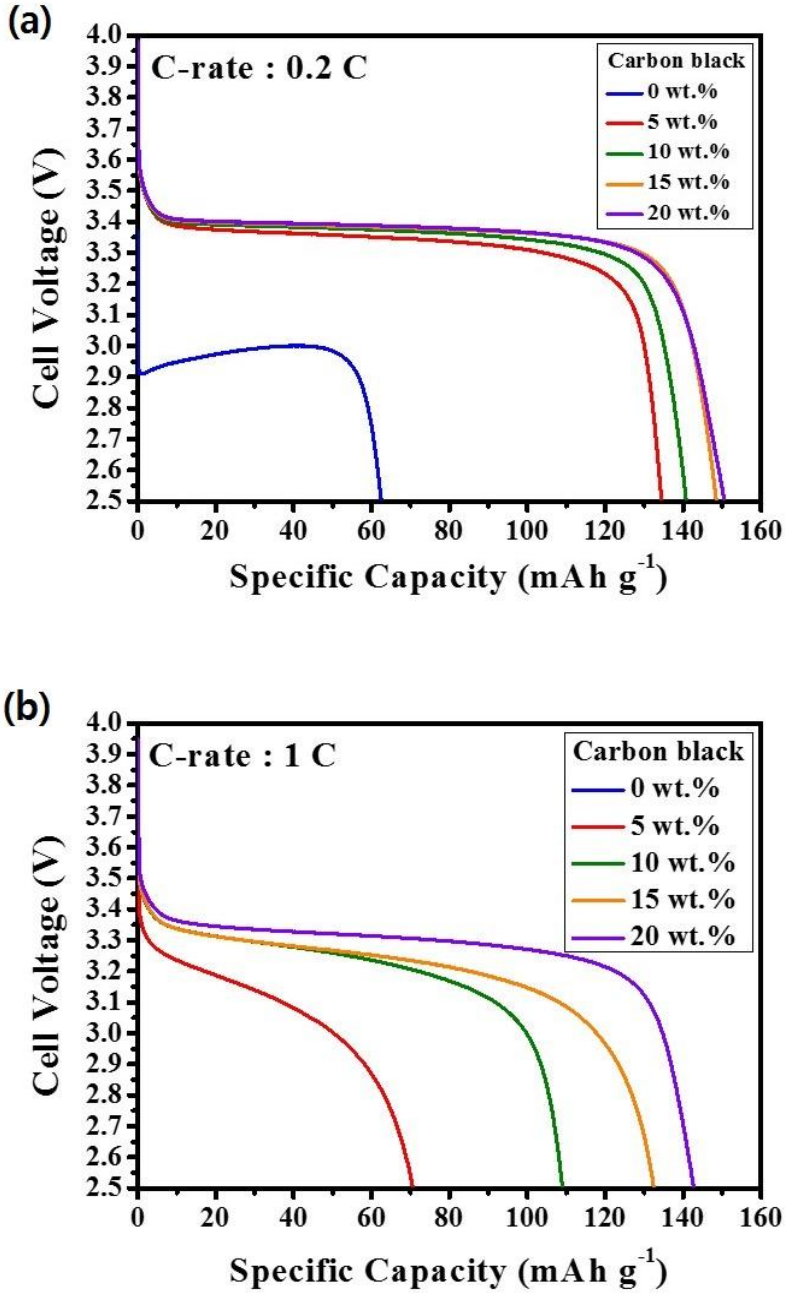

Figure 3.1.4 Comparison of the discharge curves at current rate of (a) 0.2 C and (b) 1 C.

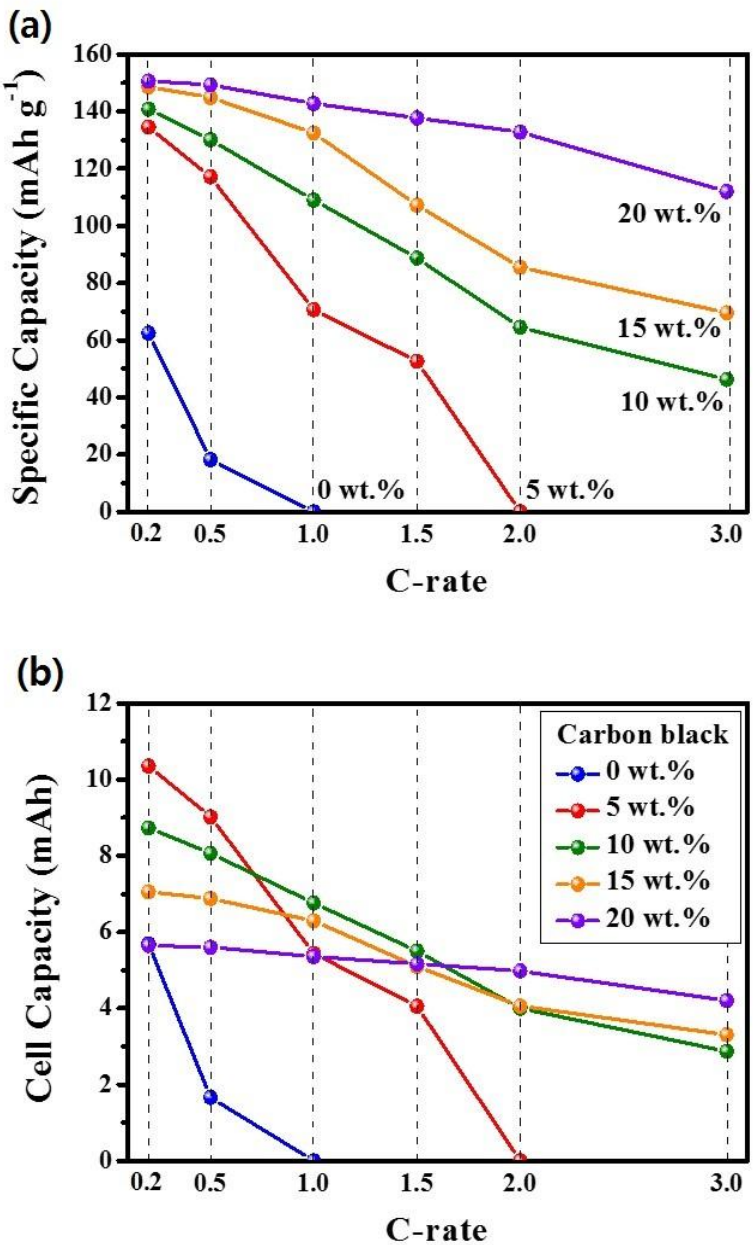

Figure 3.1.5 Comparison of the (a) specific capacity and (b) cell capacity with an increased in current rate.

Figure 3.1.6(a) shows the cycle-life performance of the cells at various discharge current rates between 0.5 and 1 C. In the case of the 15 and 20 wt.%-carbon black, the specific capacity gradually increased at the current rate of 0.5 C during initial 10 cycles. This is because as it gradually stabilizes, the captured Li-atoms at the inner part of metal foam cathode participate in redox reaction. The 10 wt.%-carbon black demonstrated an initial specific capacity of 127 mAh g^{-1}, which decreased to 55 mAh g^{-1} after 20 cycles at 0.5 and 1 C rates, showing a capacity retention of 43 %. On the other hand, 20 wt.%-carbon black showed an initial specific capacity 148 mAh g^{-1}, which decreased to 127 mAh g^{-1} after 20 cycles, demonstrating a capacity retention of 86 %. After that, the cells were carried out with 20 cycles repeated at 0.5 C. The discharge capacities showed similar values with initial 0.5 C cycles. Capacity-retention rates of 15 wt.% and 20 wt.%-carbon black were above 98 %, after 20 cycles, while it dropped to 75 % for 10 wt.%-carbon black. Obviously, cells with higher conductive carbon content showed a reduced capacity fading. Decrease of the carbon black content in the metal foam cathodes can cause capacity fade, due to loss of electrical contact between the particles, and an increase in resistance within the electrodes. Moreover, when the amount of active material increases, the volume change (expansion and contraction) also increases during charge-discharge processes. The volume change leads to severe stress accumulation within the electrode. As a result, stress accumulation induces cracking of the electrode, which eventually causes capacity degradation and resistance growth of the cell [87]. Figure 3.1.6(b) and (c) show the optical and SEM (using a back-scattered electrons (BSE) detector) images of 20 wt.%-electrode surface before and after cycle-life test. Images of electrode surface after cycle-life test (Figure 3.1.6(c)) show no exfoliation between electrode materials and metal frame of current collector due to very rough surface of the metal foam. The

rough surface enhances adhesion properties and prevents separation of the electrode materials from the metal frames during the charge-discharge process.

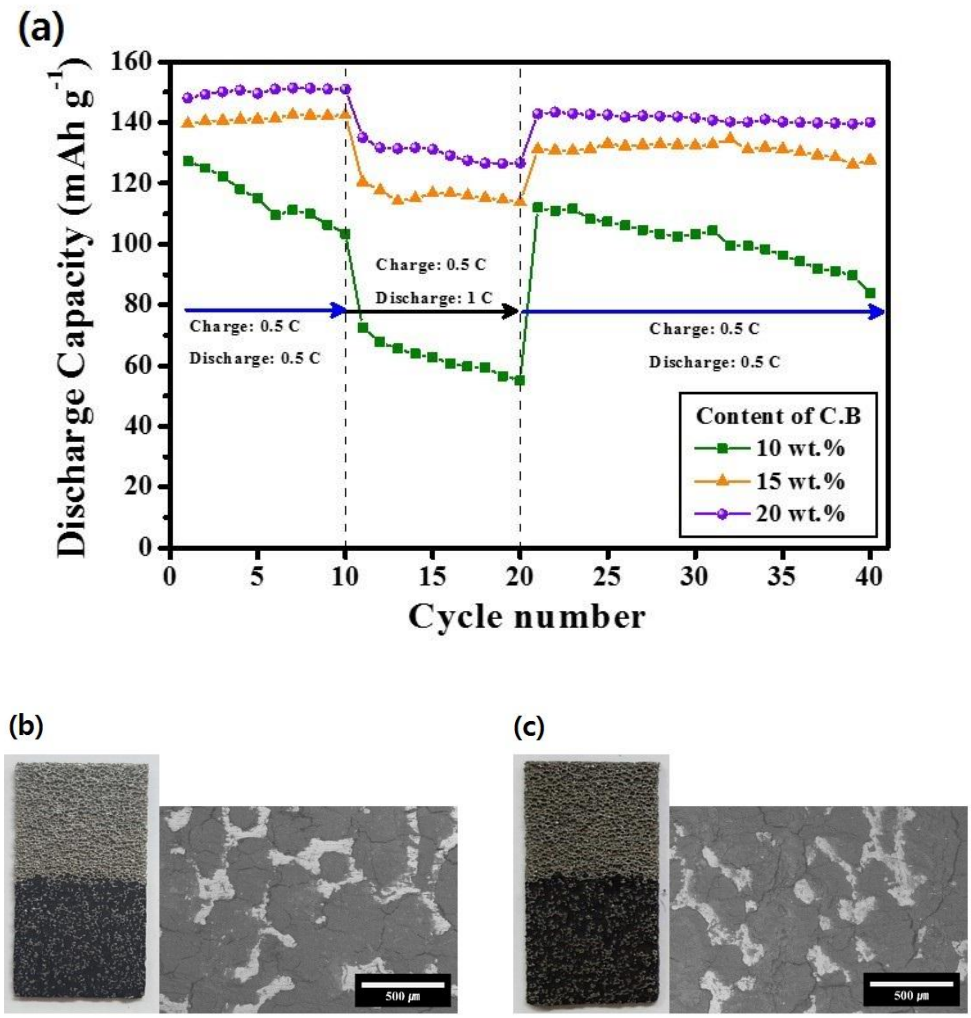

Figure 3.1.6 (a) Cycle-life performance of cells using different carbon black content under discharge rates, 0.5 C and 1 C, SEM and optical images of electrode surface (b) before and (c) after cycle-life test.

Figure 3.1.7 shows the cyclic voltammetry (CV) curves obtained from a scan rate of 0.1 mV S^{-1}. CV curves analysis is the usual technique for studying the electrochemical performance of Li-ion batteries. Information on the kinetics of the electrode reaction can be obtained from analysis of the CV curve [88]. Redox reaction of the cells occurs when the input voltage is higher or lower than the open circuit voltage (OCV, $LiFePO_4$ was 3.43 V) satisfying the Nernst equation. The results from the CV curves, kinetic performance also strongly depend on the conductive carbon content. The electrodes of lower carbon black content lead to a shift in peak position away from OCV (the oxidation and reduction peak positions of 20 wt.%-carbon black occur at 3.6 and 3.24 V, respectively, whereas those of 5 wt.%-carbon black occur at 3.7 and 3.2 V, respectively.) because the redox reaction occurs under non-equilibrium condition [88]. The shape of peak was much broader, and current intensity showed much lower, compared with the electrode of more added conductive carbon. This is due to the lower charge transfer ability and poor electronic conductivity in the electrodes inducing severe transport loss, which negatively affects the kinetic behavior. Thus, the specific diffusion flux of Li was much lower according to Fick's 1^{st} law, because the Li concentration gradient was much lower at the electrode surface for the electrode. The 0 wt.%-carbon black exhibited almost no oxidation or reduction peak. Figure 3.1.8 shows the Nyquist plots and equivalent circuit obtained from the electrodes for full discharge at 2.5 V. R_b is the bulk resistance of the cell, while R_{ct} is the charge transfer resistance of Li-ion at the electrolyte/$LiFePO_4$ interface. Z_W and C_{dl} represent the Warburg impedance related to the diffusion behavior of Li ions in the cathode active material and the capacitance double layer, respectively [89]. As a result, R_b varied very little, but R_{ct} differed greatly according to the conductive carbon content. The 0 wt.%-carbon black exhibited significantly high R_{ct} (70 Ω), and high diffusion resistance of

the electrode. Therefore, it exhibited very poor kinetic and rate performance, even at 0.2 and 0.5 C. R_{ct} significantly decreased with increased conductive carbon black; for example, the 5, 10, 15, and 20 wt.%-carbon black showed 25, 14, 11, and 4 Ω, respectively. The slopes of straight line scanned at lower frequencies also increased with more added carbon black, due to the enhanced diffusion limitation of Li-ion. Thus, conductive carbon loading is one of the most important techniques used to improve the specific capacity, rate performance, and cycling-life of $LiFePO_4$/C based on Li-ion batteries.

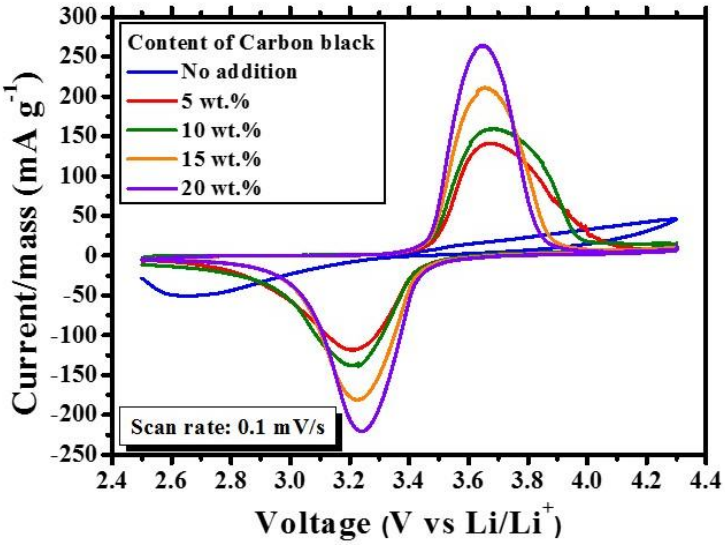

Figure 3.1.7 Comparison of the cyclic voltammetry curves at scan rate of 0.1mV S^{-1}.

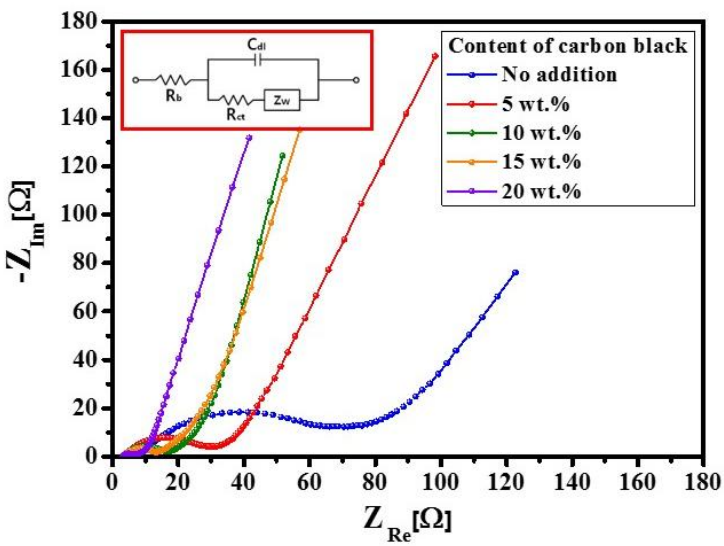

Figure 3.1.8 Nyquist plots of electrochemical impedance spectroscopy obtained from different content of carbon black at open circuit voltage (OCV) 3.43 V.

Moreover, Figure 3.1.9 shows the discharge capacity of the cells with 10 wt.% (I), 10 wt.% (II) and 20 wt.%-carbon black, respectively obtained from various current rates. In order to compare the rate performance of different carbon black content with similar areal capacity loading (10 wt.% (II) and 20 wt.%-carbon black) and different areal capacity loading with same content of carbon black (10 wt.% (I) and 10 wt.% (II)-carbon black), respectively. 10 wt.% (II) and 20 wt.%-carbon black were loaded similar mass of active materials (the 10 wt.% (II)-carbon black was 40 mg cm^{-2} and 20 wt.%-carbon black was 37.5 mg cm^{-2}, respectively), while 10 wt.% (I)-carbon black loaded 62 mg cm^{-2}. As shown in the result of the 10 wt.% (I) and (II)-carbon black, 10 wt.% (II)-carbon black exhibited a higher rate performance. It is because the lower electrode loading generally leads to improved rate performance due to the reduced kinetic barrier. Comparing the 20 wt.%-carbon black, there was no difference of discharge capacities at 0.2, 0.5, and 1 C-rate. However, discharge capacity of 10 wt.% (II)-carbon black was lower than 20 wt.%-carbon black, when c-rate exceeded 1.5 C. As the result of this figure, effects of carbon black content are more reliable.

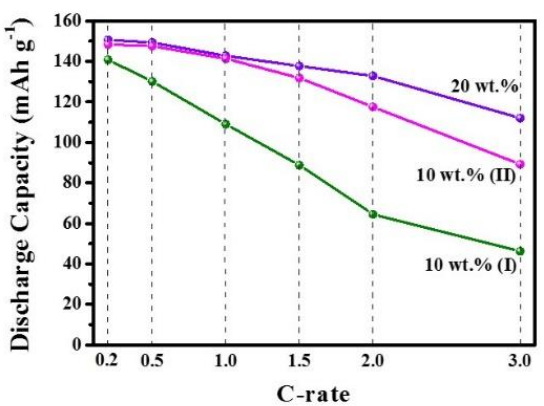

Figure 3.1.9 Comparison of the rate performance of the electrodes with 10 wt.% (I), 10 wt.% (II) and 20 wt.%, respectively, at various current rate. 10 wt.% (II) and 20 wt.%-electrodes were loaded similar mass of active materials.

Figure 3.1.10(a) show the cell capacity (mAh) of metal foam with 450 μm-pore size and 3000 μm-thickness obtained from the various discharge current densities (mA cm^{-2}). The mass of $LiFePO_4$/C were 177, 124, 93, 78, and 55 mg for the 5, 10, 15, 20, and 25 wt.%-metal foam cathodes, respectively. The detail analytical data of the metal foam cathodes was listed as shown in Table 3.1.2. Metal foam cathode of 5 wt.%-carbon black exhibited the highest cell capacity with 25.7, 23.3, 21.9, 19.1, 17.4, 15.1, and 12.3 mAh, respectively. While, metal foam cathode of 25 wt.%-carbon black exhibited the lowest cell capacity with 8.2, 8, 7.7, 7.5, 7.1, 6.6, and 5.9 mAh at 4, 6, 8, 10, 12, 15, and 20 mA cm^{-2}, respectively.

Table 3.1.2 Analytical data of metal foam cathodes with different content of carbon black. (Metal foam cathode: 450 μm-pore size and 3000 μm-thickness)

Pore size (μm)	Electrode thickness (μm)	Content of PVDF (wt.%)	Content of Carbon black (wt.%)	Content of $LiFePO_4$/C (wt.%)	Amount of $LiFePO_4$/C (mg cm^{-2})
450	3000	10	5	85	177
			10	80	124
			15	75	93
			20	70	78
			25	65	55

However, as shown in Figure 3.1.10(b), the specific capacity of the metal foam cathode of 5 wt.%-carbon black show drastically decreased and the lowest specific capacity due to the low electronic conductivity. The specific capacities were 145.5, 131.6, 123.6, 107.7, 98.3, 85.4, and 69.3 mAh g^{-1} at 4, 6, 8, 10, 12, 15, and 20 mA cm^{-2}. In addition, the metal foam cathodes of 15, 20, and 25 wt.%-carbon black show almost similar and the highest specific discharge capacity. Capacity retention rates were 48, 62, 71, 75, and 74 % for the 5, 10, 15, 20, and 25 wt.%-carbon black,

respectively. Figure 3.1.11(a) show the discharge curve at current density of 4 mA cm^{-2}. In the graph, all electrodes exhibited similar specific capacity (150 mAh g^{-1}) and the voltage of the plateau region at low current density. However, at high current density of 10 mA cm^{-2} (Figure 3.1.11(b)), the metal foam cathodes of 15, 20, and 25 wt.%-carbon black were exhibited same and the highest discharge specific capacity (138 mAh g^{-1}) and the voltage of the plateau region. While, the metal foam cathode of 5 wt.%-carbon black indicated the lowest specific capacity (108 mAh g^{-1}) and the highest over potential in the plateau region.

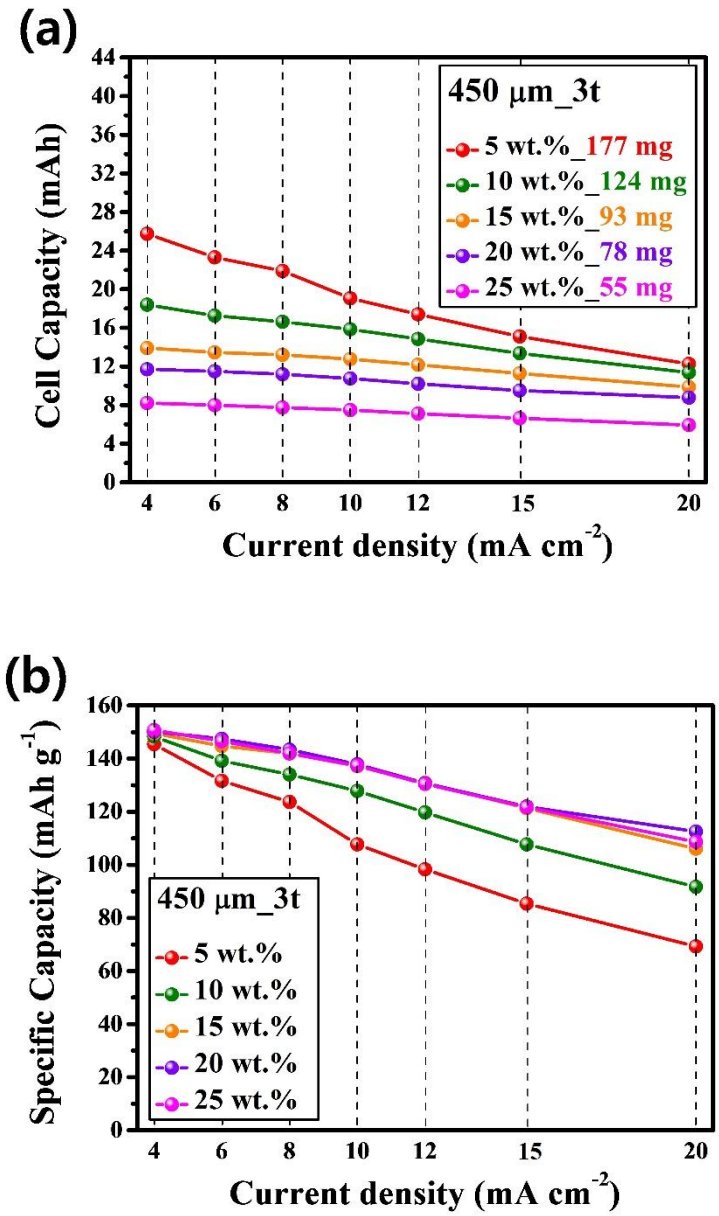

Figure 3.1.10 Comparison of the (a) cell capacity and (b) specific capacity with an increased in current density. (Metal foam cathode: 450 µm-pore size and 3000 µm-thickness)

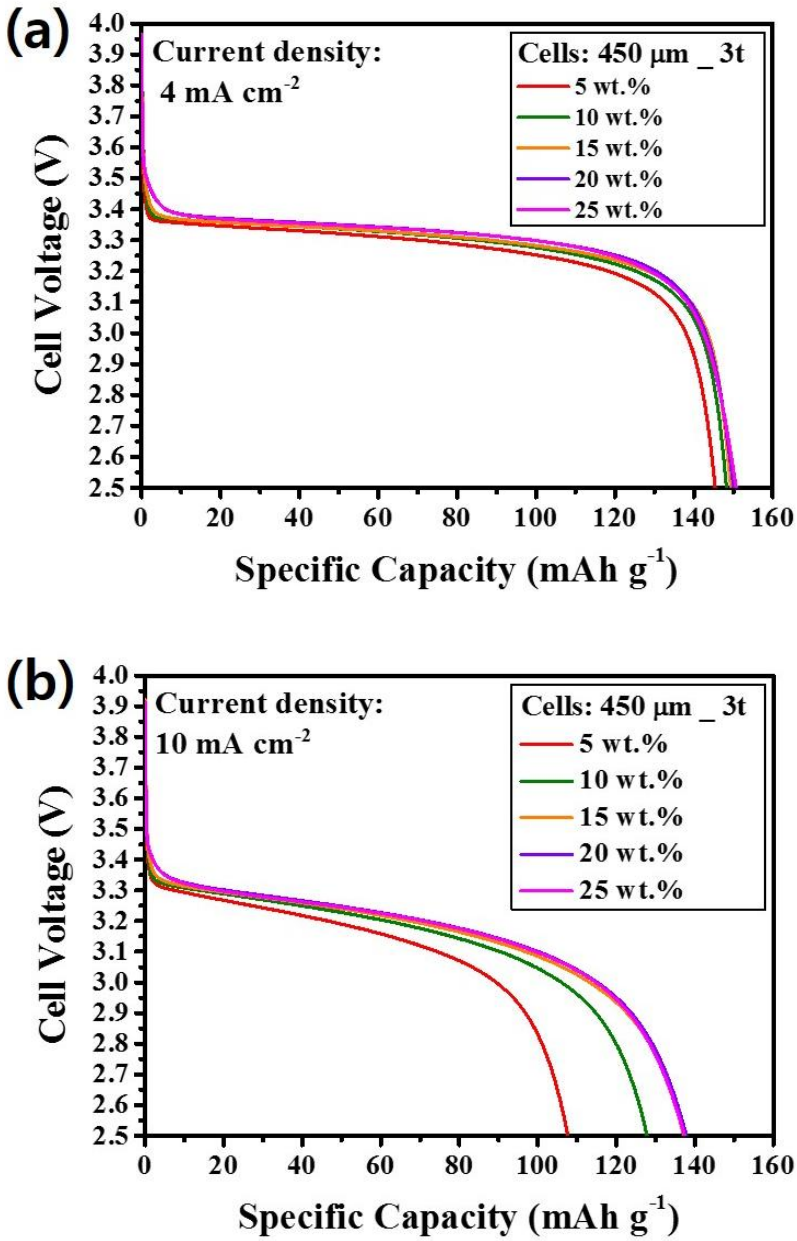

Figure 3.1.11 Comparison of the discharge curves at current density of (a) 4 mA cm^{-2} and (b) 10 mA cm^{-2}.

Figure 3.1.12(a) show the cell capacity (mAh) of metal foam with 1200 μm-pore size and 3000 μm-thickness obtained from the various discharge current densities (mA cm^{-2}). The mass of $LiFePO_4$/C were 215, 145, 113, 101, and 86 mg for the 5, 10, 15, 20, and 25 wt.%-carbon black, respectively. The detail analytical data of the metal foam cathodes was listed as shown in Table 3.1.3. Metal foam cathode of 5 wt.%-carbon black exhibited the highest cell capacity with 29.6, 27.8, and 21.1 mAh at 4, 6, and 8 mA cm^{-2}, respectively. However, as the current density increased, the cell capacity significantly decreased and showed the similar cell capacity as the metal foam cathode of 25 wt.%-carbon black at 20 mA cm^{-2}.

Table 3.1.3 Analytical data of metal foam cathodes with different content of carbon black. (Metal foam cathode: 1200 μm-pore size and 3000 μm-thickness)

Pore size (μm)	Electrode thickness (μm)	Content of PVDF (wt.%)	Content of Carbon black (wt.%)	Content of $LiFePO_4$/C (wt.%)	Amount of $LiFePO_4$/C (mg cm^{-2})
1200	3000	10	5	85	215
			10	80	145
			15	75	113
			20	70	101
			25	65	86

As shown in Figure 3.1.12(b), the specific capacity of the metal foam cathode of 5 wt.%-carbon black show drastically decreased and the lowest specific capacity. The specific capacities were 137.5, 129.4, 97.9, 82.6, 68.7, 52.8, and 35.8 mAh g^{-1} at 4, 6, 8, 10, 12, 15, and 20 mA cm^{-2}, respectively. While, metal foam cathode of 25 wt.%-carbon black was exhibited the highest specific capacity. The specific capacities were 149.5, 146.2, 143.1, 139.9, 132.2, 119.8, and 99.3 mAh g^{-1} at 4, 6, 8, 10, 12, 15, and

20 mA cm^{-2}, respectively. Capacity retention rates were 26, 42, 54, 55, and 66 % for the 5, 10, 15, 20, and 25 wt.%-carbon black, respectively. Figure 3.1.13(a) show the discharge curve at current density of 4 mA cm^{-2}. In the graph, the metal foam cathodes of 15, 20, and 25 wt.%-carbon black exhibited almost similar specific capacity (150 mAh g^{-1}) and the voltage of the plateau region. And, the metal foam cathode of 5 wt.%-carbon black was indicated the lowest discharge capacity (137 mAh g^{-1}). At high current density of 10 mA cm^{-2} (Figure 3.1.13(b)), metal foam cathode of 25 wt.%-carbon black still showed the highest discharge specific capacity (140 mAh g^{-1}) and the voltage of the plateau region. While, metal foam cathode of 5 wt.%-carbon black still indicated the lowest specific capacity (82 mAh g^{-1}) and the highest over potential in the plateau region.

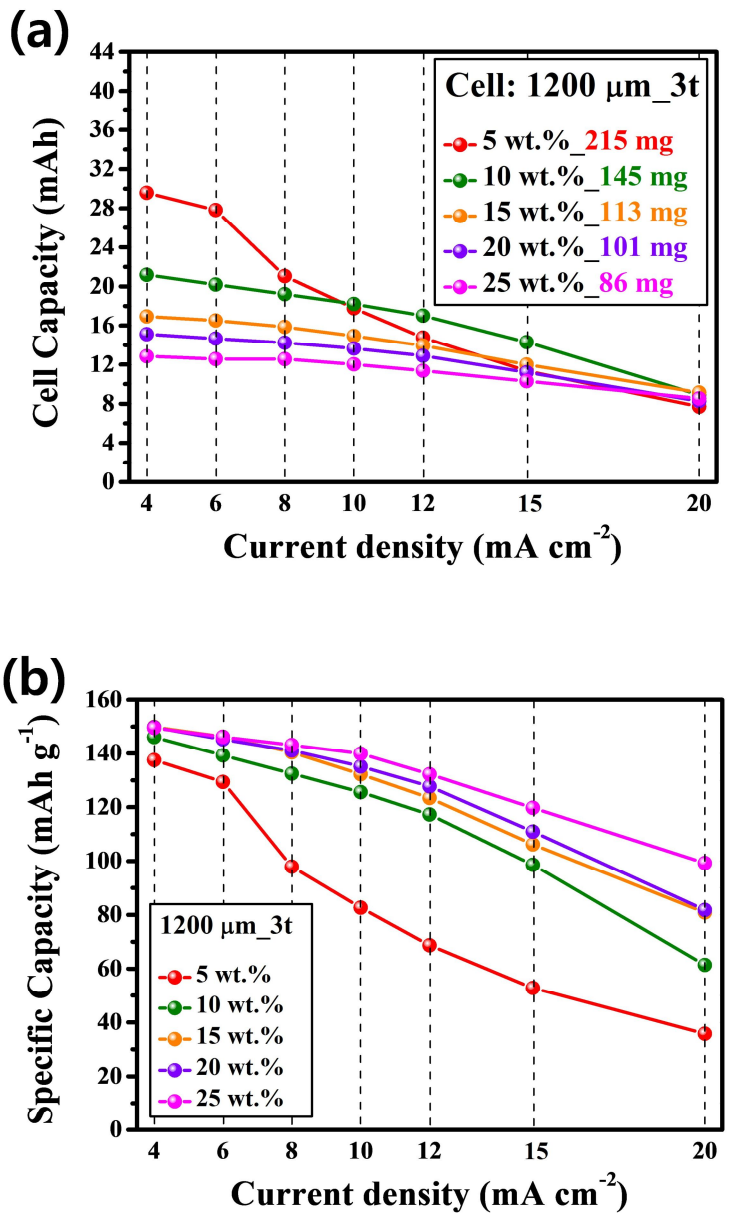

Figure 3.1.12 Comparison of the (a) cell capacity and (b) specific capacity with an increased in current density. (Metal foam cathode: 1200 µm-pore size and 3000 µm-thickness)

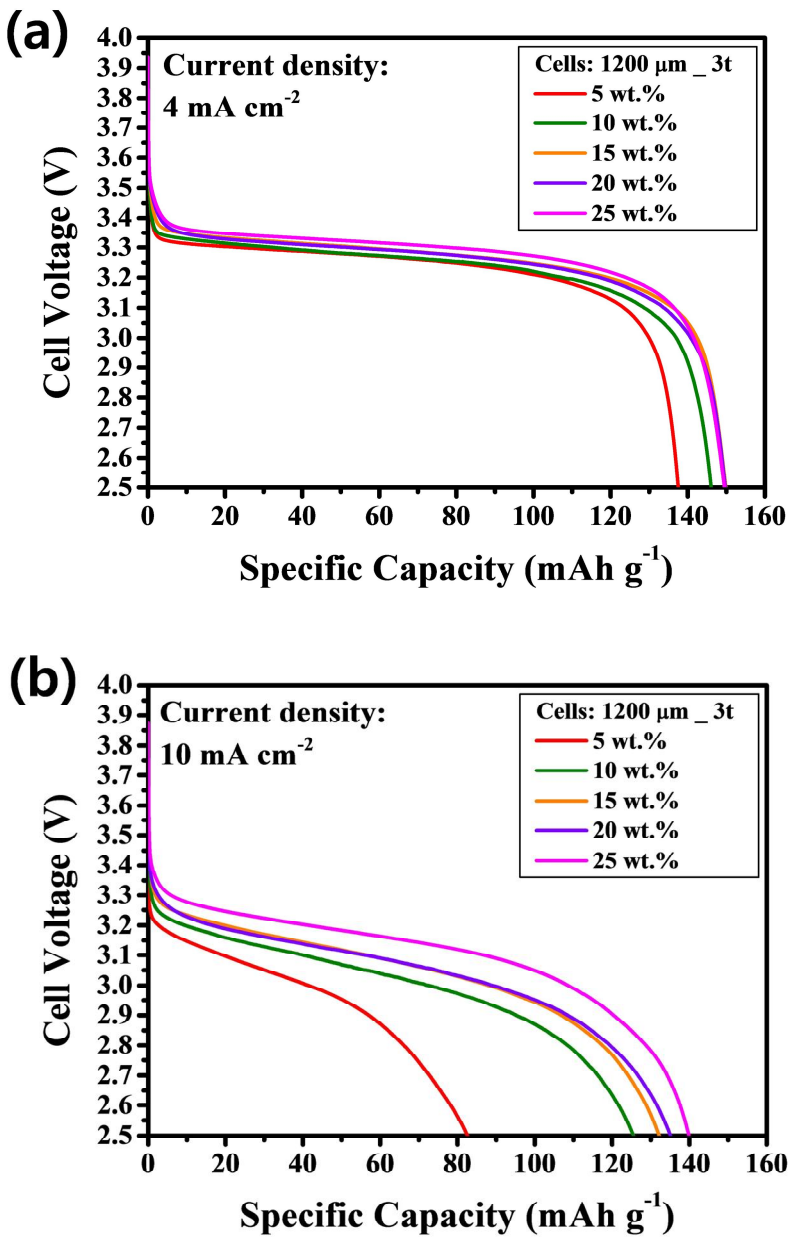

Figure 3.1.13 Comparison of the discharge curves at current density of (a) 4 mA cm^{-2} and (b) 10 mA cm^{-2}.

Moreover, Figure 3.1.14(a) show the cell capacity (mAh) of metal foam cathodes of 3000 μm-pore size and 3000 μm-thickness obtained from the various discharge current densities. The mass of $LiFePO_4$/C were 320, 230, 182, 158, 114 and 101 mg for the 5, 10, 15, 20, 25 and 30 wt.%-carbon black, respectively. The detail analytical data of the metal foam cathodes was listed as shown in Table 3.1.4. Metal foam cathode of 5 wt.%-carbon black exhibited the highest cell capacity with 40.4, 38.2, 32.6, 29.2, 24, 18.7. and 13.5 mAh at 4, 6, 8, 10, 12, 15, and 20 mA cm^{-2}, respectively. However, at 12 mA cm^{-2}, it showed the same capacity (24 mAh) as the metal foam cathode of 10 wt.%-carbon black. In addition, metal foam cathode of 15 wt.%-carbon black showed the highest cell capacity from 15 mA cm^{-2}.

Table 3.1.4 Analytical data of metal foam cathodes with different content of carbon black. (Metal foam cathode: 3000 μm-pore size and 3000 μm-thickness)

Pore size (μm)	Electrode thickness (μm)	Content of PVDF (wt.%)	Content of Carbon black (wt.%)	Content of $LiFePO_4$/C (wt.%)	Amount of $LiFePO_4$/C (mg cm^{-2})
3000	3000	10	5	85	320
			10	80	230
			15	75	182
			20	70	158
			25	65	114
			30	60	101

As shown in Figure 3.1.14(b), the specific capacity of the metal foam cathode of 5 wt.%-carbon black show drastically decreased and the lowest specific capacity. The specific capacities were 126.3, 119.5, 101.8, 91.3, 75.1, 58.3, and 42.2 mAh g^{-1} at 4, 6, 8, 10, 12, 15, and 20 mA cm^{-2}, respectively. While, metal foam cathode of 30 wt.%-carbon black exhibited the highest specific capacity and the voltage of the plateau

region. The specific capacities were 151.8, 148.6, 145.2, 141, 134.3, 126.8, and 113.3 mAh g^{-1} at 4, 6, 8, 10, 12, 15, and 20 mA cm^{-2}. Respectively. Capacity retention rates were 33, 44, 57, 58, 69 and 76 % for the 5, 10, 15, 20, 25 and 30 wt.%-carbon black, respectively. Figure 3.1.15(a) show the discharge curve at current density of 4 mA cm^{-2}. In the graph, the metal foam cathodes of 15, 20, 25 and 30 wt.%-carbon black exhibited almost similar specific capacity (150 mAh g^{-1}). However, the over potential of the plateau region was lower as carbon black was higher electrode. And, the metal foam cathode of 5 wt.%-carbon black was indicated the lowest discharge capacity (126 mAh g^{-1}). In addition, at high current density of 10 mA cm^{-2} (Figure 3.1.15(b)), the metal foam cathode of 30 wt.%-carbon black still showed the highest discharge specific capacity (141 mAh g^{-1}) and the voltage of the plateau region.

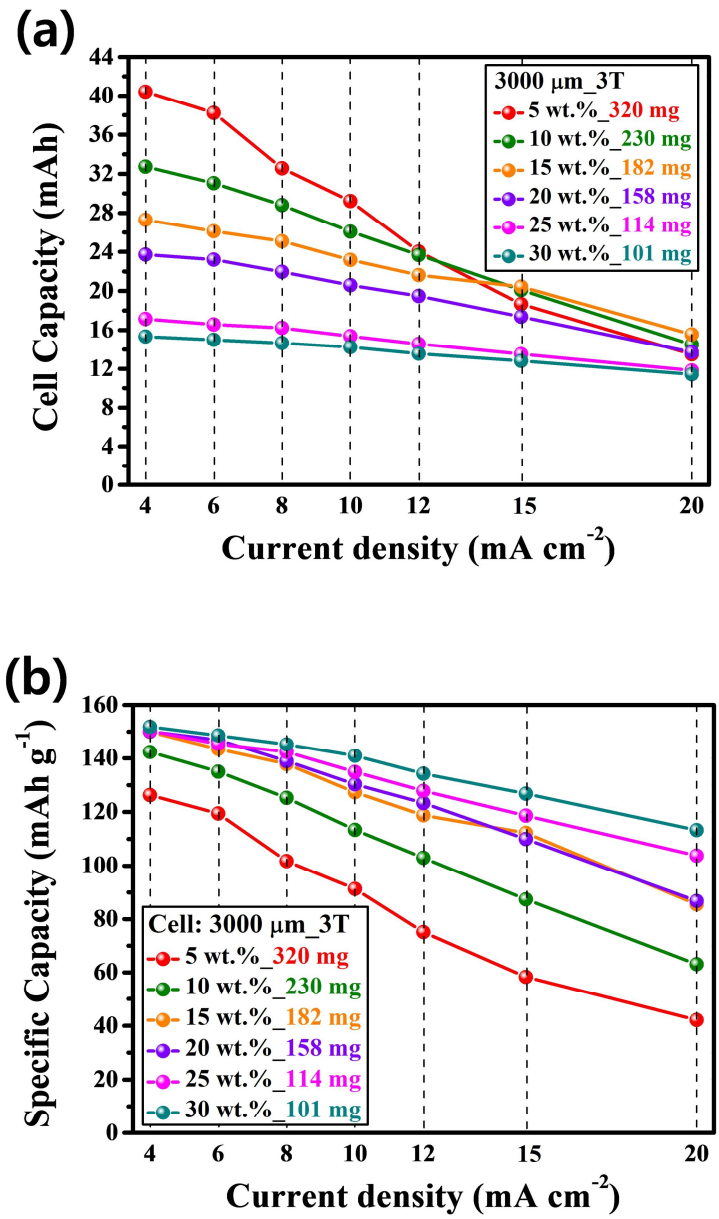

Figure 3.1.14 Comparison of the (a) cell capacity and (b) specific capacity with an increased in current density. (Metal foam cathode: 3000 µm-pore size and 3000 µm-thickness)

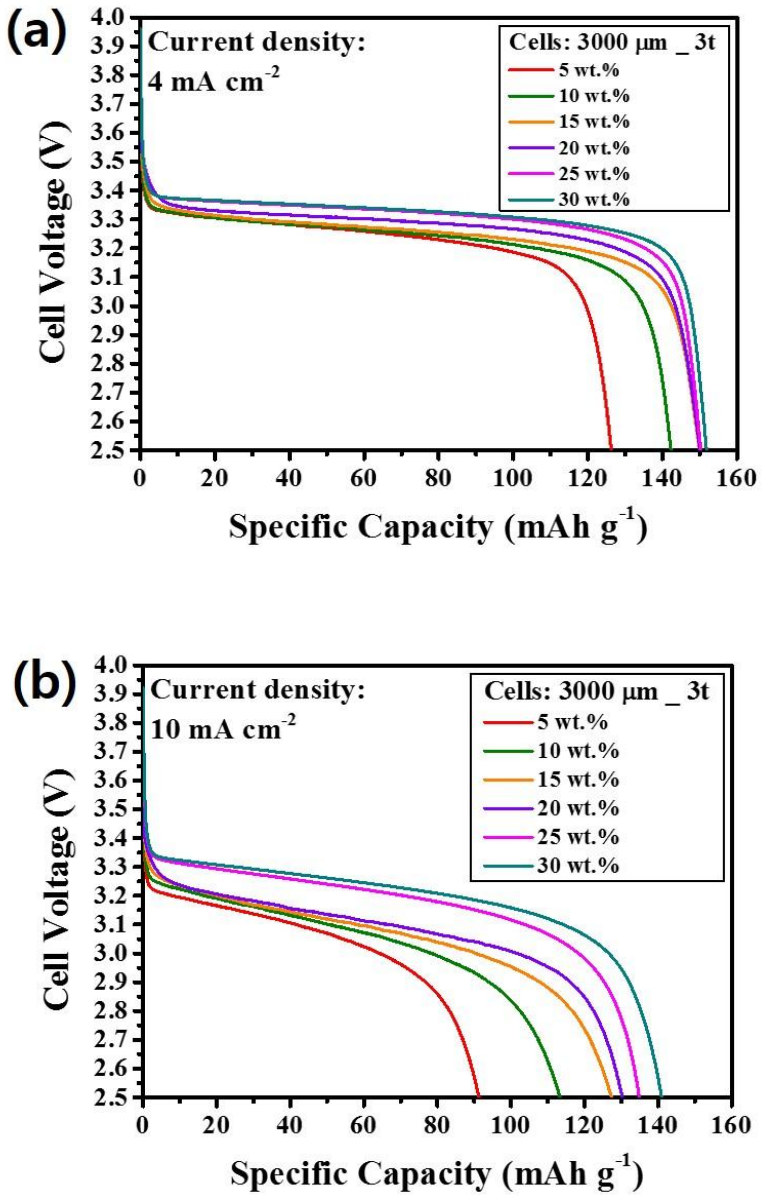

Figure 3.1.15 Comparison of the discharge curves at current density of (a) 4 mA cm^{-2} and (b) 10 mA cm^{-2}.

3.2 Effect of Pore size in metal foam

3.2.1 Similar amount of $LiFePO_4$/C

This experiment compares the electrochemical properties relate to the pore size in metal foam with the similar mass loading of $LiFePO_4$/C. The mass of $LiFePO_4$/C was around 44 mg and the thicknesses of metal foam cathode were set to 1000, 900, and 900 μm in 450, 800, and 1200 μm-pore sizes, respectively. The details analytical data of the metal foam cathodes is shown in Table 3.2.1.1.

Table 3.2.1.1 Analytical data of metal foam cathodes with different pore size. (Similar amount of active material)

Pore Size	Electrode Thickness	Amount of Active material	Content of Carbon black	Content of PVDF	Content of $LiFePO_4$/C
450 μm	1000 μm	43 mg cm^{-2}	15 wt.%	10 wt.%	75 wt.%
800 μm	900 μm	44 mg cm^{-2}			
1200 μm	900 μm	45 mg cm^{-2}			

Figure 3.2.1.1 shows the charge/discharge curve at a current density of 0.7 mA (0.1 C). In the graph, there were almost similar specific capacity (about 150 mAh g^{-1}) and potential drop in the plateau region because the diffusion limitations of Li-ion were almost similar at low current rate. Figure 3.2.1.2 shows the cycle-life performance at various current rate between 7 and 10 mA. In the graph, the metal foam cathode with larger pore size was exhibited higher capacity decrease with increase current density, due to the increase Li-ion diffusion length and charge transfer resistance. In addition, the contact area between active material and metal frame in reduced with the increase pore size. It seems that the charge transfer ability are higher for the smaller pore size of metal foam cathode [37]. Therefore, the capacity retention rates were 72, 60, and 52 %

for the 450, 800, and 1200 μm-pore sizes, respectively. Figure 3.2.1.3(a) shows the cyclic voltammetry (CV) curves obtained from a scan rate of 0.1 mV S^{-1}. The electrodes of large pore size lead to a shift in peak position away from OCV (the oxidation and reduction peak positions of 450 μm-pore size occur at 3.69 and 3.21 V, respectively, whereas those of 1200 μm-pore size occur at 3.76 and 3.16 V, respectively.) because the redox reaction occurs under non-equilibrium condition [88]. The shape of peak was much broader, and current intensity showed much lower, compared with the electrode of larger pore size. Figure 3.2.1.3(b) shows the Nyquist plots and equivalent circuit obtained from the electrodes for full discharge at 2.5 V. R_b is the bulk resistance of the cell, while R_{ct} is the charge transfer resistance of Li-ion at the electrolyte/$LiFePO_4$ interface. Z_W and C_{dl} represent the Warburg impedance related to the diffusion behavior of Li ions in the cathode active material and the capacitance double layer, respectively [89]. As a result, R_b is almost same, but R_{ct} differed according to the pore size of metal foam electrode. The 1200 μm-pore size exhibited the highest R_{ct} (20 Ω). Therefore, it exhibited very poor kinetic and cycle-life performance. R_{ct} decreased with small pore size of metal foam; for example, the 450 and 800 μm-pore sizes showed 13 and 18 Ω, respectively. Thus, pore size of metal foam electrode is one of the most important techniques used to improve the specific capacity, rate performance, and cycling-life performance of Li-ion batteries.

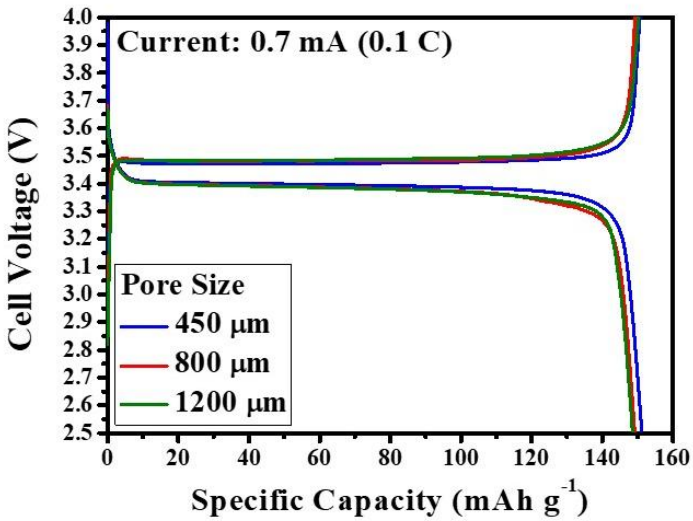

Figure 3.2.1.1 Comparison of the discharge curves at current density of 0.7 mA cm^{-2} (0.1C). (Similar amount of active material)

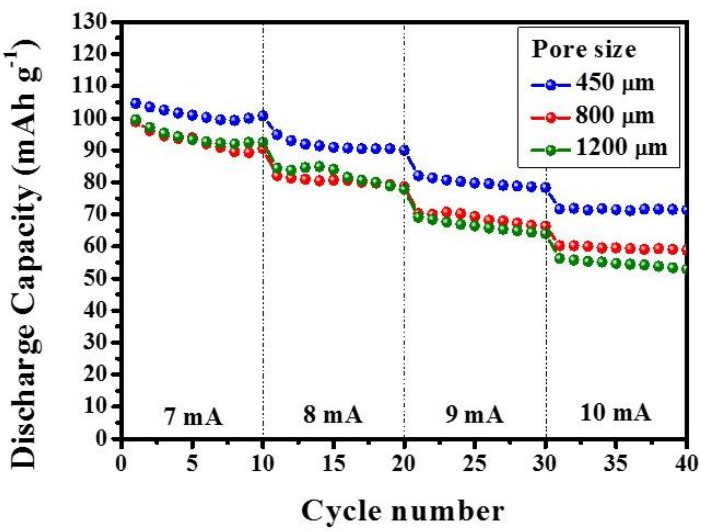

Figure 3.2.1.2 Cycle-life performance of metal foam cathodes using different pore size. (Similar amount of active material)

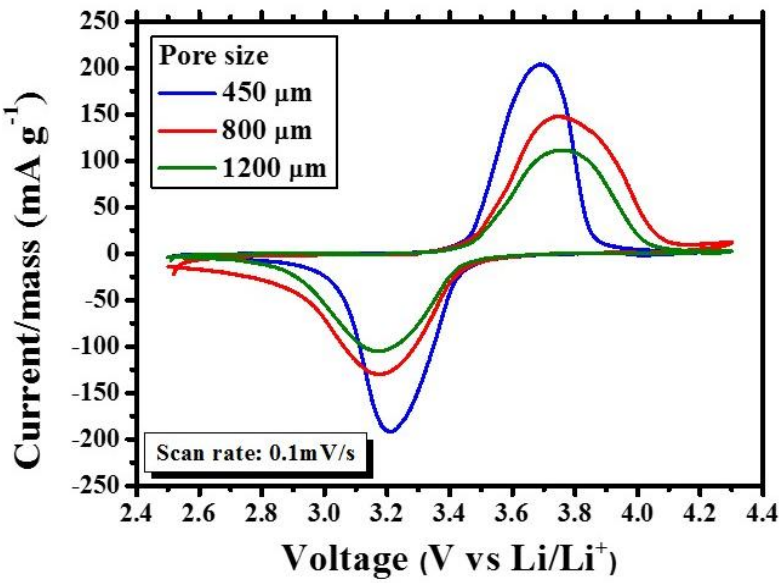

Figure 3.2.1.3 Comparison of the cyclic voltammetry curves at scan rate of 0.1mV S^{-1}. (Similar amount of active material)

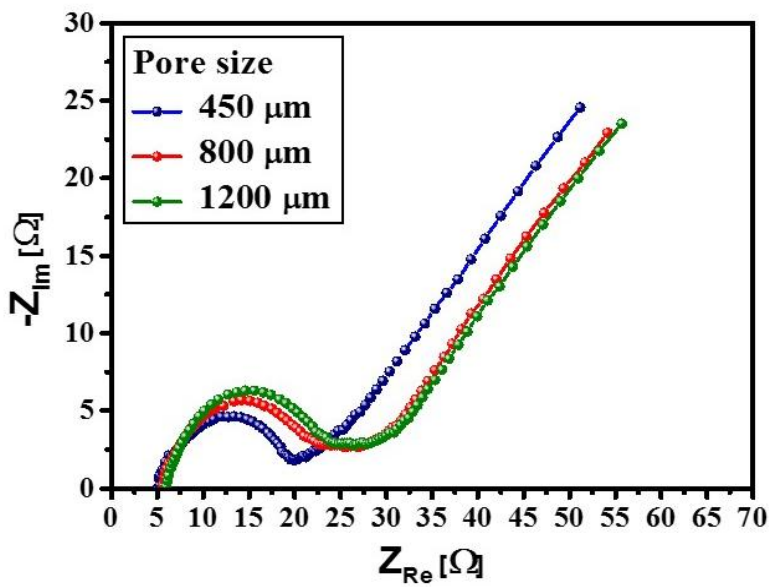

Figure 3.2.1.4 Nyquist plots of electrochemical impedance spectroscopy obtained from different pore size in metal foam cathodes at open circuit voltage (OCV) 3.43 V. (Similar amount of active material)

3.2.2 Different amount of $LiFePO_4$/C

In this part, we compared the electrochemical properties related to pore size in metal foam cathode using the 3000 μm-thickness and 15 wt.%-carbon black. The details analytical date of the metal foam cathodes is shown in Table 3.2.2.1.

Table 3.2.2.1 Analytical data of metal foam cathodes with different pore size. (Different amount of active material, metal foam cathode: 3000 μm-thickness and 15 wt.%-carbon black)

Pore Size	Thickness	Content of $LiFePO_4$/C	Content of carbon black	Content of PVDF	Mass of $LiFePO_4$/C
450 μm	3000 μm	75 wt.%	15 wt.%	10 wt.%	93 mg
1200 μm					113 mg
3000 μm					182 mg

Figure 3.2.2.1 shows the cell capacity (mAh) obtained from the various discharge current density. Analysis indicated that 3000 μm-pore size showed the highest cell capacity, followed by 1200 and 450 μm-pore sizes. Cell capacities of 3000 μm-pore size were 27.3, 26.1, 25.1, 23.2, and 21.6 mAh for the 4, 6, 8, 10, and 12 mA cm^{-2}, respectively. Whereas, 450 μm-pore size showed the lowest cell capacity with 14, 13.5, 13.2, 12.8, and 12.2 mAh because the lowest amount of $LiFePO_4$/C was loaded. However, 450 μm-pore size showed the highest LFP specific capacity due to the largest triple point and the lowest charge transfer resistance as shown in Figure 3.2.2.2. The specific capacities of 450 μm-pore size were 150, 144.8, 141.9, 137.2, and 130.9-mAh g^{-1} at the 4, 6, 8, 10, and 12 mA cm^{-2}, respectively. The capacity retention rates between 4 and 12 mA cm^{-2} of the metal foam cathodes were 88, 82, and 79 % for the 450, 1200, and 3000 μm-pore sizes, respectively. Figure 3.2.2.3(a) shows the discharge curves of different pore size of metal foam cathode at a discharge current

density of 4mA cm^{-2}. In the graph, there were almost no difference on specific capacity (about 150 mAh g^{-1}) and voltage drop in the plateau region, because the redox reaction of metal foam cathode occurs sufficiently at low current density. However, discharge curves at current density of 10 mA cm^{-2} (Figure 3.2.2.3(b)), 450 μm-pore size was indicated the highest specific capacity (138 mAh g^{-1}) and 3000 μm-pore size was indicated the lowest specific capacity (128 mAh g^{-1}). 450 μm-pore size showed the highest specific capacity and voltage of plateau region due to the largest area of redox reaction and the lowest charge transfer resistance as shown in Figure 3.2.2.5. Figure 3.2.2.4 shows the cyclic voltammetry (CV) curves obtained from a scan rate of 0.1 mV S^{-1}. The metal foam cathode of 3000 μm-pore size lead to a more shift in peak position away from OCV than 450 and 1200 μm-pore sizes. In addition, the shape of peak was much broader compared with the metal foam cathode of 450 and 1200 μm-pore size. The oxidation and reduction peak positions of 450 μm-pore size occur at 3.69 and 3.21 V, respectively, whereas those of 3000 μm-pore size occur at 3.94 and 3 V, respectively. Figure 3.2.2.5 shows the Nyquist plots obtained from the metal foam cathodes for full discharge at 2.5 V. R_b is the bulk resistance of the cell, while R_{ct} is the charge transfer resistance of Li-ion at the electrolyte/$LiFePO_4$ interface. Z_W and C_{dl} represent the Warburg impedance related to the diffusion behavior of Li ions in the cathode active material and the capacitance double layer, respectively [89]. As a result, R_b is almost similar, but R_{ct} differed according to the pore size of metal foam cathodes. The 3000 μm-pore size exhibited the highest R_{ct} (15 Ω). R_{ct} decreased with small pore size of metal foam; for example, the 450 and 1200 μm-pore sizes showed 7 and 10 Ω, respectively.

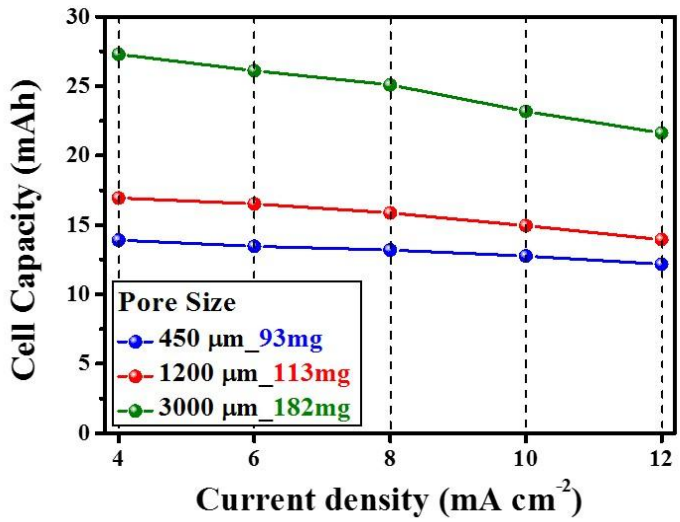

Figure 3.2.2.1 Comparison of the cell capacity (mAh) with an increased in current density. (Different amount of active material, metal foam cathode: 3000 µm-thickness and 15 wt.%-carbon black)

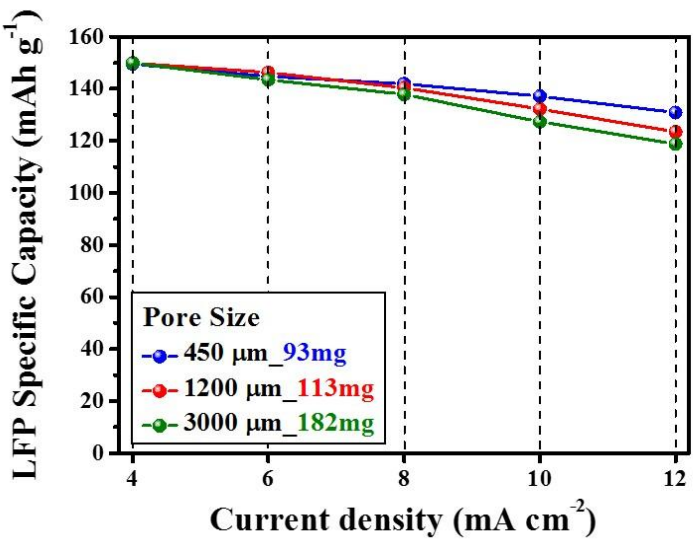

Figure 3.2.2.2 Comparison of the LFP specific capacity (mAh g^{-1}) with an increased in current density. (Different amount of active material, metal foam cathode: 3000 µm-thickness and 15 wt.%-carbon black)

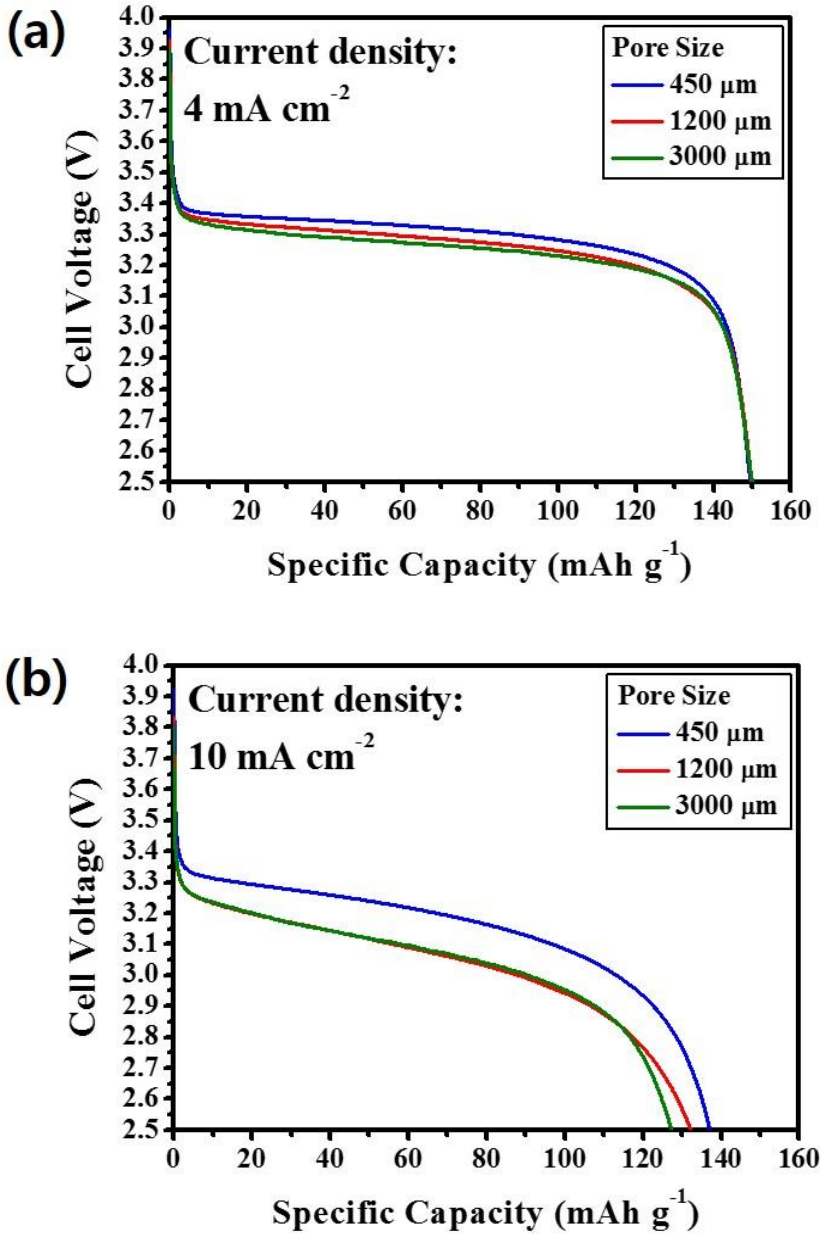

Figure 3.2.2.3 Comparison of the discharge curves at current density of (a) 4 mA cm^{-2} and (b) 10 mA cm^{-2}. (Different amount of active material, metal foam cathode: 3000 µm-thickness and 15 wt.%-carbon black)

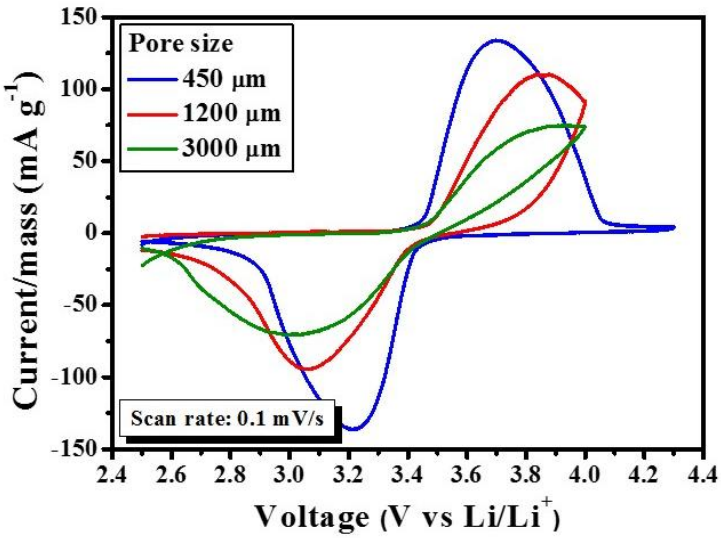

Figure 3.2.2.4 Cyclic voltammetry curves at scan rate of 0.1mV S^{-1}. (Different amount of active material, metal foam cathode: 3000 µm-thickness and 15 wt.%-carbon black)

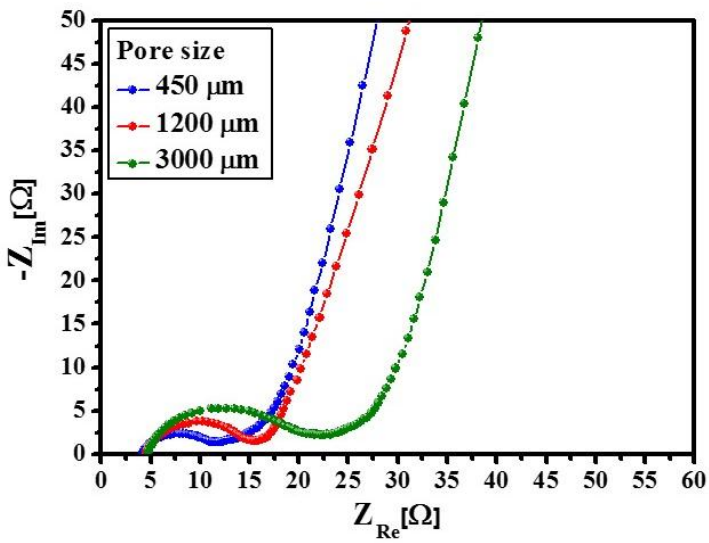

Figure 3.2.2.5 Nyquist plots of electrochemical impedance spectroscopy obtained from different pore size in metal foam cathodes at open circuit voltage (OCV) 3.43 V. (Different amount of active material, metal foam cathode: 3000 µm-thickness and 15 wt.%-carbon black)

The next experiment compared the electrochemical performances of the metal foam cathode thickness of 3000 μm-thickness and 25 wt.%-carbon black content. The details analytical data of the metal foam cathodes is shown in Table 3.2.2.2.

Table 3.2.2.2 Analytical data of metal foam cathodes with different pore size. (Different amount of active material, metal foam cathode: 3000 μm-thickness and 25 wt.%-carbon black)

Pore Size	Thickness	Content of $LiFePO_4$/C	Content of carbon black	Content of PVDF	Mass of $LiFePO_4$/C
450 μm	3000 μm	65 wt.%	25 wt.%	10 wt.%	55 mg
1200 μm					86 mg
3000 μm					114 mg

Figure 3.2.2.6(a) shows the discharge curves at current density of 4mA cm^{-2}. In the graph, there were almost no difference on specific capacity (about 150 mAh g^{-1}) and voltage drop in the plateau region, because the redox reaction of metal foam cathode occurs sufficiently at low current density. Moreover, at current density of 10 mA cm^{-2} (Figure 3.2.2.6(b)), there were almost no difference on specific capacity (about 138 mAh g^{-1}). In addition, 450 and 3000 μm-pore sizes were indicated almost similar voltage of plateau region due to the larger pore size of metal foam was influenced more by the carbon black. Figure 3.2.2.7 shows the cell capacity (mAh) obtained from the various discharge current density. Analysis indicated that 3000 μm-pore size showed the highest cell capacity, followed by 1200 and 450 μm-pore sizes. Cell capacities of 3000 μm-pore size were 17.1, 16.6, 16.2, 15.4, and 14.6 mAh for the 4, 6, 8, 10, and 12 mA cm^{-2}, respectively. whereas, 450 μm-pore size showed the lowest cell capacity with 8.2, 8, 7.7, 7.5, and 7.1 mAh due to the lowest amount of active material ($LiFePO_4$/C) was loaded. Figure 3.2.2.8 shows the LFP specific capacity (mAh g^{-1}). In the graph,

there were almost similar LFP specific capacity and rate performance. Capacity retention rates between 4 and 12 mA cm^{-2} of the electrodes were 86, 87, and 85% for the 450, 1200, and 3000 µm-pore sizes, respectively.

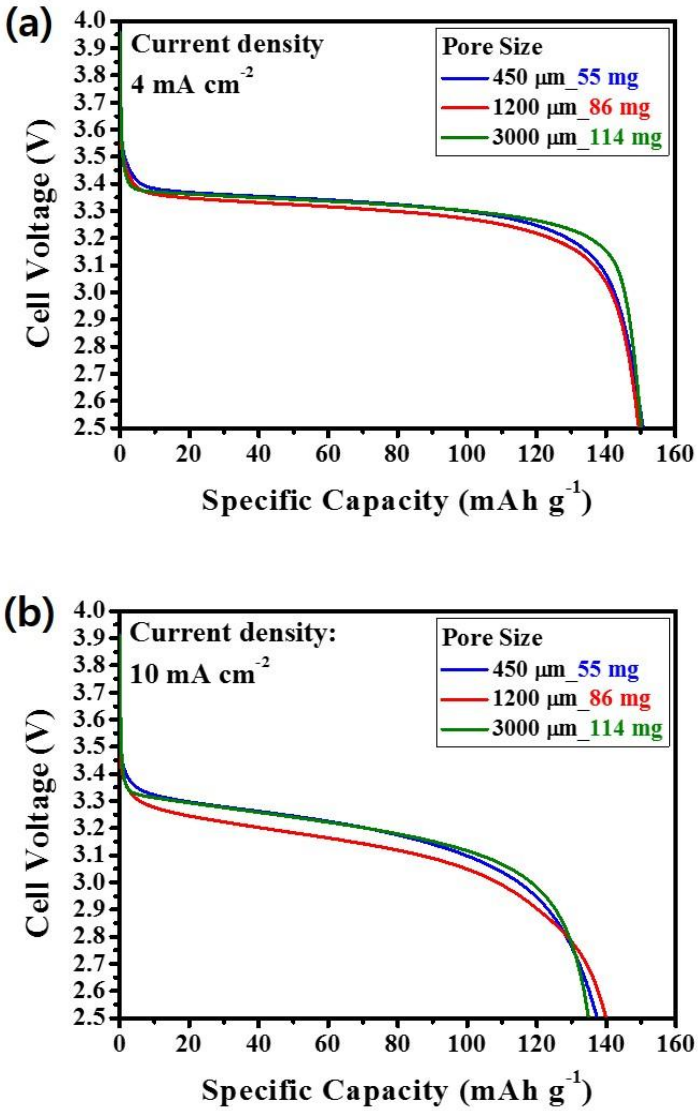

Figure 3.2.2.6 Comparison of the discharge curves at current density of (a) 4 mA cm^{-2} and (b) 10 mA cm^{-2}. (Different amount of active material, metal foam cathode: 3000 µm-thickness and 25 wt.%-carbon black)

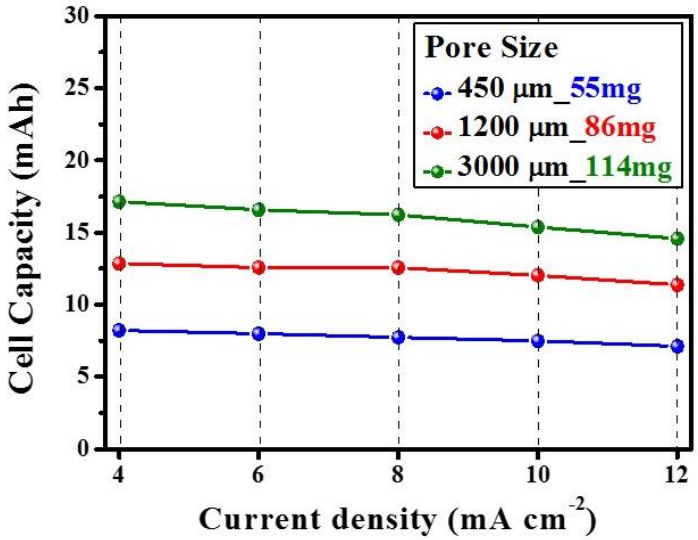

Figure 3.2.2.7 Comparison of the cell capacity (mAh) with an increased in current density. (Different amount of active material, metal foam cathode: 3000 µm-thickness and 25 wt.%-carbon black)

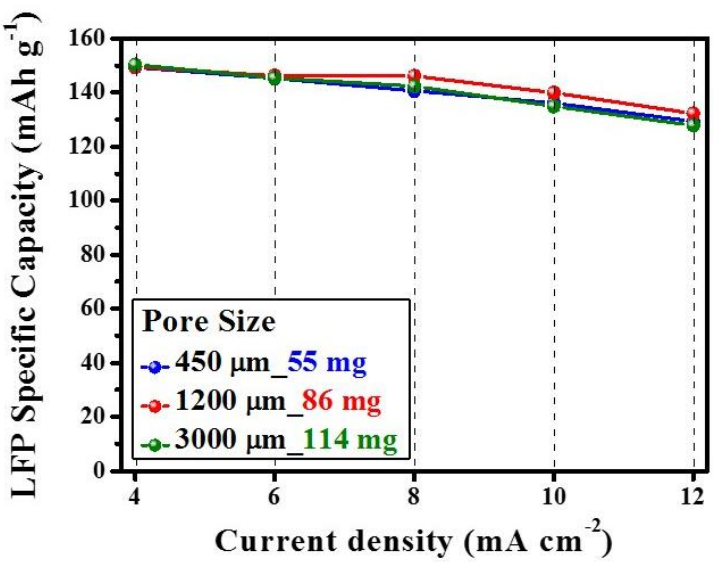

Figure 3.2.2.8 Comparison of the LFP specific capacity (mAh g^{-1}) with an increased in current density. (Different amount of active material, metal foam cathode: 3000 µm-thickness and 25 wt.%-carbon black)

The next experiment evaluated metal foam cathodes fabrication method that is most suitable for manufacture a light and high capacity battery. The details analytical data of the metal foam cathodes are shown in Table 3.2.2.3.

Table 3.2.2.3 Analytical data of metal foam cathodes with different pore size and content of carbon black.

Pore size (µm)	Electrode thickness (µm)	Content of PVDF (wt.%)	Content of Carbon black (wt.%)	Content of $LiFePO_4$/C (wt.%)	Mass of $LiFePO_4$/C (mg cm^{-2})	Mass of Cathode materials (LFP+C.B+PVDF) (mg cm^{-2})	Mass of NiCrAl Metal Foam (mg cm^{-2})	Mass of metal foam cathode (mg cm^{-2})
450	3000	10	15	75	**93**	124	240	**364**
450	3000	10	25	65	**55**	84	240	**324**
1200	3000	10	15	75	**113**	151	150	**301**
1200	3000	10	25	65	**86**	132	150	**282**
3000	3000	10	15	75	**182**	242	80	**322**
3000	3000	10	25	65	**114**	152	80	**232**

Figure 3.2.2.9 shows the cell capacity (mAh) obtained from the various discharge current densities. The metal foam cathode with 3000 µm-pore size and 15 wt.%-carbon black exhibited the highest cell capacity with 27.3, 26.1, 25.1, 23.2, and 21.6 mAh at 4, 6, 8, 10, and 12 mA cm^{-2}, respectively. Whereas, the metal foam cathode with 450 µm-pore size and 25 wt.%-carbon black exhibited the lowest cell capacity with 8.2, 8, 7.7, 7.5, and 7.1 mAh at 4, 6, 8, 10, and 12 mA cm^{-2}. The reason was that metal foam cathode of 450 µm-pore size and 25 wt.%-carbon black has the lowest mass loadings of active material. Figure 3.2.2.10 shows the LFP specific capacity (mAh g^{-1}). LFP specific capacity was obtained the cell capacity divided by the mass loadings of active material. In the graph, the metal foam cathode of 450 µm-pore size and 15 wt.%-carbon black, the metal foam cathode of 450 µm-pore size and 25 wt.%-carbon black, and the metal foam cathode 3000 µm-pore size and 25 wt.%-carbon black was exhibited the similar LFP specific capacity. On the other hands, the metal foam cathode of 3000 µm-pore size and 15 wt.%-carbon black was indicated the

lowest LFP Specific capacity with 150, 143.5, 137.8, 127.3, and 118.8 mAh g^{-1} at 4, 6, 8, 10, and 12 mA cm^{-2}. The reason was that the metal foam cathode of 3000 μm-pore size and 15 wt.%-carbon black has low triple point and electric conductivity due to the large pore size of metal foam and low content of carbon black. However, the difference in LFP specific capacity was very small. Figure 3.2.2.11 shows the cell specific capacity (mAh g^{-1}). Cell specific capacity was obtained the cell capacity divided by the total mass of the metal foam cathodes (total mass of active material, carbon black, PVDF, and metal foam). In the graph, the metal foam cathode of 3000 μm-pore size and 15 wt.%-carbon black showed the highest cell specific capacity because the highest mass loading of active materials and the lightest weight of metal foam current collector. Cell specific capacities of the metal foam cathode of 3000 μm-pore size and 15 wt.%-carbon black were 84.8, 81.1, 78, 87, and 67.2 mAh g^{-1} at 4, 6, 8, 10, and 12 mA cm^{-2}, respectively. Therefore, metal foam cathode of 3000 μm-pore size and 15 wt.%-carbon black was found to be the most suitable to manufacture a light and high capacity battery.

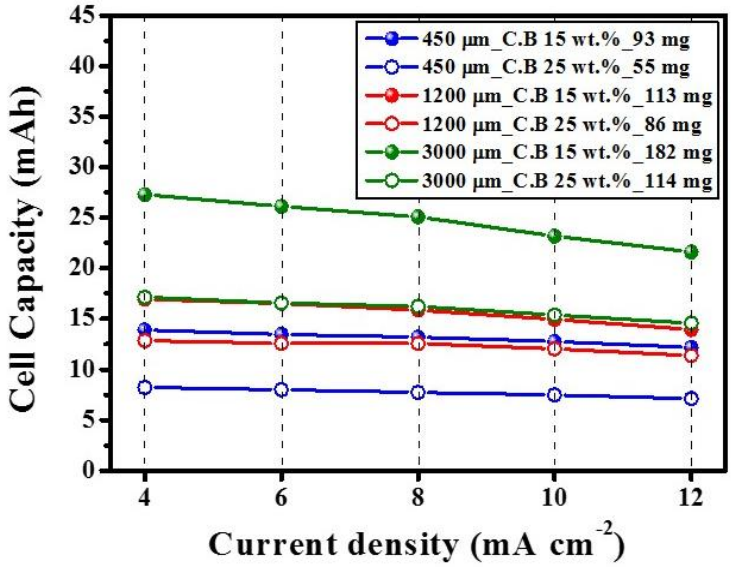

Figure 3.2.2.9 Comparison of the cell capacity (mAh) related to pore size and content of carbon black with an increased in current density.

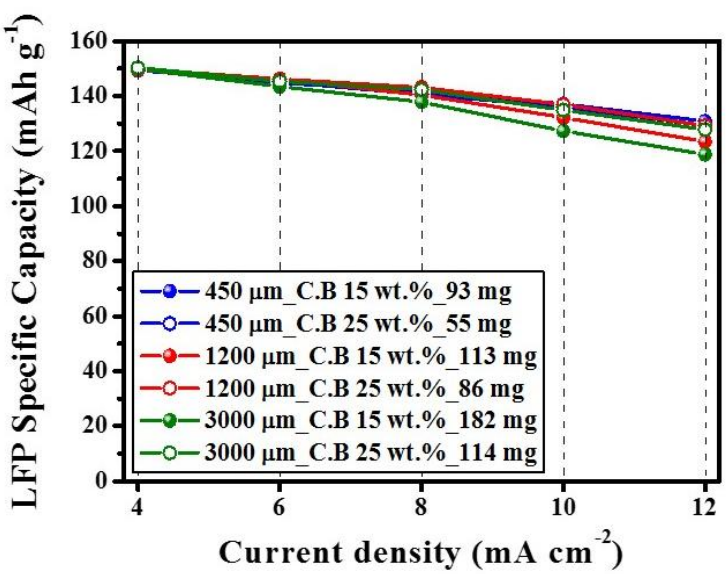

Figure 3.2.2.10 Comparison of the LFP specific capacity (mAh g^{-1}) related to pore size and content of carbon black with an increased in current density.

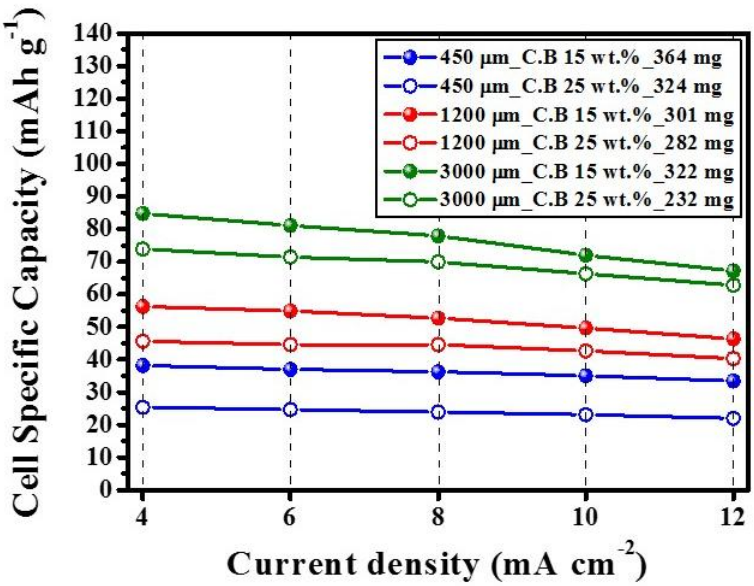

Figure 3.2.2.11 Comparison of the cell specific capacity (mAh g^{-1}) related to pore size and content of carbon black with an increased in current density.

3.3 Effect of metal foam cathode thickness

In this chapter, compare to the electrochemical performances related to thickness of metal foam cathodes and an amount of active material [97]. The electrode thickness and mass loading of active materials are significant factors for achieving high power and high specific energy for Li secondary batteries [97].

The metal foam cathodes were prepared using the NiCrAl metal foam with pore size of around 450 μm, thickness of 1600 μm, and porosity of 85 %. The metal foam thicknesses of 500, 1000, and 3000 μm, respectively, were prepared *via* mechanical polishing or bonding two metal foam (see Figure 3.3.1(a)-(c)). The mass of metal foam current collectors was 40, 80, and 240 mg cm^{-2} and the amount of $LiFePO_4$/C loaded into each of the electrodes was 28, 49, and 130 mg cm^{-2}, respectively. The analytical data such as thickness of metal foam cathodes and amount of active materials was listed in Table 3.3.1.

Table 3.3.1 Analytical data of metal foam cathodes with different thickness. (Pore size: 450 μm)

Pore size	Metal foam Thickness	Amount of Active material	Content of $LiFePO_4$/C	Content of Carbon black	Content of PVDF
450 μm	500 μm (0.5t)	28 mg cm^{-2}	75 %	15 %	10 %
	1000 μm (1t)	49 mg cm^{-2}			
	3000 μm (3t)	130 mg cm^{-2}			

Figure 3.3.2(a) shows the discharge curves at current density of 2 mA cm^{-2}. In the graph, there were almost no difference in discharge capacity and voltage in the plateau region (3.39 V). The plateau region was attributed to the coexistence of two phases ($LiFePO_4$ and $FePO_4$), with no change in the cell potential. Deviating from the plateau

region changed the composition from two phase to single phase, causing the voltage to rapidly increase or decrease. At the low current density, there is almost no difference in rate-performance regardless of electrode thickness, because there was no difference in the diffusion limitation of Li-ion. However, at discharge current density of 10 mA cm^{-2} (Figure 3.3.2(b)), metal foam cathode of 500 µm-thickness exhibited the highest voltage drop in the plateau region and the lowest discharge specific capacity (116 mAh g^{-1}), because it carried the highest current rate (2.4 C), due to the lowest mass loading of active material in the metal foam cathode. Whereas, metal foam cathode of 3000 µm-thickness showed the lowest voltage drop in the plateau region and the highest specific capacity (121 mAh g^{-1}), because it carried the lowest current rate (0.5 C). Figure 3.3.3 shows the cell capacity (mAh) obtained from the various discharge current density. Analysis indicated that 3000 µm-thickness showed the highest cell capacity, followed by 1000 and 500 µm-thickness. Cell capacities of 3000 µm-thickness were 19.6, 19, 17.7, 17.1, and 15.7 mAh for the 2, 4, 6, 8, and 10 mA cm^{-2}, respectively. Whereas, 500 µm-thickness showed the lowest cell capacity with 4.1, 4, 3.7, 3.5, and 3.2 mAh because the lowest amount of $LiFePO_4$/C was loaded. Figure 3.3.4 shows the LFP specific capacity (mAh g^{-1}). In the graph, there were almost similar LFP specific capacity and rate performance. Capacity retention rate was 78, 79, and 81 %, for the 500, 1000, and 3000 µm-thickness, respectively. That is, the thick metal foam cathodes are electrochemically more stable than the thin metal foam cathodes. Figure 3.3.5 shows the cyclic voltammetry curves at a 0.1 mV S^{-1} scan rate using different thickness of metal foam cathodes and mass of active material. The midpoint of the oxidation and reduction peaks is about 3.43 V, which corresponds to the open-circuit voltage (OCV) of $LiFePO_4$. According to the CV curve results, voltage of redox peaks occurs much earlier for the thinner electrode. For example, the

oxidation peak and reduction peak of 500 μm-thickness metal foam cathode occur at 3.59 and 3.28 V, respectively, whereas those of 3000 μm-thickness metal foam cathodes occur at 3.78 and 3.19 V, respectively. Additionally, the oxidation and reduction current intensity also exhibit much higher for the thinner electrode. Figure 3.3.6 shows Nyquist plots of electrochemical impedance spectroscopy (EIS) of the metal foam cathodes using different thickness, where R_b is the bulk resistance of the cell, and R_{ct} is the Li-ion charge transfer resistance at the electrode/electrolyte interface, which mostly determines the internal cell resistance. C_{dl} is the double-layer capacitance, and Z_w is the Warburg impedance related to the diffusion behavior of Li-ions in the active material [89]. The inset of Figure 3.3.6 shows the AC impedance spectra analyzed using the equivalent circuit. According to the EIS results, there was almost no difference in the R_b (3 Ω) and R_{ct} (10 Ω).

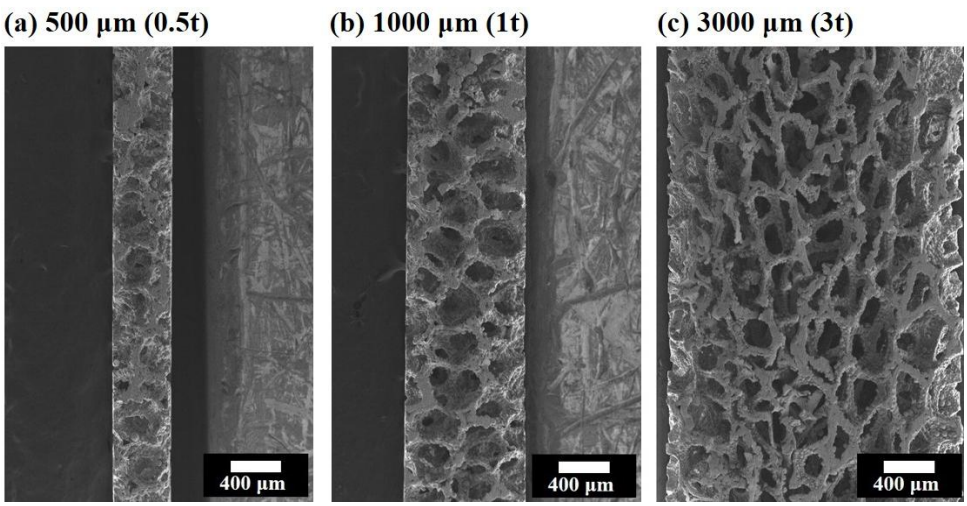

Figure 3.3.1 SEM images of NiCrAl metal foam current collector. The cross-section of (a) 500 μm-thickness, (b) 1000 μm-thickness, and (c) 3000 μm-thickness.

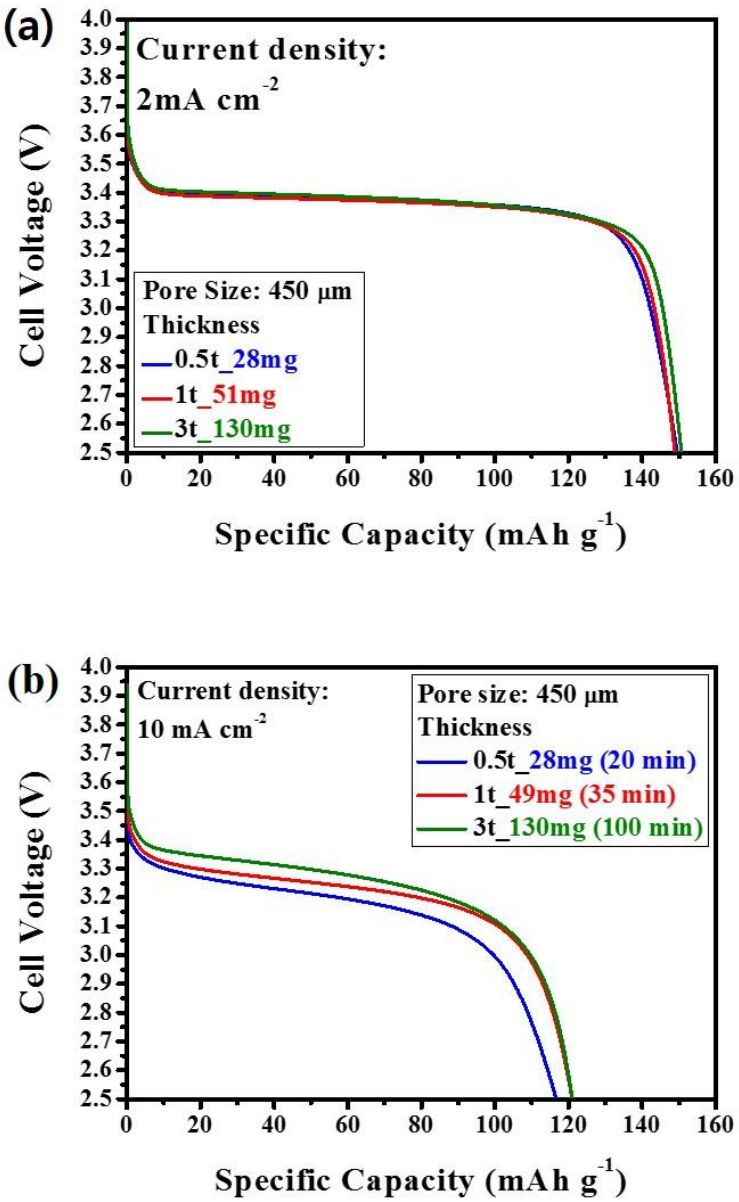

Figure 3.3.2 Comparison of the discharge curves related to thickness of metal foam cathodes at current density of (a) 2 mA cm^{-2} and (b) 10 mA cm^{-2}. (Pore size: 450 µm)

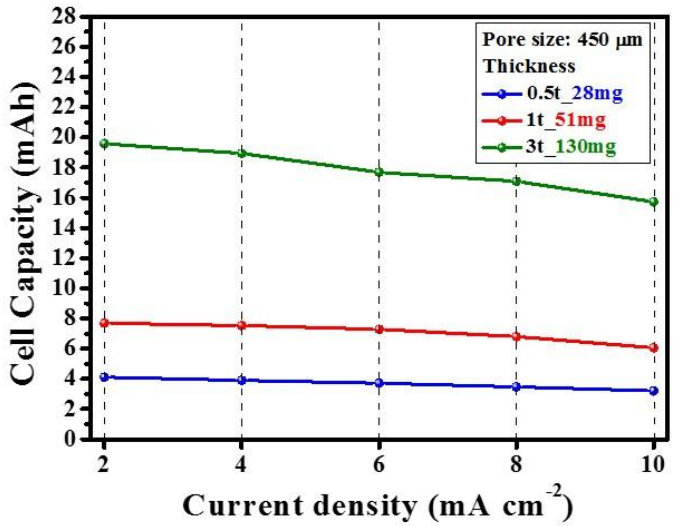

Figure 3.3.3 Comparison of the cell capacity (mAh) related to thickness of metal foam cathodes with an increased in current density. (Pore size: 450 µm)

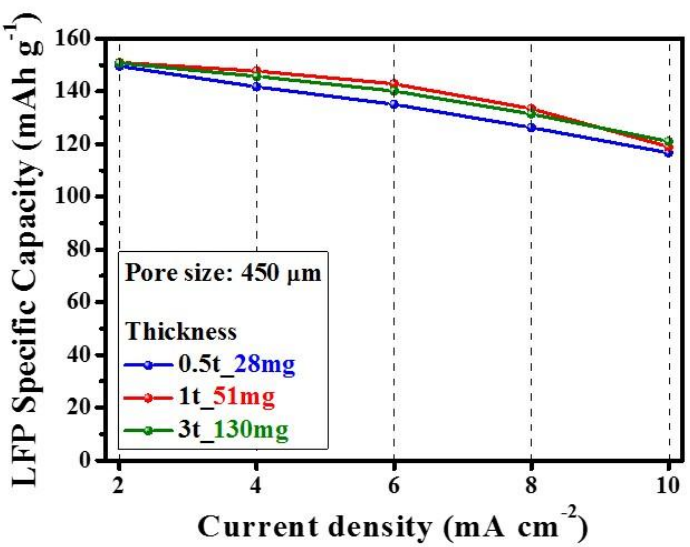

Figure 3.3.4 Comparison of the LFP specific capacity (mAh g^{-1}) related to thickness of metal foam cathodes with an increased in current density. (Pore size: 450 µm)

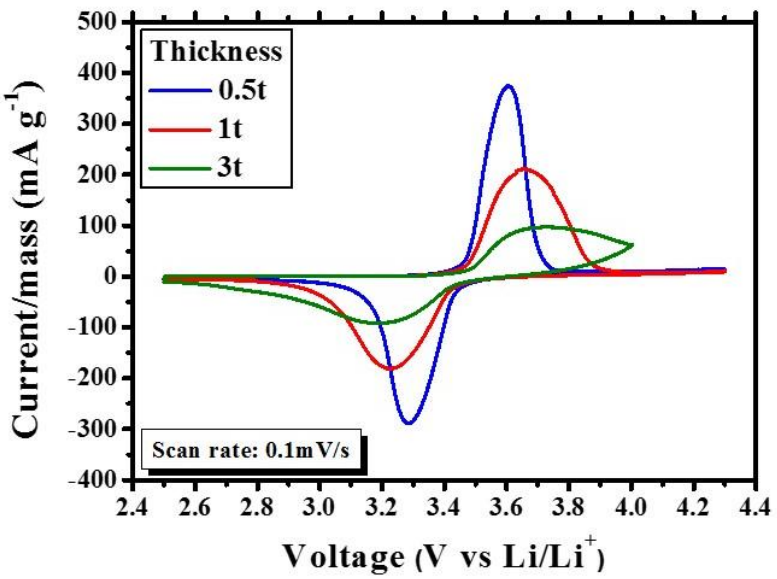

Figure 3.3.5 Cyclic voltammetry curves related to thickness of metal foam cathodes at scan rate of 0.1mV S^{-1}. (Pore size: 450 µm)

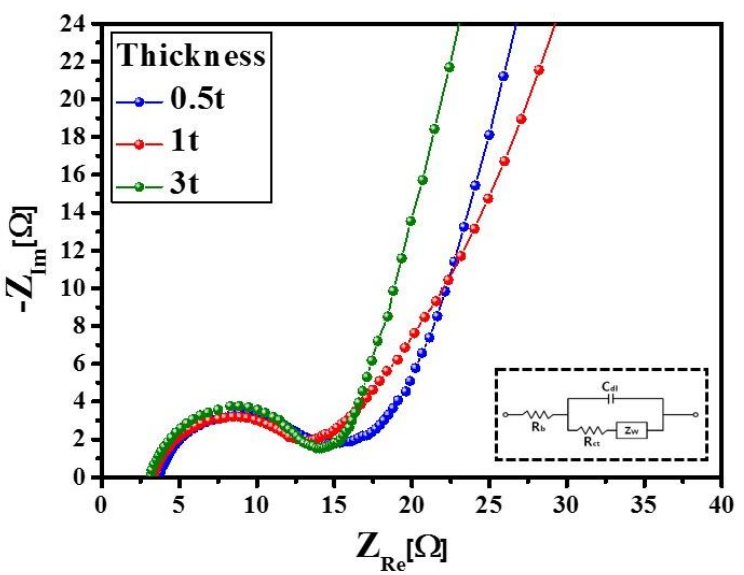

Figure 3.3.6 Nyquist plots of electrochemical impedance spectroscopy obtained from different thickness at open circuit voltage (OCV) 3.43 V. (Pore size: 450 µm)

The next experimental, the metal foam cathodes were prepared using the NiCrAl metal foam with pore size of around 1200 µm, thickness of 3000 µm, and porosity of 90 %. The metal foam thicknesses of 1000 and 3000 µm, respectively, were prepared *via* mechanical polishing. The amount of $LiFePO_4$/C loaded into each of the electrodes was 64 and 145 mg cm^{-2}, respectively. The analytical data such as thickness of metal foam cathodes and amount of active materials was listed in Table 3.3.2.

Table 3.3.2 Analytical data of metal foam cathodes with different thickness. (Pore size: 1200 µm)

Pore size	Metal foam Thickness	Amount of Active material	Content of $LiFePO_4$/C	Content of Carbon black	Content of PVDF
1200 µm	1000 µm (1t)	64 mg cm^{-2}	75 %	15 %	10 %
	3000 µm (3t)	145 mg cm^{-2}			

Figure 3.3.7(a) shows the discharge curves at current density of 2 mA cm^{-2}. In the graph, there were almost no difference in discharge capacity and voltage in the plateau region (3.37 V). However, at discharge current density of 10 mA cm^{-2} (Figure 3.3.7(b)), metal foam cathode of 1000 µm-thickness exhibited higher voltage drop in the plateau region and lower discharge specific capacity (110 mAh g^{-1}) than metal foam cathode of 3000 µm-thickness due to the lowest mass loading of active material in the metal foam cathode. Whereas, metal foam cathode of 3000 µm-thickness showed the low voltage drop in the plateau region and high specific capacity (128 mAh g^{-1}). Figure 3.3.8 shows the cell capacity (mAh) obtained from the various discharge current density. In the graph, 3000 µm-thickness showed higher cell capacity than 1000 µm-thickness. Cell capacities of 3000 µm-thickness were 21.8, 21.2, 18.4, 14.8, and 11.7 mAh for the 2, 5, 10, 15, and 20 mA cm^{-2}, respectively. Whereas, 1000 µm-thickness showed the lowest

cell capacity with 9.6, 8.9, 7.1, 5.5, and 4.3 mAh because the lowest amount of $LiFePO_4$/C was loaded. Figure 3.3.9 shows the LFP specific capacity (mAh g^{-1}). In the graph, 3000 μm-thickness showed higher specific capacity than 1000 μm-thickness. Capacity retention rate was 45 and 54 % for the 1000 and 3000 μm-thickness, respectively. That is, the thick metal foam cathodes are electrochemically more stable than the thin metal foam cathodes.

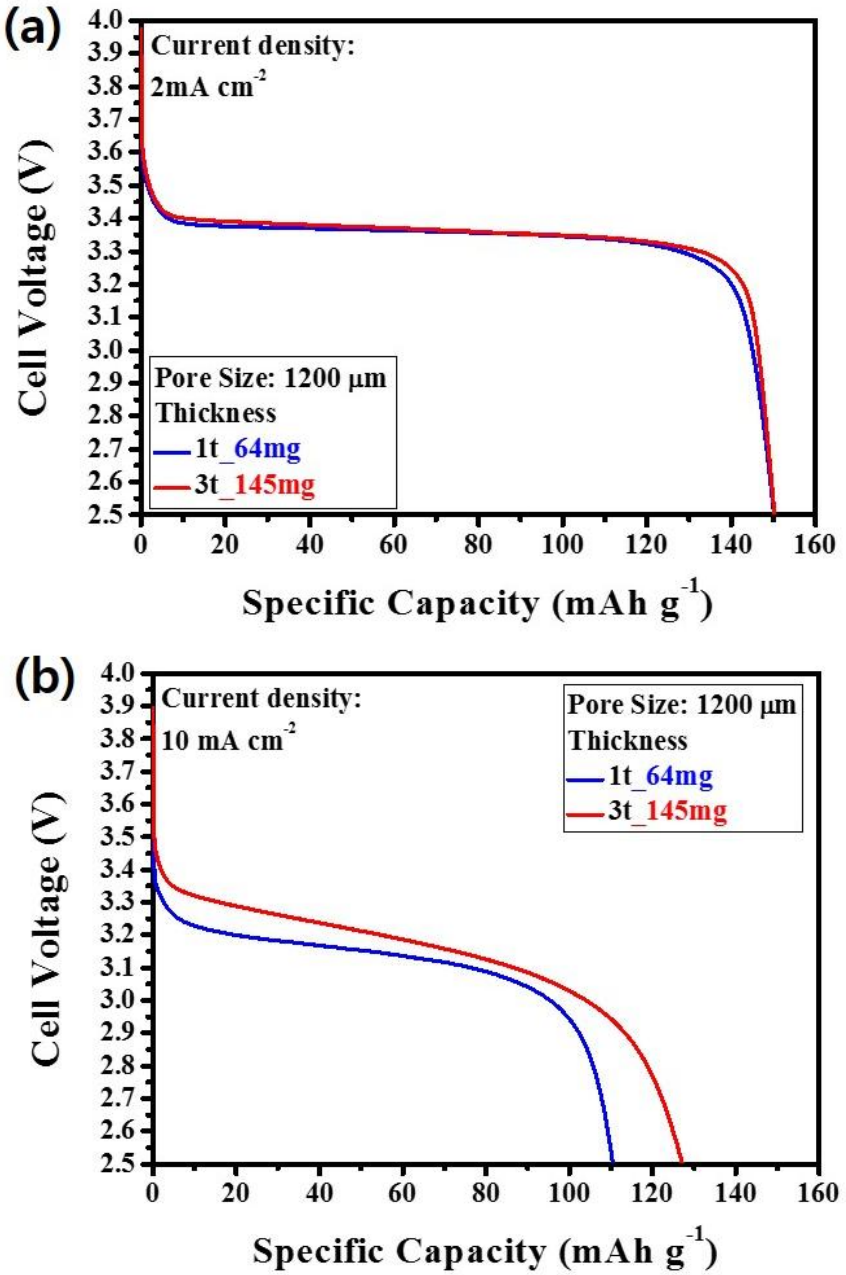

Figure 3.3.7 Comparison of the discharge curves related to thickness of metal foam cathodes at current density of (a) 2 mA cm^{-2} and (b) 10 mA cm^{-2}. (Pore size: 1200 µm)

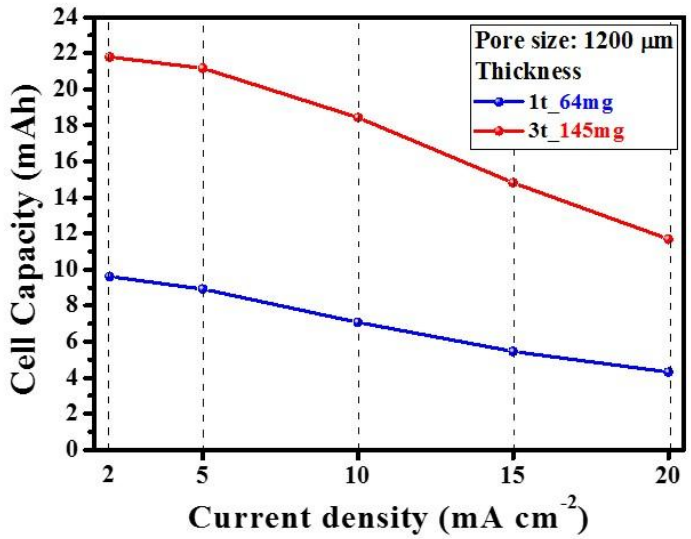

Figure 3.3.8 Comparison of the cell capacity (mAh) related to thickness of metal foam cathodes with an increased in current density. (Pore size: 1200 µm)

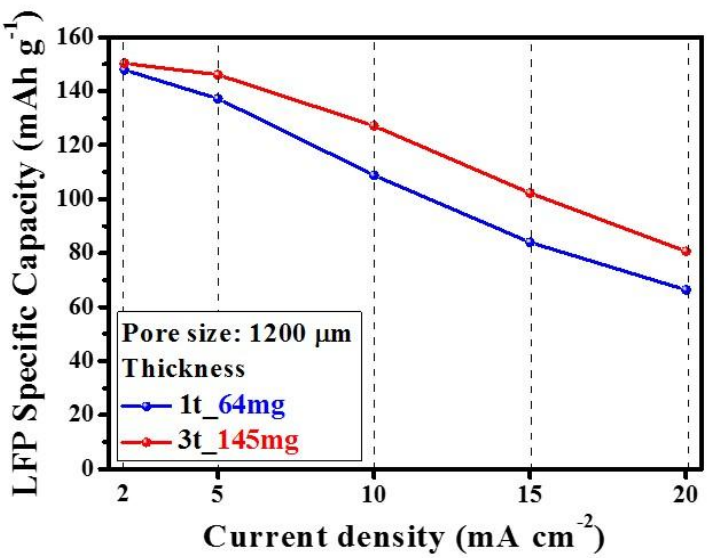

Figure 3.3.9 Comparison of the LFP specific capacity (mAh g^{-1}) related to thickness of metal foam cathodes with an increased in current density. (Pore size: 1200 µm)

The following experimental, the metal foam cathodes were prepared using the NiCrAl metal foam with pore size of around 3000 μm, thickness of 5000 μm, and porosity of 94 %. The metal foam thicknesses of 1500, 3000 and 5000 μm, respectively, were prepared *via* mechanical polishing. The amount of $LiFePO_4$/C loaded into each of the metal foam cathodes was 81, 170, and 230 mg cm^{-2}, respectively. The analytical data such as thickness of metal foam cathodes and amount of active materials was listed in Table 3.3.3.

Table 3.3.3 Analytical data of metal foam cathodes with different thickness. (Pore size: 3000 μm)

Pore size	Metal foam Thickness	Amount of Active material	Content of $LiFePO_4$/C	Content of Carbon black	Content of PVDF
3000 μm	1500 μm (1.5t)	81 mg cm^{-2}	75 %	15 %	10 %
	3000 μm (3t)	170 mg cm^{-2}			
	5000 μm (5t)	230 mg cm^{-2}			

Figure 3.3.10(a) shows the discharge curves at current density of 4 mA cm^{-2}. In the graph, there were almost no difference in discharge capacity and voltage in the plateau region. However, at discharge current density of 20 mA cm^{-2} (Figure 3.3.10(b)), metal foam cathode of 1500 μm-thickness exhibited the highest voltage drop in the plateau region and the lowest discharge specific capacity (77 mAh g^{-1}), due to the lowest mass loading of active material in the metal foam cathode. Whereas, metal foam cathode of 5000 μm-thickness showed the lowest voltage drop in the plateau region and the highest specific capacity (112 mAh g^{-1}), because it carried the lowest current rate. Figure 3.3.11 shows the cell capacity (mAh) obtained from the various discharge current density. Analysis indicated that 5000 μm-thickness showed the highest cell capacity, followed

by 3000 and 1500 μm-thickness. Cell capacities of 5000 μm-thickness were 34.6, 33.9, 32.9, 30.6, 29.8, and 25.6 mAh for the 4, 6, 8, 10, 12, and 20 mA cm^{-2}, respectively. Whereas, 1500 μm-thickness showed the lowest cell capacity with 12.1, 11.2, 10.8, 9.6, 8.6, and 6.2 mAh because the lowest amount of $LiFePO_4$/C was loaded. Figure 3.3.12 shows the LFP specific capacity (mAh g^{-1}). In the graph, there were almost similar LFP specific capacity and rate performance. Capacity retention rate was 51, 65, and 74 %, for the 1500, 3000, and 5000 μm-thickness, respectively.

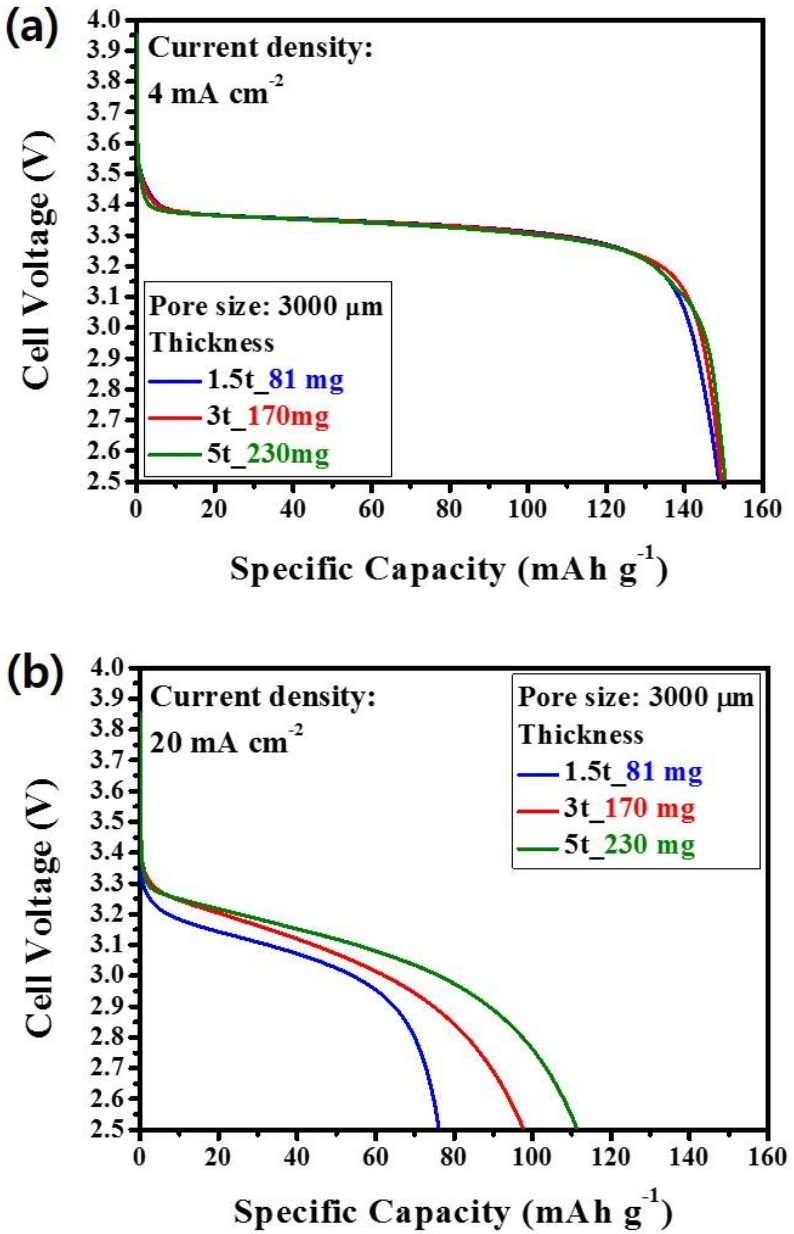

Figure 3.3.10 Comparison of the discharge curves related to thickness of metal foam cathodes at current density of (a) 4 mA cm^{-2} and (b) 20 mA cm^{-2}. (Pore size: 3000 μm)

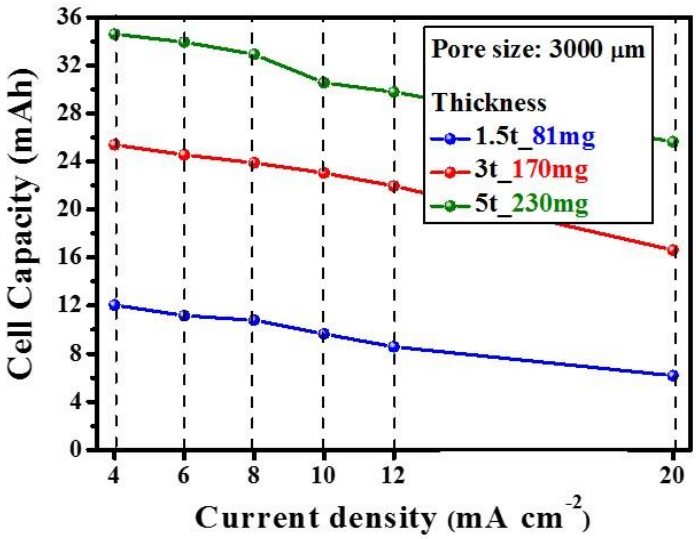

Figure 3.3.11 Comparison of the cell capacity (mAh) related to thickness of metal foam cathodes with an increased in current density. (Pore size: 3000 µm)

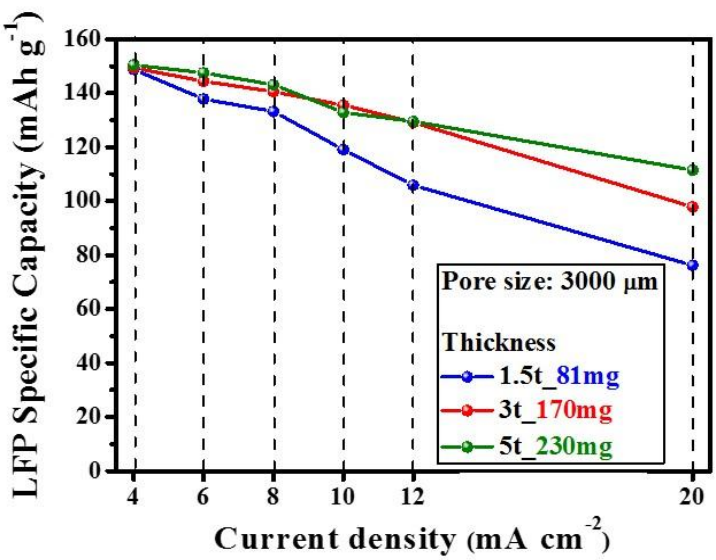

Figure 3.3.12 Comparison of the LFP specific capacity (mAh g^{-1}) related to thickness of metal foam cathodes with an increased in current density. (Pore size: 3000 µm)

3.4 Effect of Cell designs

In this part, we compared the electrochemical performances of the Li anode when placed on both and single side of the metal foam cathode as shown in Figure 3.4.1. First experiment was used metal foam cathode of 450 μm-pore size and 1000 μm-thickness. Figure 3.4.2(a) shows specific capacity (mAh g^{-1}) obtained from the various discharge current (mA). In the graph, both sides cell showed higher specific capacity than single side cell. Because the both sides cell has wider surface area of redox reaction than single side cell. However, at low current, there were almost similar specific capacity. Specific capacities of both sides cell were 150, 145.7, 132.5, 107.2, 85.5, and 70 mAh g^{-1} for the 2, 4, 8, 10, 15, and 20 mA, respectively. Whereas, single side cell was 142.2, 137.8, 125.6, 100.6, 74.4, and 40.3 mAh g^{-1}, respectively. In addition, Figure 3.4.2(b) shows the discharge curves at current of 4 mA. In the graph, both sides cell exhibited lower voltage drop in the plateau region and higher specific capacity (145.7 mAh g^{-1}) than single side cell. Figure 3.4.3 shows the cyclic voltammetry curves at a scan rate of 0.1 mV S^{-1}. In the graph, voltage of redox peaks occurs much earlier for the both sides cell. For example, the oxidation and reduction peak of both sides cell occur at 3.64 and 3.23 V, respectively, whereas those of single side cell occur at 3.72 and 3.17 V, respectively. In addition, the oxidation and reduction current intensity also exhibit much higher for the both sides cell than single side cell. Figure 3.4.4 shows Nyquist plots of electrochemical impedance spectroscopy (EIS). In the graph, R_b and R_{ct} significantly decreased with both sides cell due to wider surface area of redox reaction than single side cell. For instance, R_b and R_{ct} of both sides cell was 7 Ω and 8 Ω, respectively, whereas single side cell was 10 Ω and 20 Ω, respectively. Figure 3.4.5(a) shows specific capacity (mAh g^{-1}) obtained from the various discharge current density (mA cm^{-2}). Current density was applied a twice

current to a battery in which lithium metal placed on both sides of a metal foam cathode. In the graph, single side cell showed higher specific capacity than both sides cell. This is because even if lithium placed only on single side, the redox reaction also occurs on the opposite side of metal foam cathode. However, at low current, there were almost similar specific capacity. Specific capacities of single side cell according to current density were 142.2, 137.8, 125.6, and 100.6 mAh g^{-1} for the 2, 4, 8, and 10 mA cm^{-2}, respectively. Whereas, both sides cell was 144.9, 132.5, 85.5, and 69.6 mAh g^{-1}, respectively. In addition, Figure 3.4.2(b) shows the discharge curves at current of 4 mA cm^{-2}. In the graph, single side cell exhibited lower voltage drop in the plateau region and higher specific capacity (137.8 mAh g^{-1}) than both sides cell.

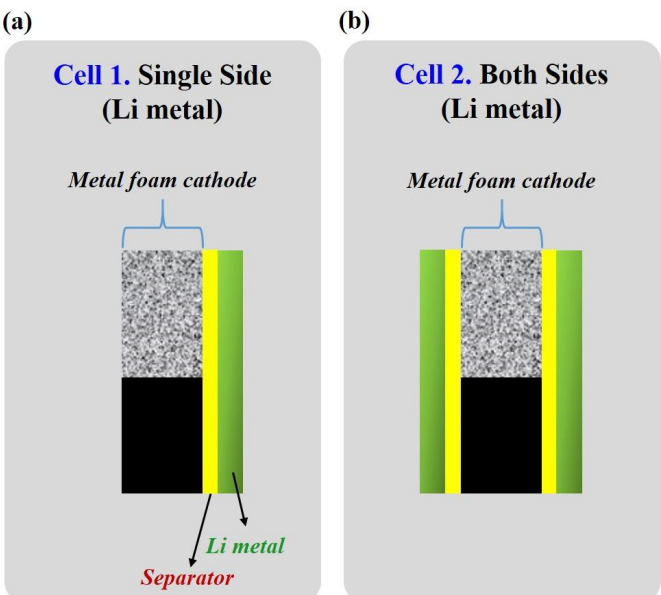

Figure 3.4.1 Schematic view of placement of electrodes; Li metal is placed at (a) single side and (b) both sides of metal foam cathode

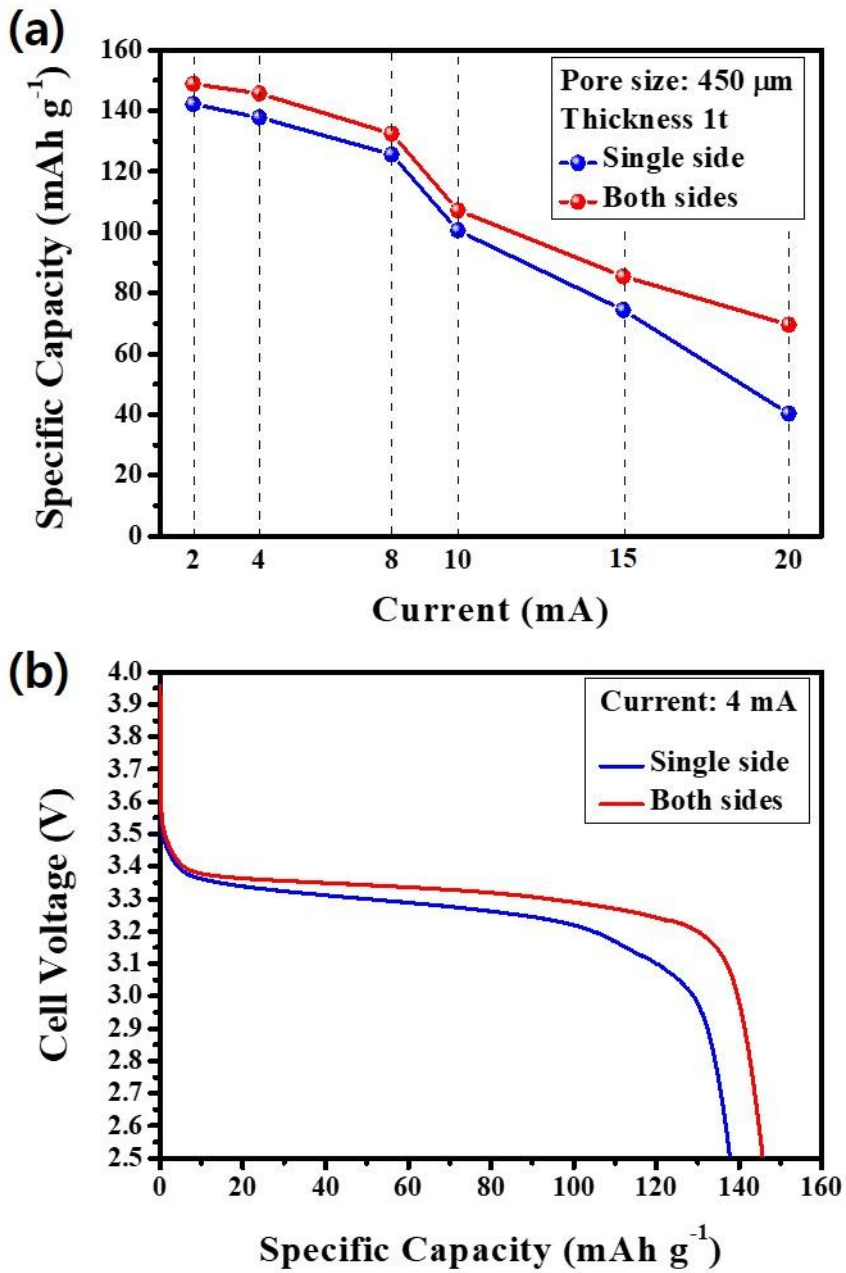

Figure 3.4.2 Comparison of (a) the specific capacity (mAh g^{-1}) with an increased in current (mA) and (b) the discharge curves at 4 mA, when Li anode placed on single and both sides of the metal foam cathodes. (Metal foam cathode of 450 μm-pore size and 1000 μm-thickness)

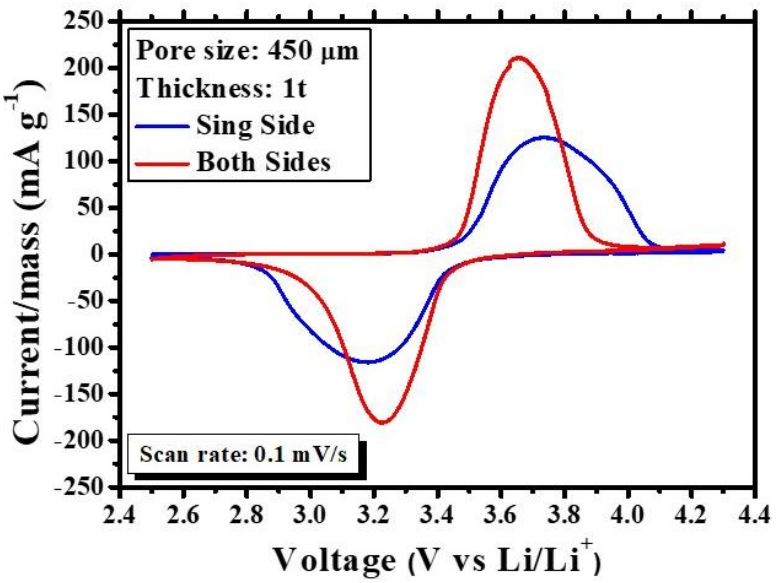

Figure 3.4.3 Cyclic voltammetry curves at scan rate of 0.1mV S^{-1}. (Metal foam cathode of 450 µm-pore size and 1000 µm-thickness)

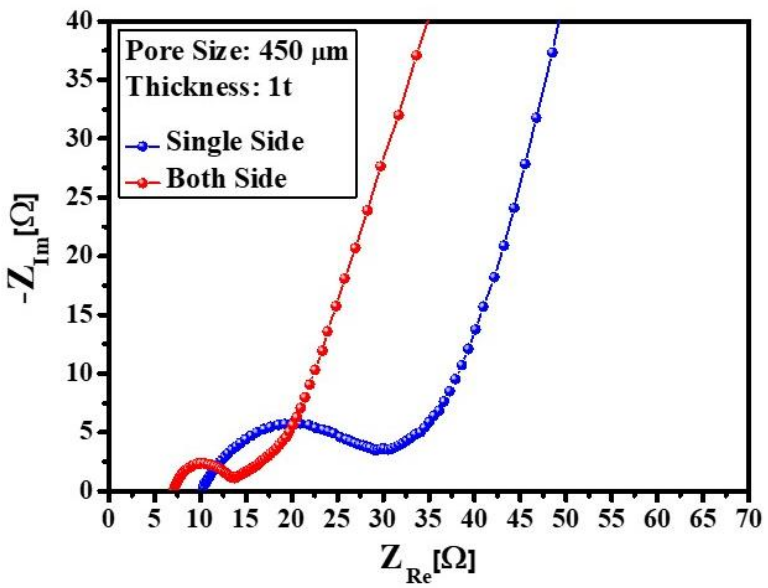

Figure 3.4.4 Nyquist plots of electrochemical impedance spectroscopy obtained from open circuit voltage (OCV) 3.43 V. (Metal foam cathode of 450 µm-pore size and 1000 µm-thickness)

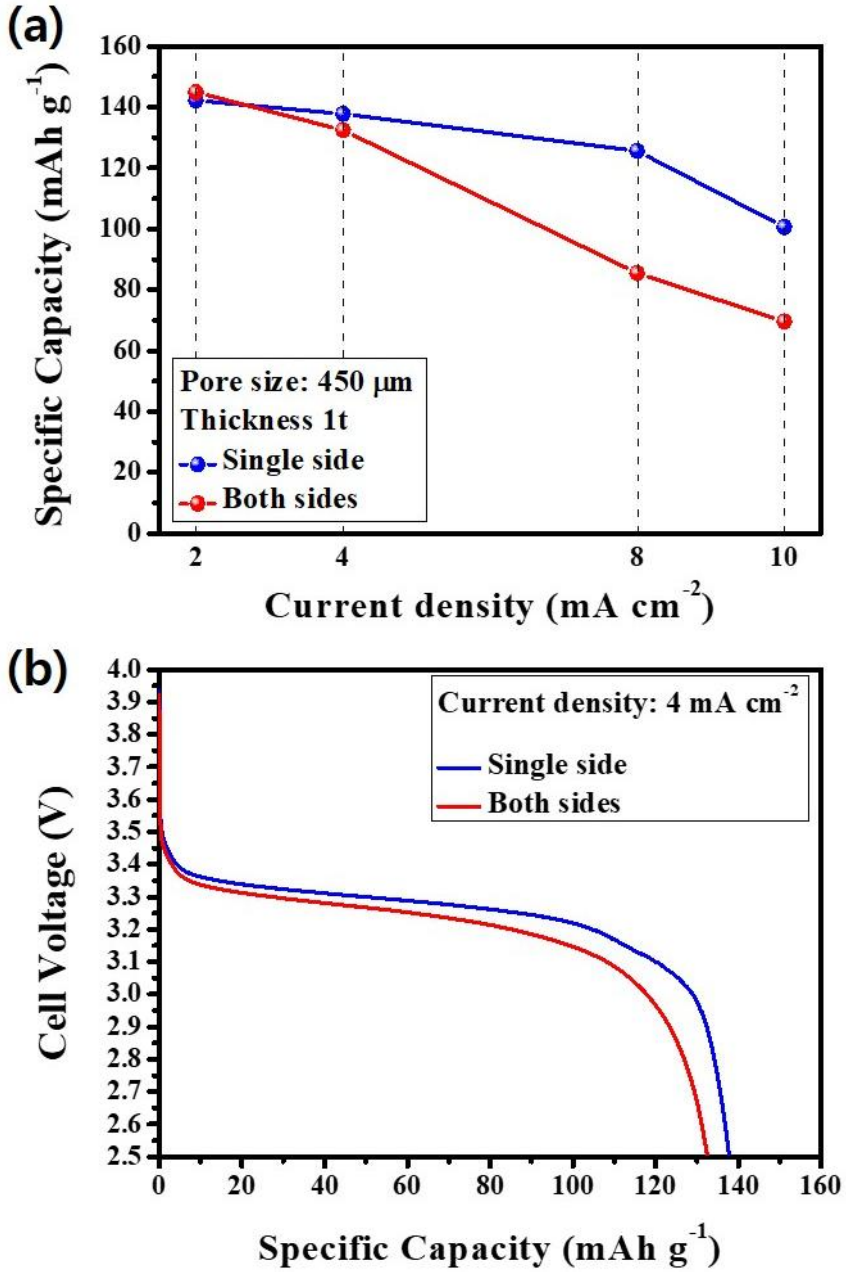

Figure 3.4.5 Comparison of (a) the specific capacity (mAh g^{-1}) with an increased in current density (mA cm^{-2}) and (b) the discharge curves at 4 mA cm^{-2}, when Li anode placed on single and both sides of the metal foam cathodes. (Metal foam cathode of 450 μm-pore size and 1000 μm-thickness)

The following experiment was used metal foam cathode of 450 μm-pore size and 3000 μm-thickness. Figure 3.4.6(a) shows specific capacity (mAh g^{-1}) obtained from the various discharge current (mA). In the graph, both sides cell also showed higher specific capacity than single side cell. Because the both sides cell has wider surface area of redox reaction than single side cell. However, at low current, there were almost similar specific capacity. Specific capacities of both sides cell were 150.7, 145.9, 136.1, 131.4, 121.1, 111.7, 99.1, and 88.2 mAh g^{-1} for the 2, 4, 6, 8, 10, 12, 16, and 20 mA, respectively. Whereas, single side cell was 148.6, 143.9, 133.7, 128.3, 118.1, 108.6, 90.5, and 71.5 mAh g^{-1}, respectively. In addition, Figure 3.4.6(b) shows the discharge curves at current of 6 mA. In the graph, both sides cell exhibited lower voltage drop in the plateau region and higher specific capacity (136.1 mAh g^{-1}) than single side cell. Figure 3.4.7(a) shows specific capacity (mAh g^{-1}) obtained from the various discharge current density (mA cm^{-2}). Current density was applied a twice current to a battery in which lithium metal placed on both sides of a metal foam cathode. In the graph, single side cell showed higher specific capacity than both sides cell. This is because even if lithium placed only on single side, the redox reaction also occurs on the opposite side of metal foam cathode. However, at 2mA cm^{-2}, there were almost similar specific capacity. Specific capacities of single side cell according to current density were 148.6, 143.9, 133.7, 128.3 and 118.1 mAh g^{-1} for the 2, 4, 6, 8, and 10 mA cm^{-2}, respectively. Whereas, both sides cell was 145.9, 131.4, 111.7, 99.1, and 88.2 mAh g^{-1}, respectively. In addition, Figure 3.4.2(b) shows the discharge curves at current of 6 mA cm^{-2}. In the graph, single side cell exhibited lower voltage drop in the plateau region and higher specific capacity (133.7 mAh g^{-1}) than both sides cell.

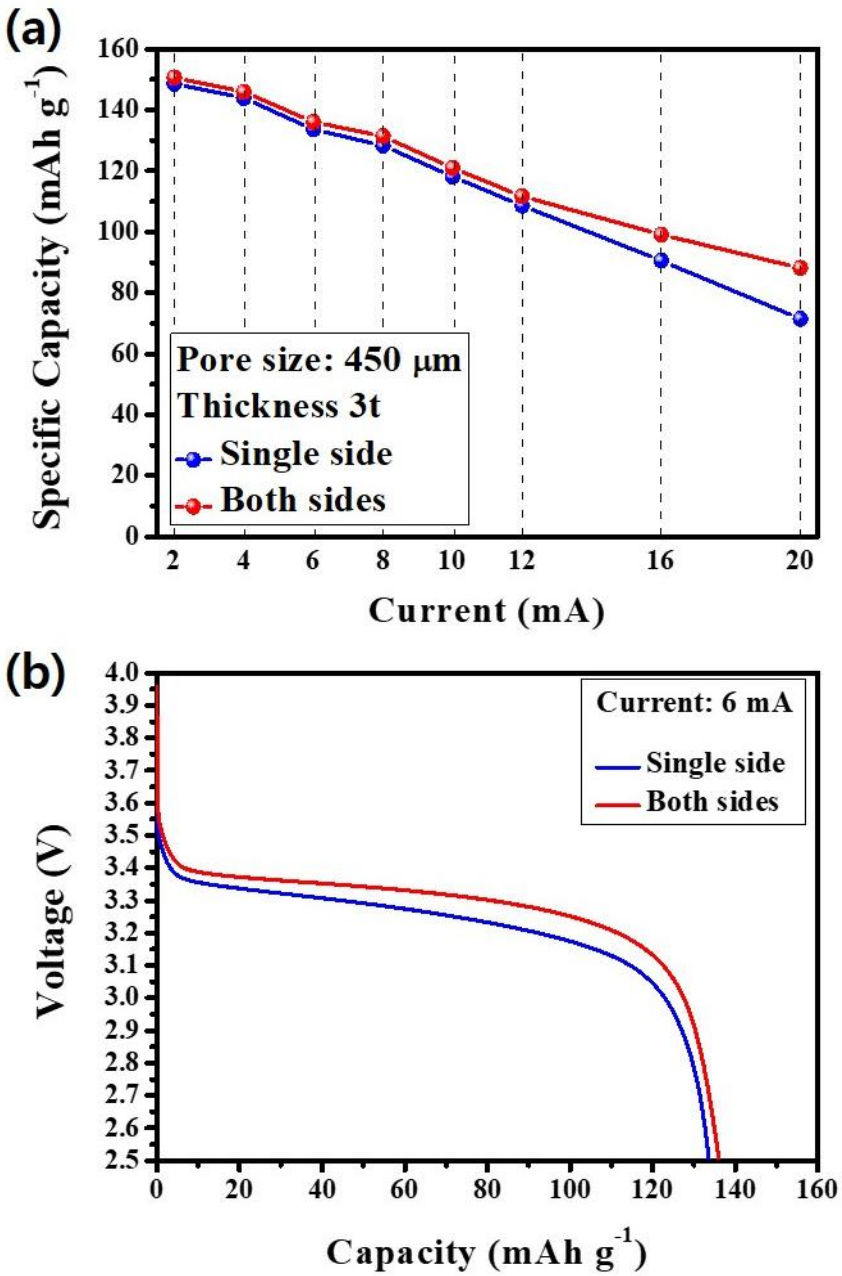

Figure 3.4.6 Comparison of (a) the specific capacity (mAh g^{-1}) with an increased in current (mA) and (b) the discharge curves at 6 mA, when Li anode placed on single and both sides of the metal foam cathodes. (Metal foam cathode of 450 µm-pore size and 3000 µm-thickness)

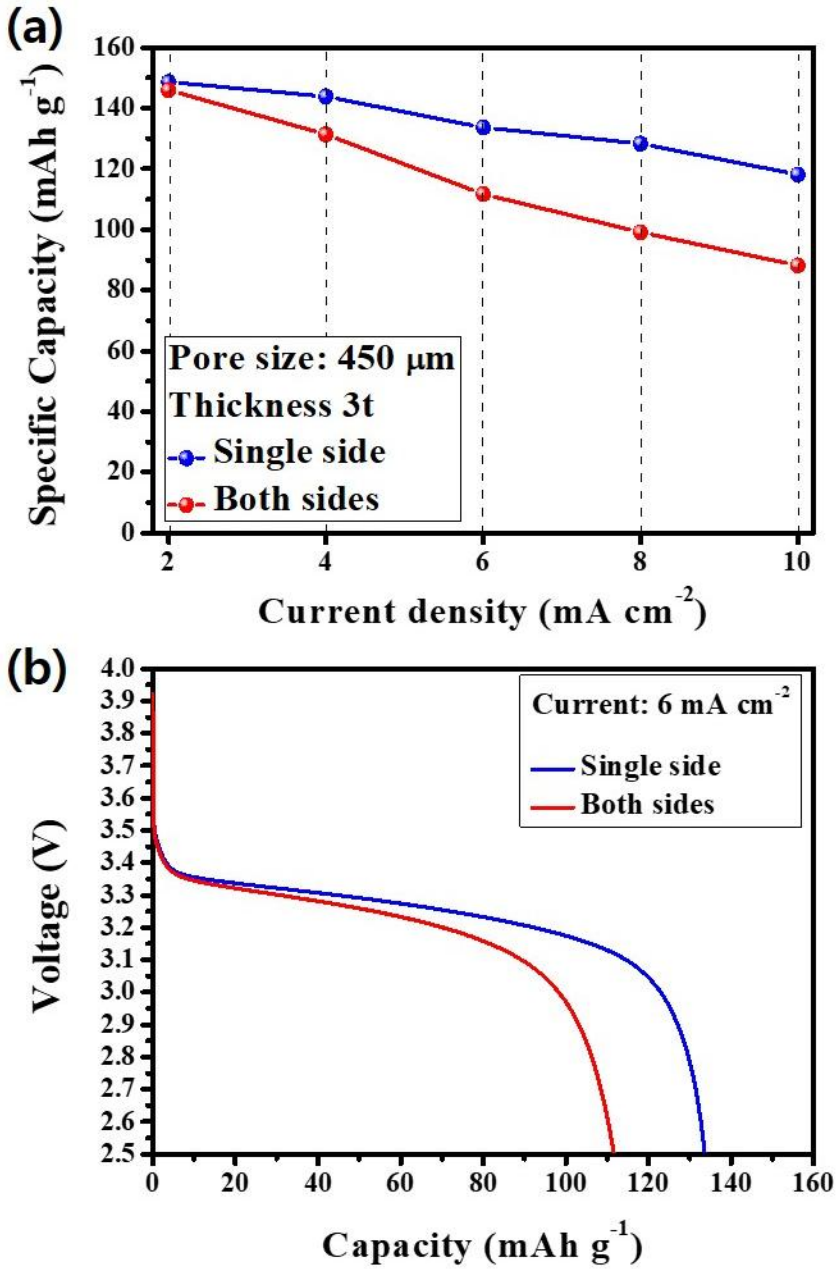

Figure 3.4.7 Comparison of (a) the specific capacity (mAh g^{-1}) with an increased in current density (mA cm^{-2}) and (b) the discharge curves at 6 mA cm^{-2}, when Li anode is placed on single and both sides of the metal foam cathodes. (Metal foam cathode of 450 µm-pore size and 3000 µm-thickness)

The following experiment was used metal foam cathode of 1200 μm-pore size and 3000 μm-thickness. Figure 3.4.8(a) shows specific capacity (mAh g^{-1}) obtained from the various discharge current (mA). In the graph, both sides cell showed higher specific capacity than single side cell. Because the both sides cell has wider surface area of redox reaction than single side cell. However, at low current, there were almost similar specific capacity. Specific capacities of both sides cell were 150.3, 149, 146.1, 139.4, 127.1, 102.2, and 80.6 mAh g^{-1} for the 2, 4, 5, 8, 10, 15, and 20 mA, respectively. Whereas, single side cell was 149.3, 145.6, 135, 118.9, 114, 73.2, and 47.7 mAh g^{-1}, respectively. In addition, Figure 3.4.8(b) shows the discharge curves at current of 5 mA. In the graph, both sides cell exhibited lower voltage drop in the plateau region and higher specific capacity (146.1 mAh g^{-1}) than single side cell. Figure 3.4.9 shows the cyclic voltammetry curves at a scan rate of 0.1 mV S^{-1}. In the graph, voltage of redox peaks occurs much earlier for the both sides cell. For example, the oxidation and reduction peak of both sides cell occur at 3.65 and 3.23 V, respectively, whereas those of single side cell occur at 3.73 and 3.14 V, respectively. In addition, the oxidation and reduction current intensity also exhibit much higher for the both sides cell than single side cell. Figure 3.4.10 shows Nyquist plots of electrochemical impedance spectroscopy (EIS). In the graph, R_b and R_{ct} significantly decreased with both sides cell due to wider surface area of redox reaction than single side cell. For instance, R_b and R_{ct} of both sides cell was 5 Ω and 16 Ω, respectively, whereas single side cell was 9 Ω and 31 Ω, respectively. Figure 3.4.11(a) shows specific capacity (mAh g^{-1}) obtained from the various discharge current density (mA cm^{-2}). In the graph, single side cell showed higher specific capacity than both sides cell. Specific capacities of single side cell according to current density were 149.3, 145.6, 135, and 114 mAh g^{-1} for the 2, 4, 5, and 10 mA cm^{-2}, respectively. Whereas, both sides cell was 149, 139.4, 127.1, and

80.6 mAh g^{-1}, respectively. In addition, Figure 3.4.11(b) shows the discharge curves at current of 5 mA cm^{-2}. In the graph, single side cell exhibited lower voltage drop in the plateau region and higher specific capacity (135 mAh g^{-1}) than both sides cell.

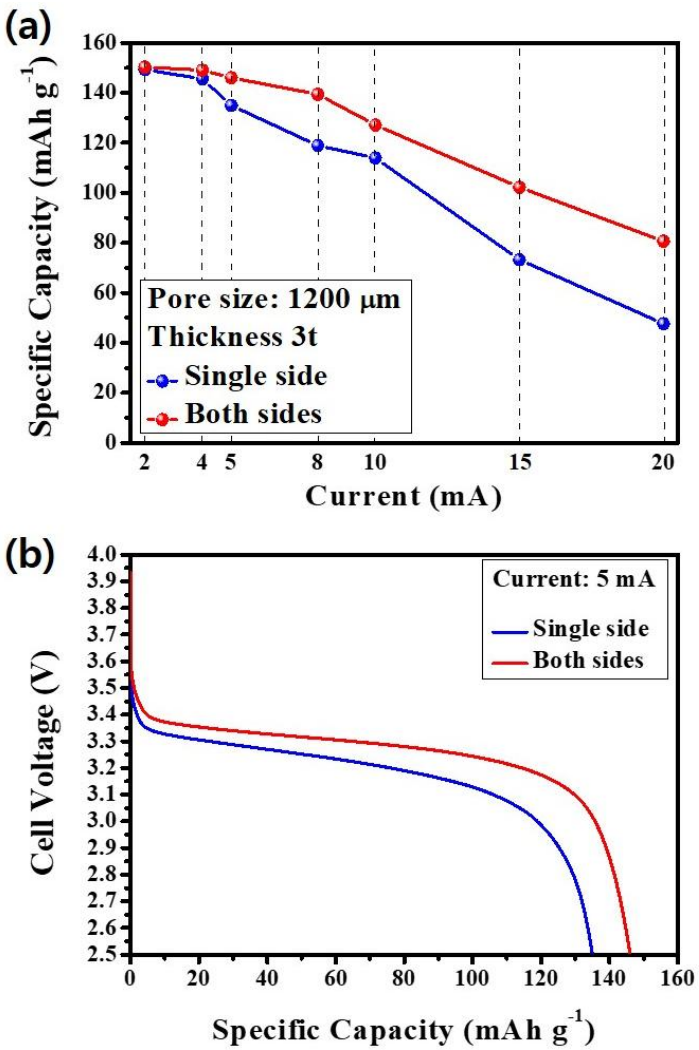

Figure 3.4.8 Comparison of (a) the specific capacity (mAh g^{-1}) with an increased in current (mA) and (b) the discharge curves at 5 mA, when Li anode placed on single and both sides of the metal foam cathodes. (Metal foam cathode of 1200 µm-pore size and 3000 µm-thickness)

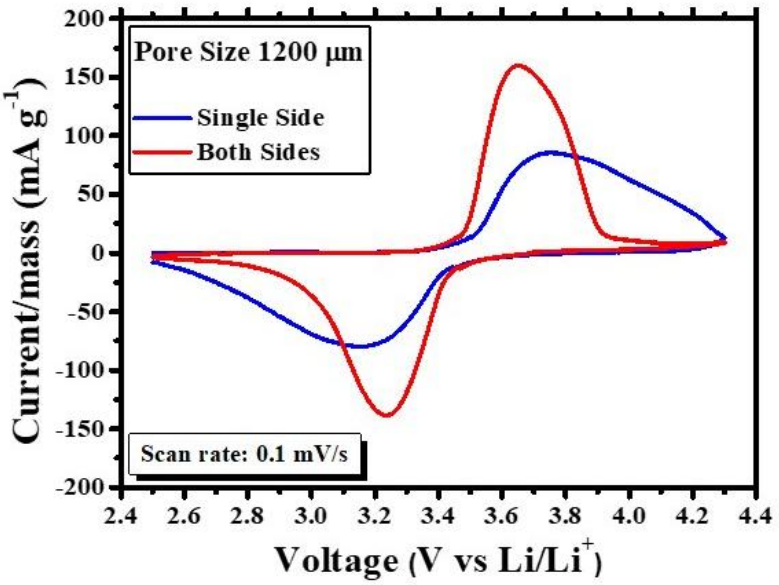

Figure 3.4.9 Cyclic voltammetry curves at scan rate of 0.1mV S^{-1}. (Metal foam cathode of 1200 µm-pore size)

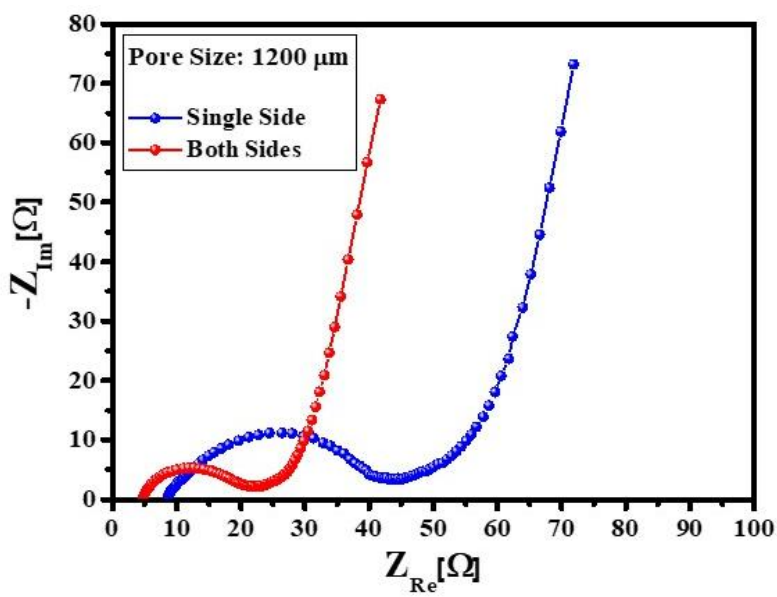

Figure 3.4.10 Nyquist plots of electrochemical impedance spectroscopy obtained from open circuit voltage (OCV) 3.43 V. (Metal foam cathode of 1200 µm-pore size)

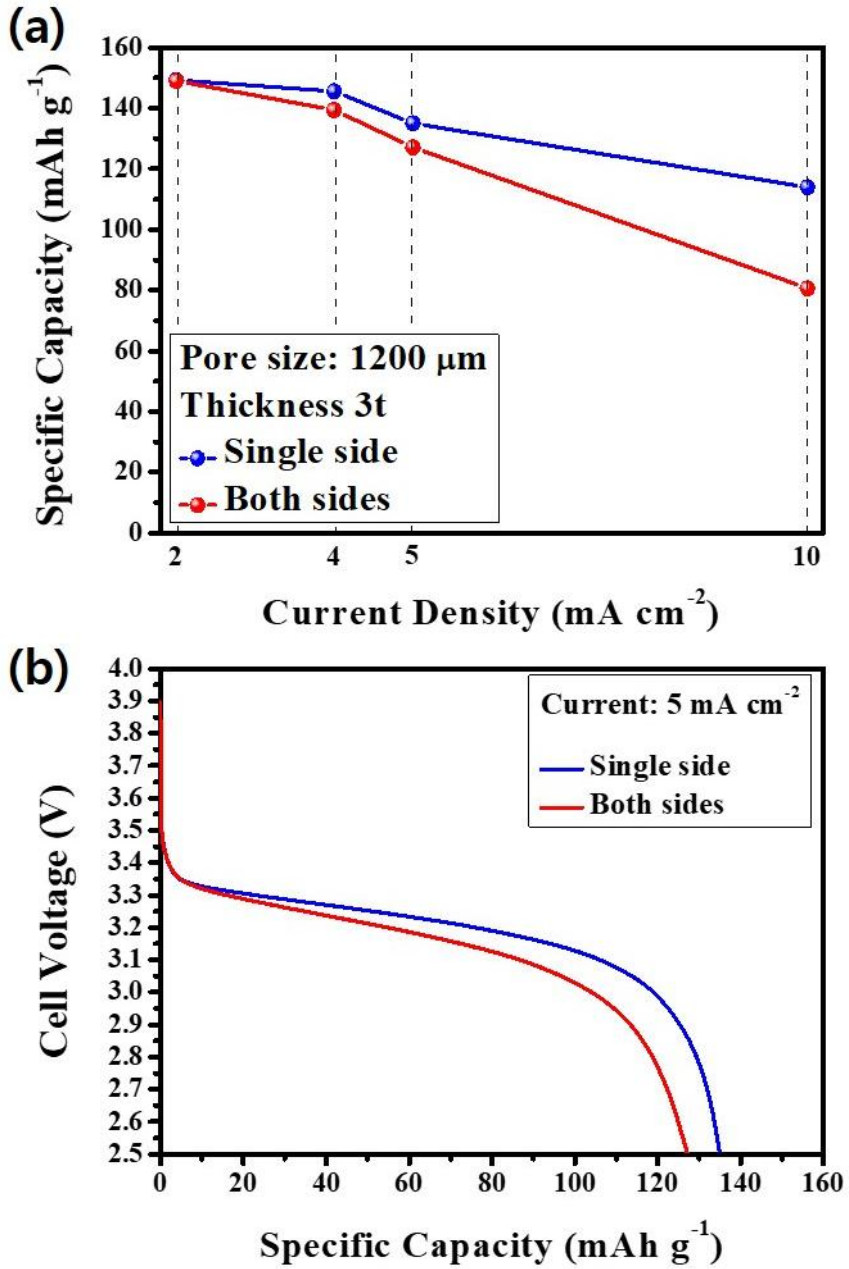

Figure 3.4.11 Comparison of (a) the specific capacity (mAh g^{-1}) with an increased in current density (mA cm^{-2}) and (b) the discharge curves at 5 mA cm^{-2}, when Li anode placed on single and both sides of the metal foam cathodes. (Metal foam cathode of 1200 µm-pore size and 3000 µm-thickness)

The following experiment was used metal foam cathode of 3000 μm-pore size and 3000 μm-thickness. Figure 3.4.12(a) shows specific capacity (mAh g^{-1}) obtained from the various discharge current (mA). In the graph, both sides cell also showed higher specific capacity than single side cell. However, at low current, there were almost similar specific capacity. Specific capacities of both sides cell were 152, 152, 149.3, 145.8, 142.2, 135.4, and 125.7 mAh g^{-1} for the 2, 4, 6, 8, 10, 12, and 15 mA, respectively. Whereas, single side cell was 149.7, 148.4, 143.2, 136.9, 130.6, 124.1, and 116.5 mAh g^{-1}, respectively. In addition, Figure 3.4.12(b) shows the discharge curves at current of 6 mA. In the graph, both sides cell exhibited lower voltage drop in the plateau region and higher specific capacity (149.3 mAh g^{-1}) than single side cell. Figure 3.4.13(a) shows specific capacity (mAh g^{-1}) obtained from the various discharge current density (mA cm^{-2}). In the graph, single side cell showed higher specific capacity than both sides cell. Specific capacities of single side cell according to current density were 149.7, 148.4, 143.2, 136.9, and 130.6 mAh g^{-1} for the 2, 4, 6, 8, and 10 mA cm^{-2}, respectively. Whereas, both sides cell was 152.3, 145.8, 135.4, 125.7, and 106.3 mAh g^{-1}, respectively. In addition, Figure 3.4.13(b) shows the discharge curves at current of 6 mA cm^{-2}. In the graph, single side cell exhibited lower voltage drop in the plateau region and higher specific capacity (143.2 mAh g^{-1}) than both sides cell.

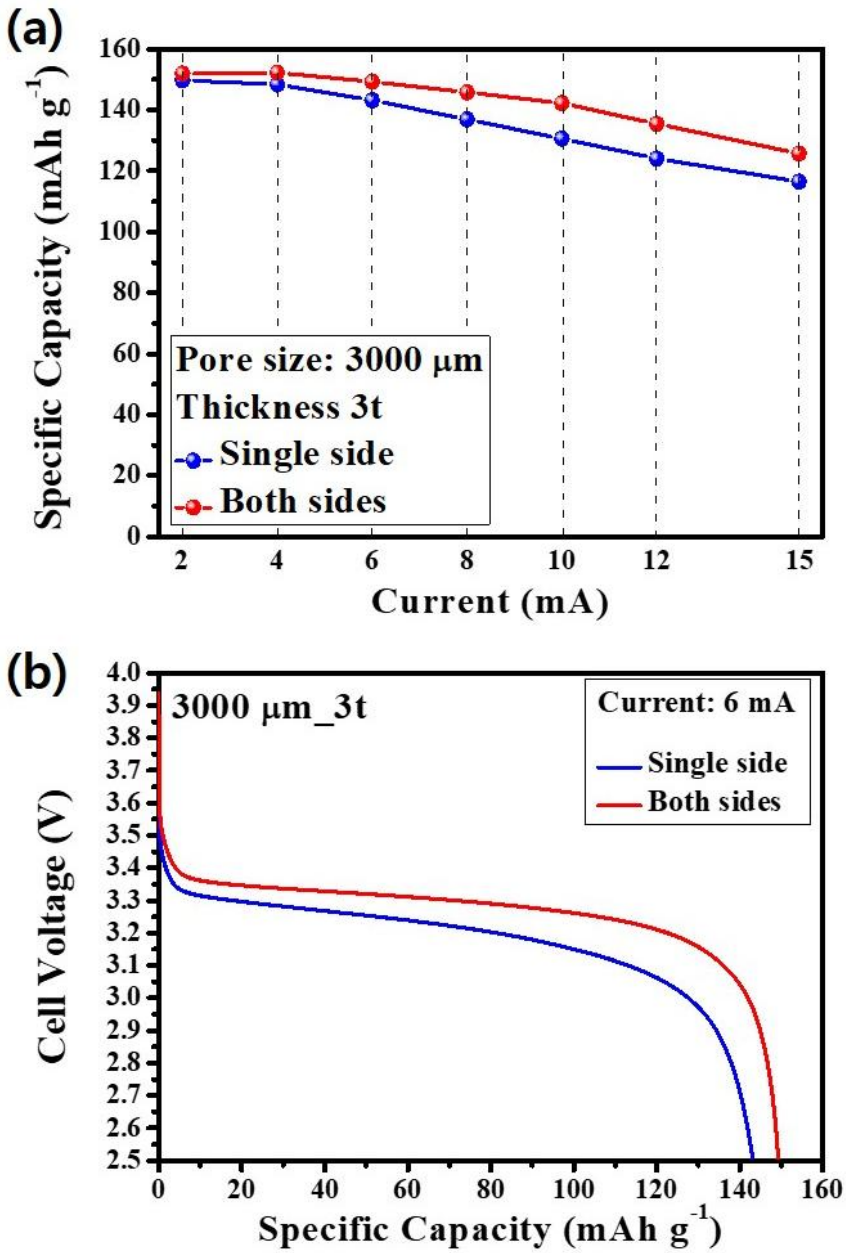

Figure 3.4.12 Comparison of (a) the specific capacity (mAh g^{-1}) with an increased in current (mA) and (b) the discharge curves at 6 mA, when Li anode placed on single and both sides of the metal foam cathodes. (Metal foam cathode of 3000 µm-pore size and 3000 µm-thickness)

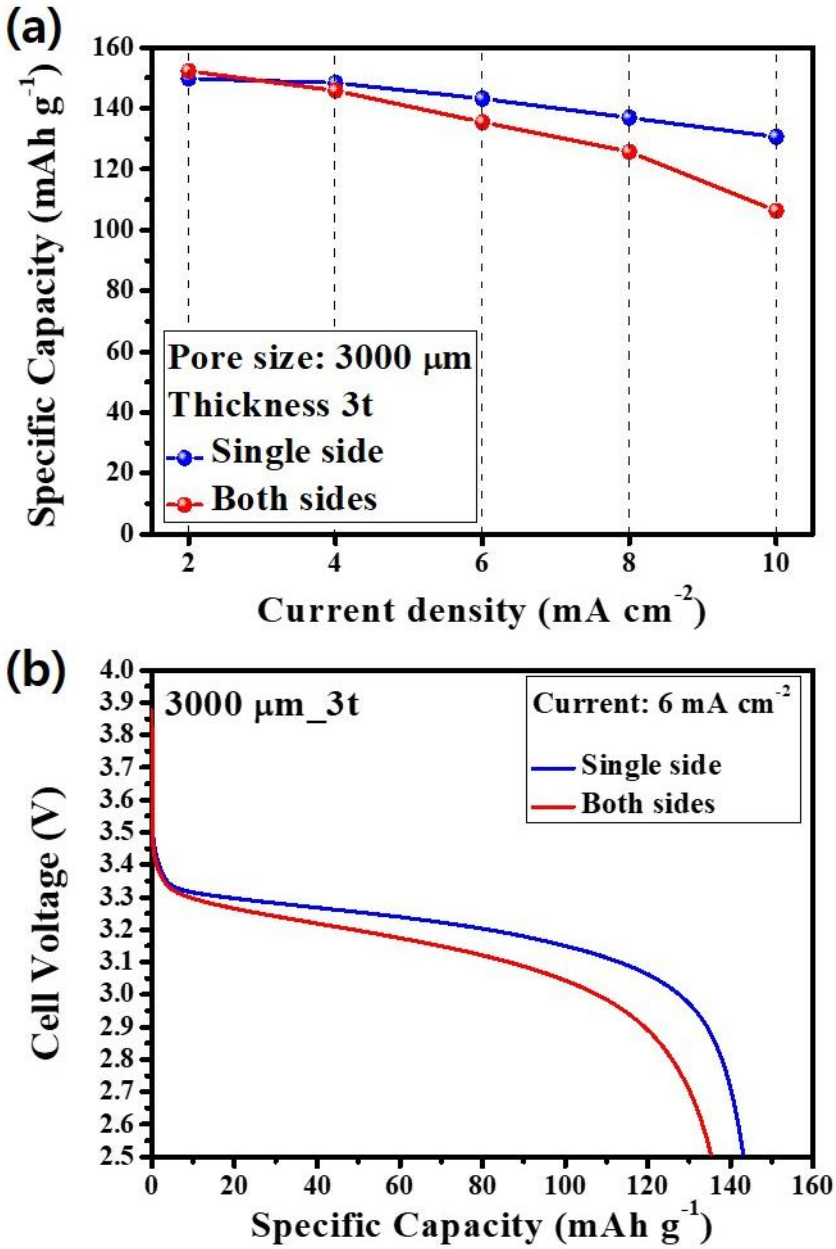

Figure 3.4.13 Comparison of (a) the specific capacity (mAh g^{-1}) with an increased in current density (mA cm^{-2}) and (b) the discharge curves at 6 mA cm^{-2}, when Li anode placed on single and both sides of the metal foam cathodes. (Metal foam cathode of 3000 µm-pore size and 3000 µm-thickness)

The following part was compared the electrochemical performances related to cell structures as shown in Figure 3.4.14. Cell structures were two cathodes system, two anodes system, and layered system. Metal foam cathode were fabricated by using 450 μm-pore size metal foam. Figure 3.4.15(a) shows the discharge curves at current of 2 mA. In the graph, there were almost similar voltage drop in the plateau region and specific capacity (150 mAh g^{-1}) due to low current. In addition, cycle-life performance was also exhibited similar performance at 4 mA as shown in Figure 3.4.15(b). Capacity retention rate were 89, 92, and 95 % for the two cathodes system, two anodes system, and layered system. However, at current density of 12 mA (Figure 3.4.16), layered structure was indicated the highest specific capacity (138 mAh g^{-1}) and voltage in the plateau region due to the largest surface area for the redox reactions. Therefore, to manufacture a high-energy (capacity) battery that uses a low current density, thick electrode offers more efficiency. This is due to the decreased mass of inactive materials, such as the current collector and separator. However, to manufacture a high-power battery that uses a high current density, it is preferable to stack thin metal foam cathode. Figure 3.4.17 shows the cyclic voltammetry curves at a scan rate of 0.1 mV S^{-1}. In the graph, voltage of redox peaks occurs much earlier for the layered structure than two cathodes and two anodes systems. For example, the oxidation and reduction peak of layered structure occur at 3.6 and 3.28 V, respectively. In addition, the oxidation and reduction current intensity also exhibit much higher for the layered structure than two cathodes and two anodes systems. Figure 3.4.18 shows Nyquist plots of electrochemical impedance spectroscopy (EIS). In the graph, R_b was almost similar. However, R_{ct} significantly decreased with layered structure due to the widest surface area of redox reaction.

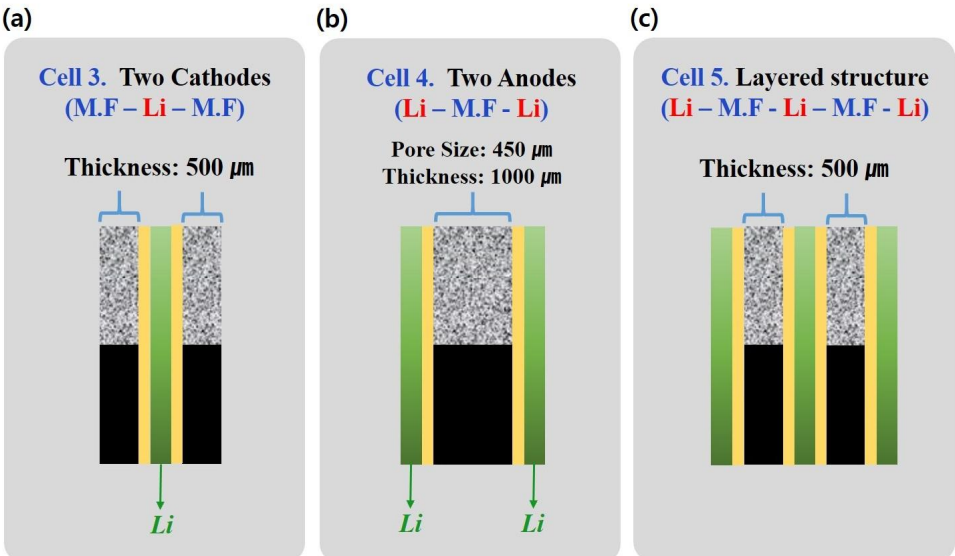

Figure 3.4.14 Schematic view of cell structures; (a) two cathodes system, (b) two anode system, and (c) layered structure.

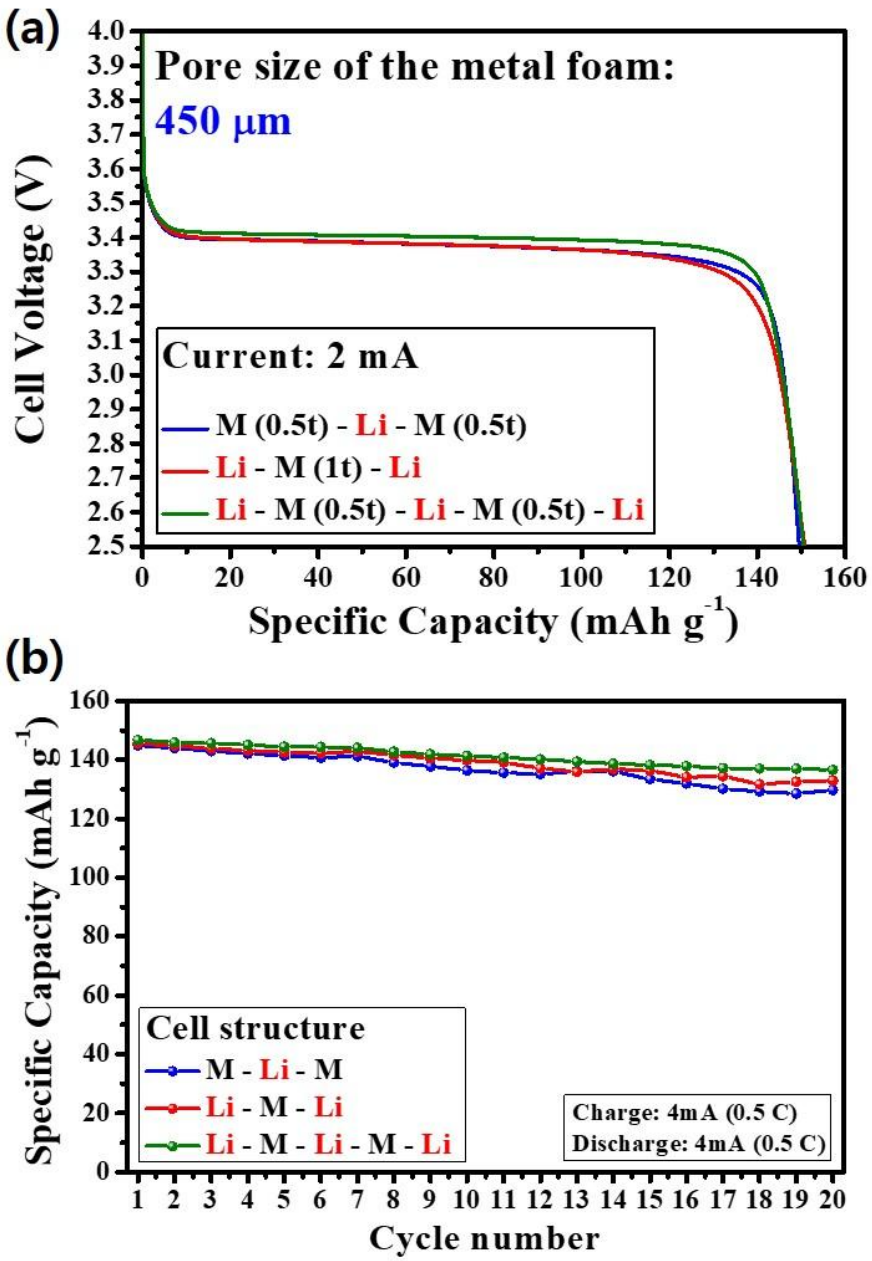

Figure 3.4.15 (a) Discharge curves related to the cell structures at 2 mA. (b) cycle-life performances at 4 mA (0.5 C).

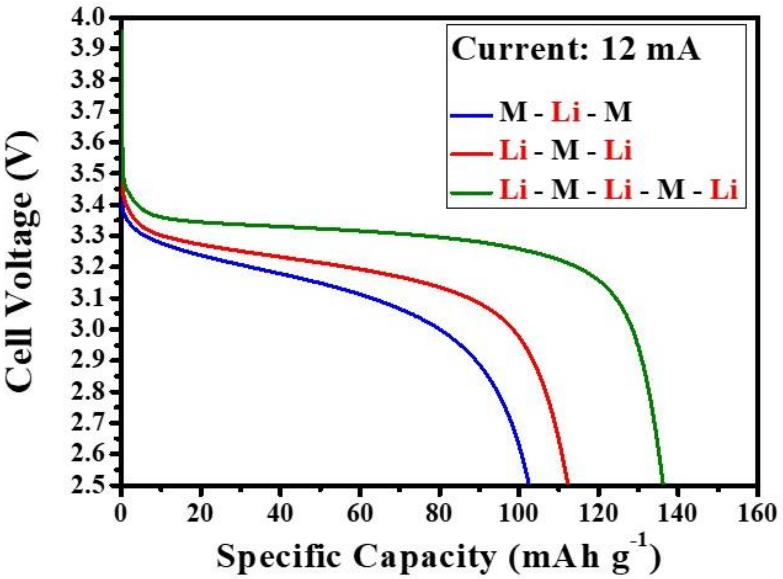

Figure 3.4.16 Discharge curves relate to the cell structures at 12 mA.

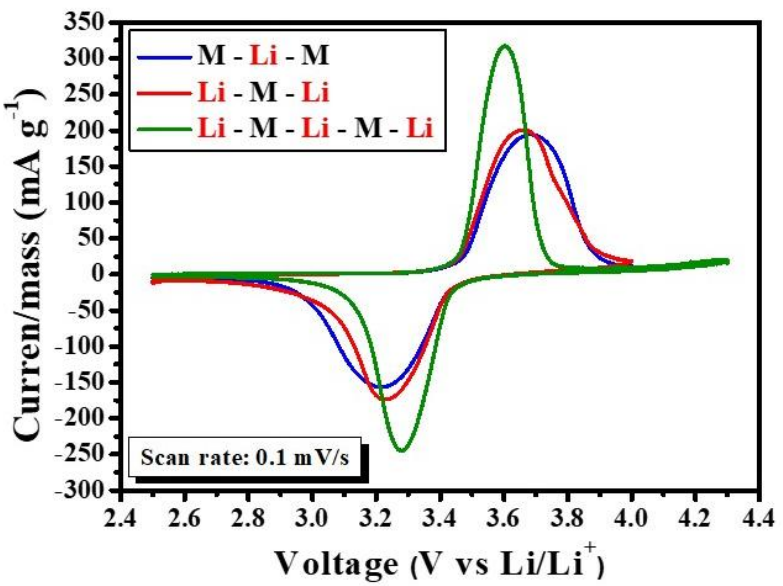

Figure 3.4.17 Cyclic voltammetry curves at scan rate of 0.1mV S^{-1}.

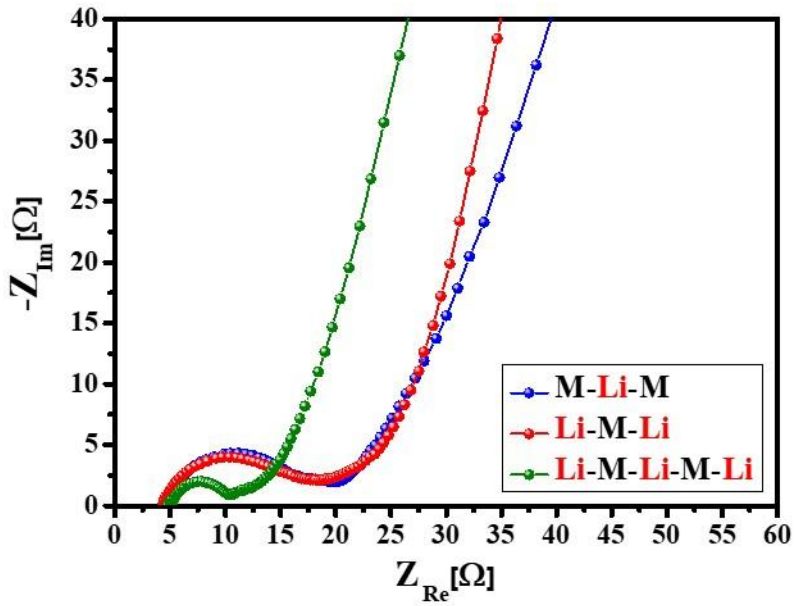

Figure 3.4.18 Nyquist plots of electrochemical impedance spectroscopy obtained from open circuit voltage (OCV) 3.43 V.

3.5 Effect of Porosity in metal foam cathodes

To investigate the electrochemical properties related to the press intensities after annealing. We fabricated the electrodes for no pressed (1000 μm), 20% pressed (1000→800 μm), and 50% pressed (1000→500 μm) after annealing using metal foam cathode of 450 μm-pore size. The fabrication and detail information about the cells are shown in Table 3.5.1.

Table 3.5.1 Analytical data of metal foam cathodes with press intensity after firing process. (Pore size: 450 μm)

Pore size	Content of LFP	Content of C.B	Content of PVDF	Fabrication of electrodes	Amount of $LiFePO_4$/C	Electrode density
450 μm	75 wt.%	15 wt.%	10 wt.%	1000 μm (1t) – Load – Fire	41 mg cm^{-2}	0.48 g cm^{-3}
				1000 μm (1t) – Load – Fire – 800 μm (0.8t) Press	41 mg cm^{-2}	0.76 g cm^{-3}
				1000 μm (1t) – Load – Fire – 500 μm (0.5t) Press	39 mg cm^{-2}	1.79 g cm^{-3}

Figures 3.5.1(a) and (b) show the discharge curves at the current densities of 2 and 10 mA cm^{-2}, respectively. No pressed and 20 % pressed cells show similar specific capacity (about 150 mAh g^{-1} at 2 mA cm^{-2} and about 100 mAh g^{-1} at 10 mA cm^{-2}, respectively) and voltages of the plateau region, which is higher than the 50 % pressed cell (about 128 mAh g^{-1} at 2 mA cm^{-2} and about 12 mAh g^{-1} at 10 mA cm^{-2}, respectively). However, at a rate performance of above 12 mA cm^{-2} (Figure 3.5.2), the 20 % pressed cell also showed less specific capacity than the not pressed cell. In addition, metal foam cathode of 50 % pressed showed a much greater reduction in specific capacity than that of other cells. That is, as the intensity of the press increased, the reduction in the specific capacity increased. This is because the higher electrode

density leads to a reduction of the rate performance due to the increased kinetic barrier. When the discharge rate exceeded 10 mA cm^{-2}, no discharge capacity was observed due to the electrochemical reaction mostly taking place at the metal foam cathode surface. As a result, the cell potential of the electrode to the discharge cut-off voltage was greatly reduced. The active material density of no pressed, 20 % pressed, and 50 % pressed electrodes is 0.48, 0.76, and 1.79 g cm^{-3}, respectively.

Moreover, Figure 3.5.3 shows the cycle-life behaviors. Capacity retention rates of the no pressed, 20 % pressed, and 50 % pressed electrodes were around 91, 80, and 37 %, respectively, after 30 cycles at 0.5 C. Figure 3.5.4 shows the cyclic voltammetry (CV) curves obtained at a scan rate of 0.1 mV S^{-1}. The CV curves analysis is the general technique used for studying the kinetic performance of the electrode reaction in Li secondary batteries [88]. Redox reaction of the cells occurs when the input voltage is higher or lower than the open circuit voltage (OCV, $LiFePO_4$ was 3.43 V) satisfying the Nernst equation. The results from the graph show that the CV curves also strongly depend on the density and porosity of the active materials in the electrode. The no pressed and 20 % pressed cells showed almost similar peaks. While, the 50 % pressed cell lead to a shift in peak position away from OCV (the oxidation and reduction peak positions of the no pressed and 20 % pressed cells occurred at around 3.65 and 3.22 V, respectively, whereas those of the 50 % pressed cell occur at 3.75 and 3.13 V, respectively). This is because the redox reaction occurs under non-equilibrium condition [88]. The shape of the peak was much broader and the current intensity was much lower than the other metal foam cathodes. This is due to the severe transport loss, which negatively affects the kinetic behavior.

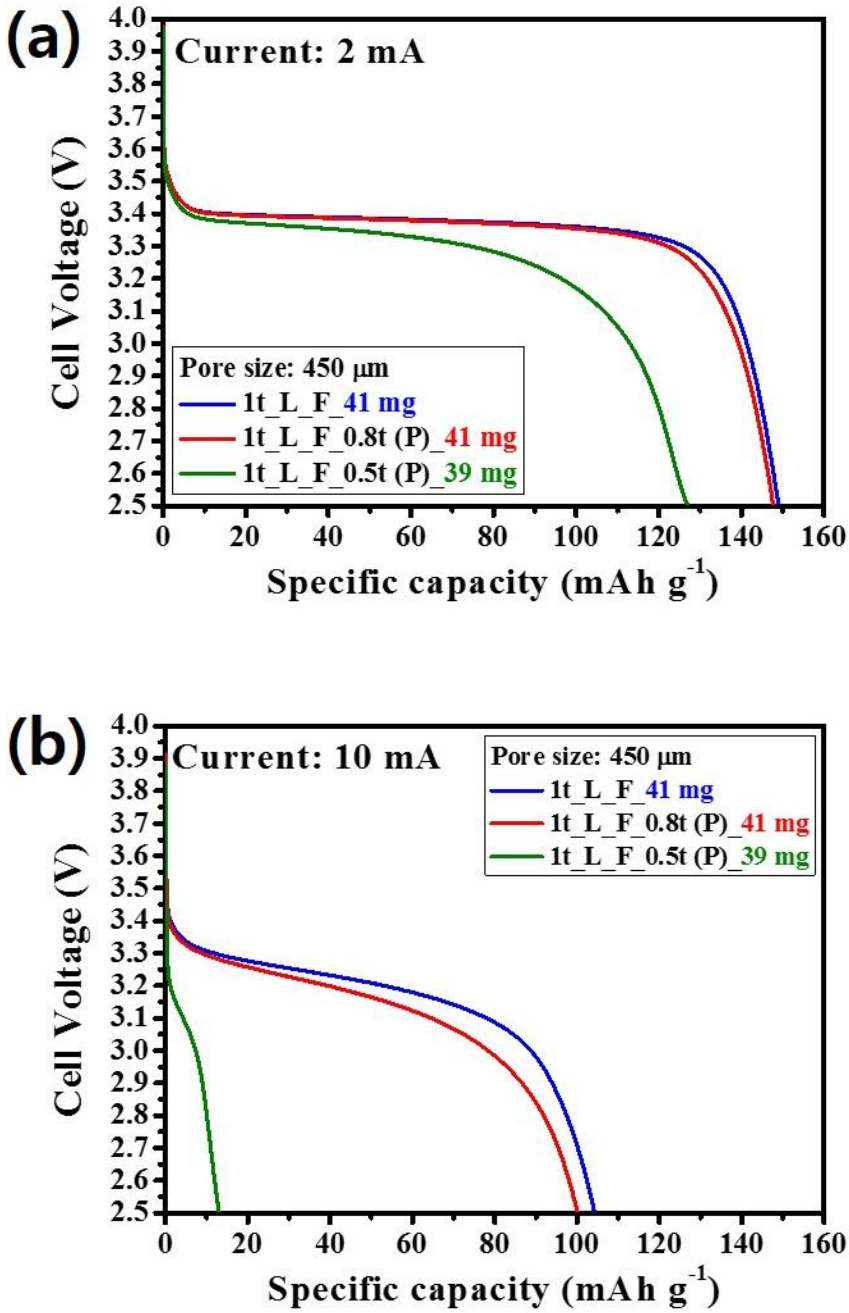

Figure 3.5.1 Comparison of the discharge curves related to press intensity after firing process at current density of (a) 2 mA cm^{-2} and (b) 10 mA cm^{-2}. (Pore size: 450 µm)

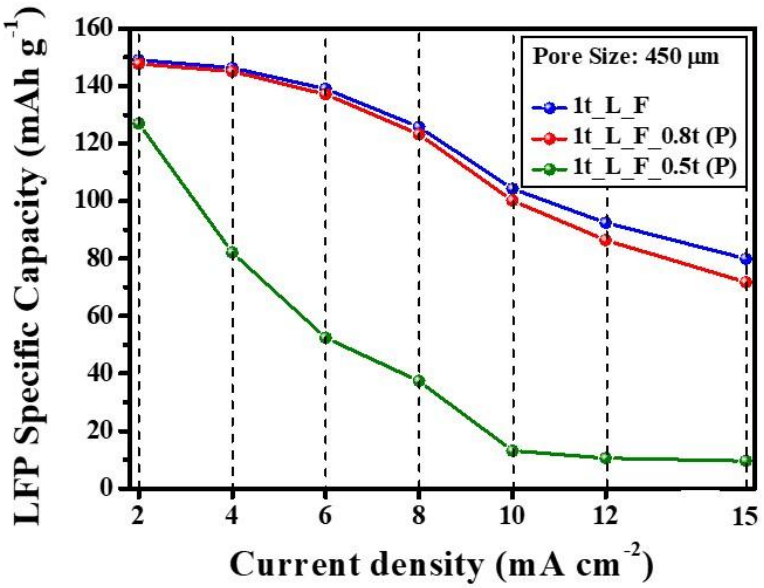

Figure 3.5.2 Comparison of the LFP specific capacity (mAh g^{-1}) related to press intensity after firing process with an increased in current density. (Pore size: 450 µm)

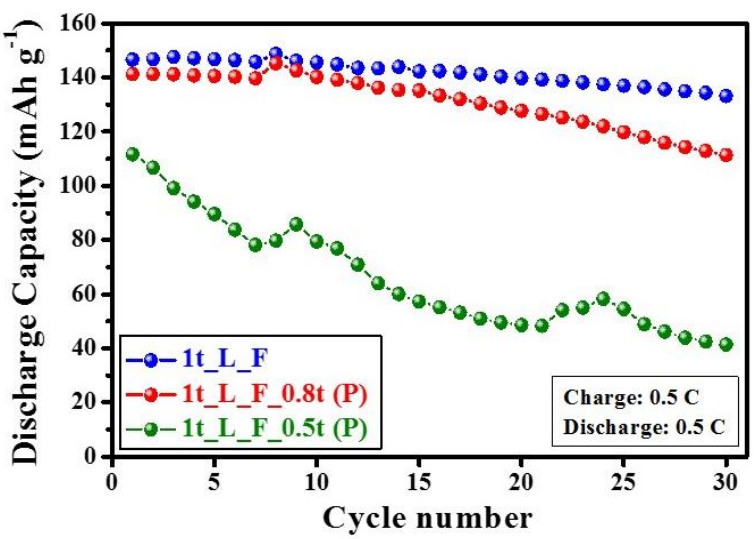

Figure 3.5.3 Cycle-life performance related to press intensity after firing process at 0.5 C. (Pore size: 450 µm)

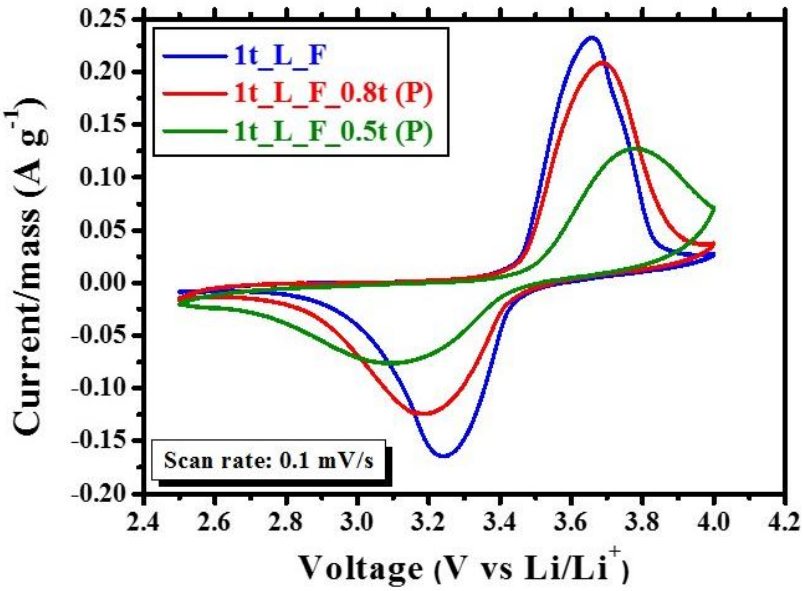

Figure 3.5.4 Cyclic voltammetry curves related to press intensity after firing process at scan rate of 0.1mV S^{-1}.

The next experimental, we fabricated the electrodes for no pressed (5000 μm), 20 % pressed (5000→4000 μm), and 40 % pressed (5000→3000 μm) after annealing using metal foam cathode of 3000 μm-pore size. Active material density of the no pressed, 20 % pressed, and 50 % pressed electrodes is 0.5, 0.72, and 1.1 g cm^{-3}, respectively. The fabrication and detail information about the cells are shown in Table 3.5.2.

Table 3.5.2 Analytical data of metal foam cathodes with press intensity after firing process. (Pore size: 3000 μm)

Pore size	Content of LFP	Content of C.B	Content of PVDF	Fabrication of electrodes	Amount of $LiFePO_4$/C	Electrode Density
3000 μm	75 wt.%	15 wt.%	10 wt.%	5000 μm (5t) – Load – Fire	0.234 g cm^{-2}	0.5 g cm^{-3}
				5000 μm (5t) – Load – Fire – 4000 μm (4t) Press	0.216 g cm^{-2}	0.72 g cm^{-3}
				5000 μm (5t) – Load – Fire – 3000 μm (3t) Press	0.190 g cm^{-2}	1.1 g cm^{-3}

Figures 3.5.5 shows the discharge curves at the current densities of 10 mA cm^{-2}, respectively. In the graph, no pressed and 20% pressed cells were indicated similar specific capacity (about 133 mAh g^{-1}) and voltages of the plateau region, which is higher than the 40 % pressed metal foam cathode (about 114 mAh g^{-1}). In addition, metal foam cathodes of no pressed and 20 % pressed showed similar specific capacity in the rate performance (Figure 3.5.6). Whereas, metal foam cathode of 40 % pressed showed a much greater reduction in specific capacity. Capacity retention rates of the no pressed, 20 % pressed, and 40 % pressed electrodes were around 62, 63, and 54 %, respectively. This shows that the formation of the third pores into which the electrolyte can enter is very important factor when the batteries are manufactured using the metal foam current collector.

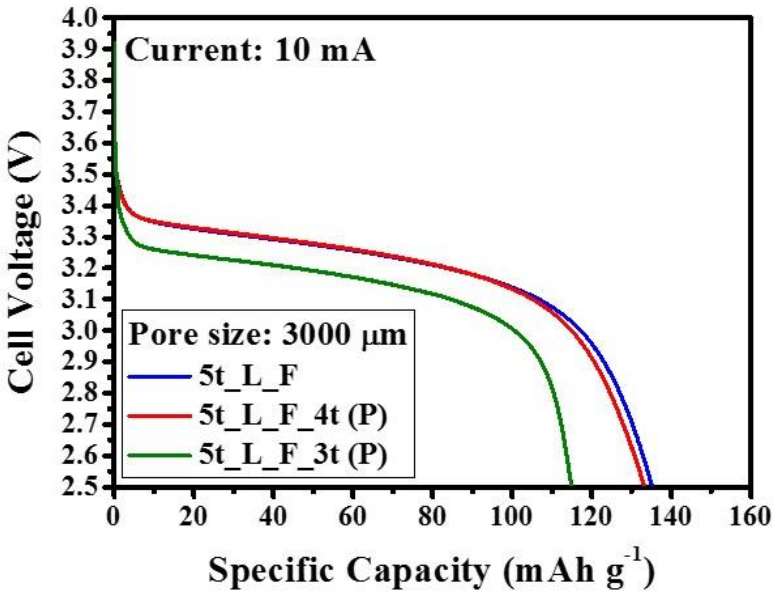

Figure 3.5.5 Comparison of the discharge curves related to press intensity after firing process at current density of 10 mA cm^{-2}. (Pore size: 3000 μm)

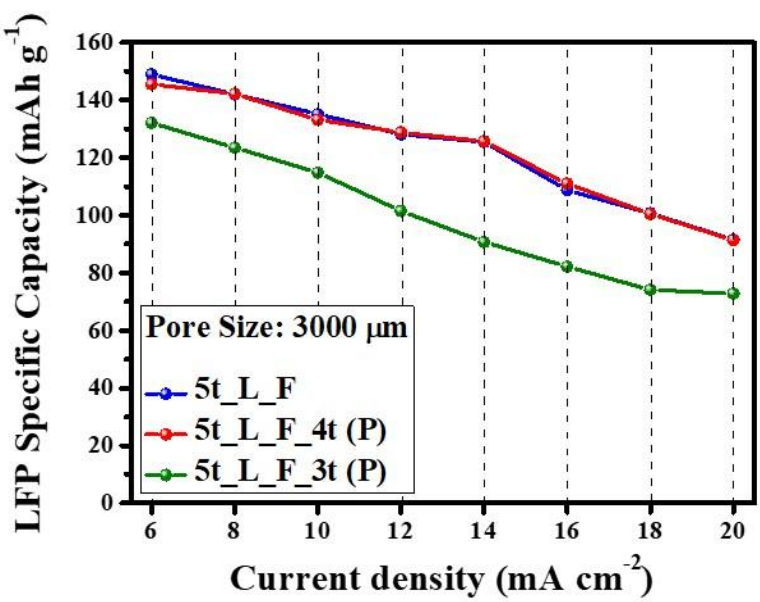

Figure 3.5.6 Comparison of the LFP specific capacity (mAh g^{-1}) related to press intensity after firing process with an increased in current density. (Pore size: 450 μm)

The next experiment was compared the electrochemical properties according to the proportion of the metal frame in the metal alloy foam and the active material density. The metal foam thickness of 1000 µm was prepared *via* mechanical pressing. Each amount of active materials of no pressed, pressed before firing, and pressed after firing were 37, 29, and 55 mg, respectively. The metal foam cathodes fabrication and information are shown in Table 3.5.3.

Table 3.5.3 Analytical data of metal foam cathodes related to the proportion of the metal frame and press methods.

Pore size	Fabrication of electrodes	Amount of $LiFePO_4$/C	Content of $LiFePO_4$/C	Content of Carbon black	Content of PVDF
450 µm	1000 µm (1t) - Load-Fire	37 mg	75 wt.%	15 wt.%	10 wt.%
	1500 µm (1.5t) – 1000 µm (1t) pressed - Load - Fire	29 mg			
	1500 µm (1.5t) - Load – Fire – 1000 µm (1t) pressed	55 mg			

The metal foam cathode of pressed before firing was indicated the highest rate performance as shown in Figure 3.5.7. The reason is that the highest proportion of the metal frame and electrode porosity in the metal foam cathode. However, as shown in the cell capacity (mAh) of Figure 3.5.8, metal foam cathode of pressed after firing showed the high cell capacity due to filled the active material the highest. Nevertheless, the capacity retention rate was the lowest (50 %) due to the cell capacity was significantly decreased with current density increased. That is, high-energy batteries were advantageous to have a pressed process after firing, whereas produce high-power batteries was advantageous to have a high proportion of metal frame. As shown in the CV curves (Figure 3.5.9), the metal foam cathode of pressed before firing was showed the best kinetic performance. The oxidation and reduction peak

positions of the metal foam cathode of pressed before firing occur at 3.65 and 3.23 V, respectively, whereas those of the metal foam cathode of pressed after firing occur at 3.75 and 3.13 V, respectively. In addition, the maximum oxidation current of no pressed, pressed before firing, and pressed after firing were showed 160, 231, and 137 mA g^{-1}, respectively.

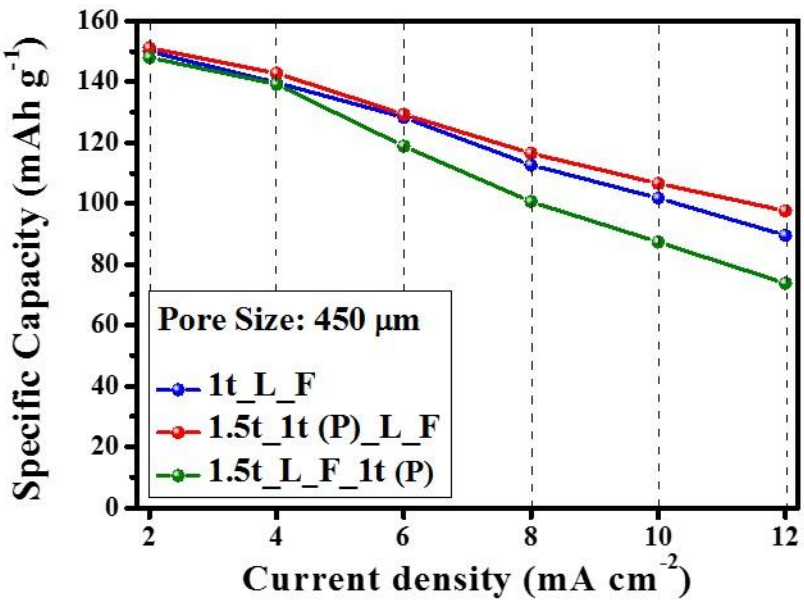

Figure 3.5.7 Comparison of the LFP specific capacity (mAh g^{-1}) related to the proportion of the metal frame and press methods with an increased in current density.

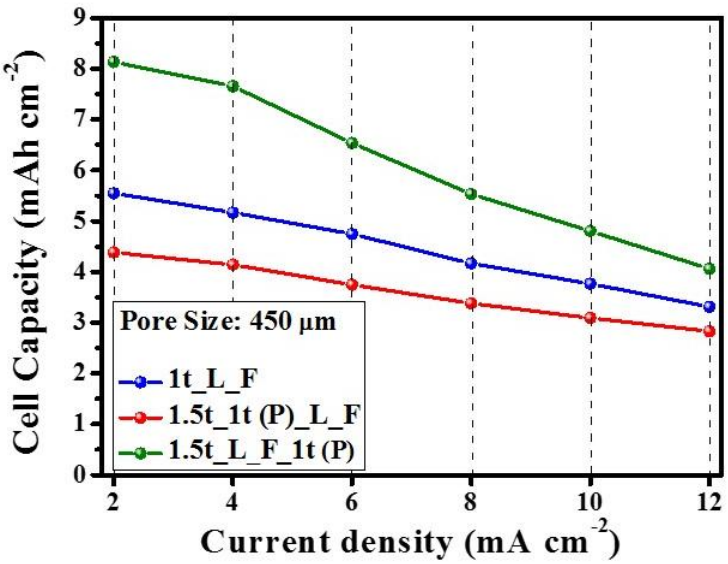

Figure 3.5.8 Comparison of the cell capacity (mAh) related to the proportion of the metal frame and press methods with an increased in current density.

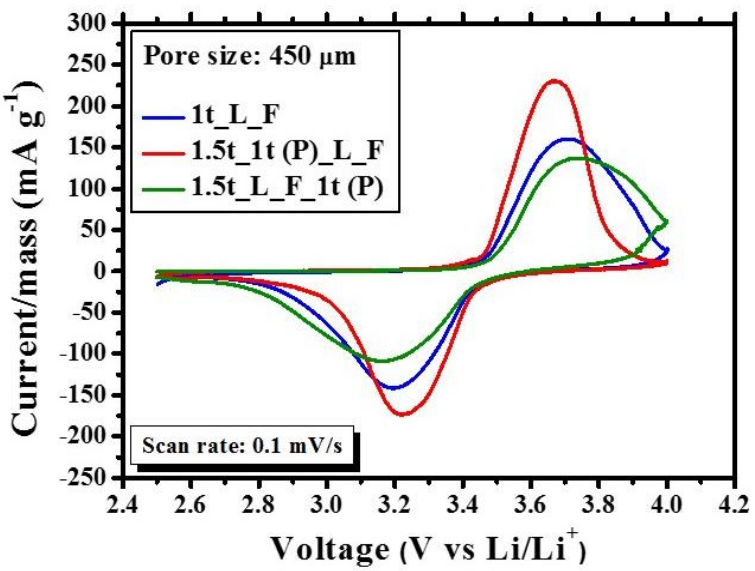

Figure 3.5.9 Cyclic voltammetry curves related to the proportion of the metal frame and press methods at scan rate of 0.1mV S^{-1}.

The following was an experiment in which metal foam cathodes manufactured by pre-firing process. The reason for the pre-firing process is to increase the active material density and electrode porosity. Metal foam cathodes were used 3000 μm-pore size in metal foam. The fabrication and information of the cells are shown in Table 3.5.4.

Table 3.5.4 Analytical data of metal foam cathodes manufactured by pre-firing process.

Pore size	Fabrication of electrodes	Active material (mg cm^{-2})	Content of $LiFePO_4$/C	Content of Carbon black	Content of PVDF
3000 μm	2t – 1t Press - Load – Fire	43	75 wt.%	15 wt.%	10 wt.%
	2t – Load – Pre-fire (100 °C, 30 min) – 1t press – Fire	75			
	2t – Load – Pre-fire (100 °C, 1h) – 1t press – Fire	105			
	2t – Load – Fire – 1t press	120			

Figure 3.5.10 shows the cell capacity (mAh) obtained from the various discharge current densities. In the graph, metal foam cathode of press after firing process showed the highest cell capacity (16.8 mAh) at 2 mA, due to the highest mass loadings of active material. However, at above 4 mA, metal foam cathode of 1h pre-firing process showed the highest cell capacity. Because metal foam cathode of 1h pre-firing process has higher mass loadings of active material than metal foam cathode with 30 min pre-firing process and metal foam cathode of press before firing process. In addition, it has wider surface area of redox reaction than metal foam cathode of press after firing process due to the maintained third pores. Figure 3.5.11 shows the LFP specific capacity (mAh g^{-1}) at various discharge current densities. In the graph, metal foam cathodes of press before firing process, 30 min pre-firing process, and 1h pre-firing process were almost similar LFP specific capacity and rate performance.

Capacity retention rate was 70, 73, and 73 %, for the metal foam cathodes of press before firing process, 30 min pre-firing process, and 1h pre-firing process, respectively. While, metal foam cathode of press after firing process was indicated the lowest capacity retention rate (50 %). It was noted that pre-firing process increases the active materials density and the formation of third pores through which the electrolyte can permeate into the metal foam cathode. Figure 3.5.12(a) shows the discharge curves at current density of 2 mA cm^{-2}. In the graph, there were almost no difference in discharge capacity and voltage in the plateau region. However, at discharge current density of 10 mA cm^{-2} (Figure 3.5.12(b)), metal foam cathode of 1h pre-firing process exhibited the lowest voltage drop in the plateau region and the highest discharge specific capacity (110 mAh g^{-1}). Whereas, metal foam cathode of press after firing process showed the lowest specific capacity (70 mAh g^{-1}).

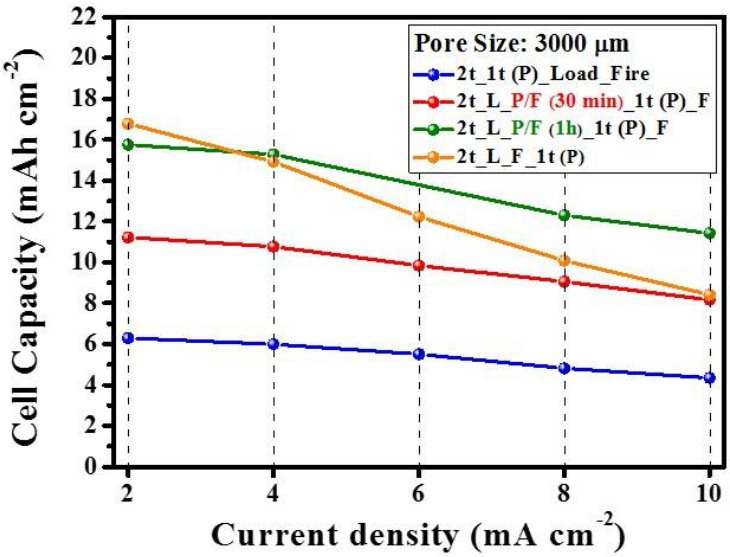

Figure 3.5.10 Comparison of the cell capacity (mAh) related to the pre-firing process with an increased in current density.

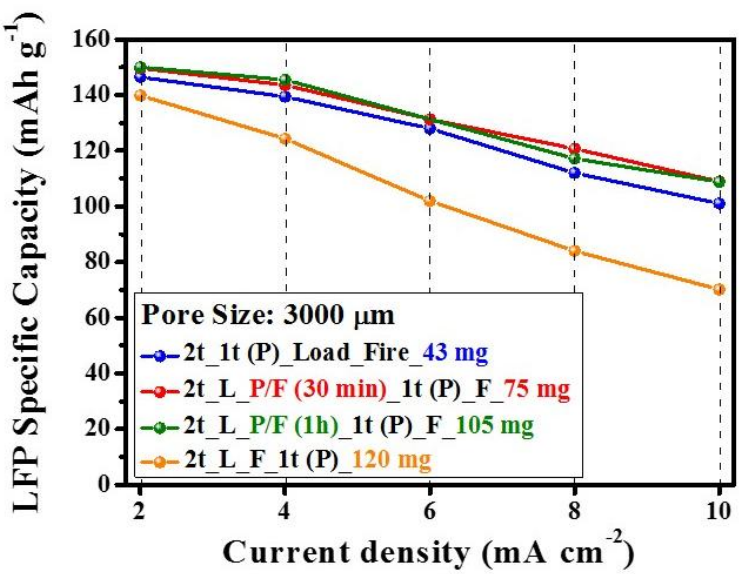

Figure 3.5.11 Comparison of the LFP specific capacity (mAh g^{-1}) related to the pre-firing process with an increased in current density.

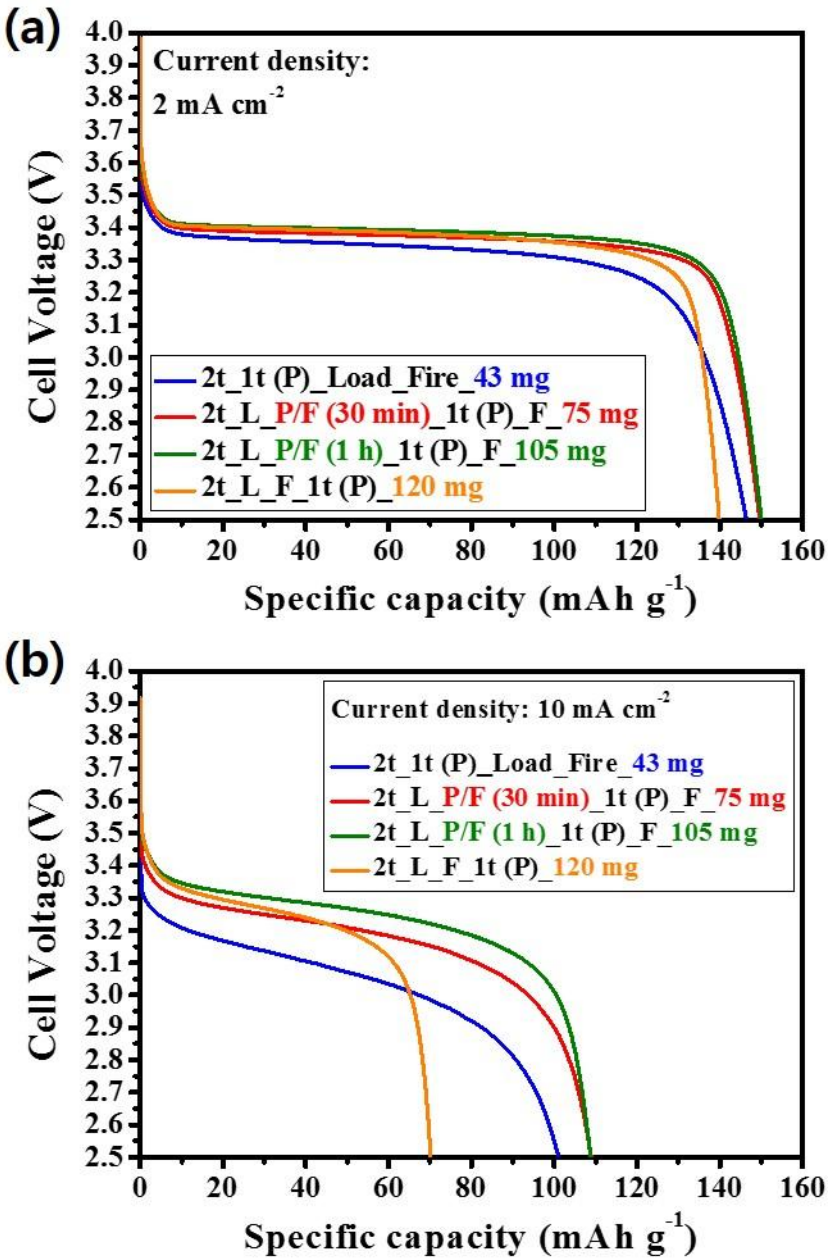

Figure 3.5.12 Comparison of the discharge curves related to the pre-firing process at current density of (a) 2 mA cm^{-2} and (b) 10 mA cm^{-2}.

3.6 Bendable Li pouch battery

Flexible LIBs have been studied due to the rapid development unique devices such as wearables, rollup displays, and conformable health-monitoring electronic skin [46-54]. It is critical for flexible LIBs to have lightweight, good flexibility, high energy density and cycling stability. In this paper, we describe a positive electrode fabricated using a 3D structured nickel-chromium (NiCr) alloy metal foam as the current collector for use in bendable pouch LIBs [98].

The NiCr alloy metal foam was obtained using foam-type polyurethane following the manufacturing process reported by Yao et al. [34] and Yang et al. [37] First, Ni foam was prepared by nickel plating onto polyurethane, and the polyurethane was then removed via heat treatment. After that, NiCr alloy powder was adsorbed onto the Ni foam, and the substrate was then reheated to obtain the NiCr alloy foam [34]. The weight ratio of Ni to Cr was 75 : 25. The metal foam was supplied by Alantum Corporation (Korea). The NiCr alloy metal foam had around 400 μm-1st pore size, around 150 μm-2nd pore size and 700 μm-thickness. The thickness of the metal foam was controlled *via* mechanical pressing to around 500 μm. The slurry for the metal foam cathode was prepared by mixing $LiFePO_4$/C as the cathode active material, carbon black as the conductive material, and polyvinylidene fluoride (PVDF) as the binder at a weight ratio of 75 : 15 : 10 with *N*-methyl-2-pyrrolidone (NMP). The prepared slurry was filled in the pore space of the NiCr alloy metal foam and was annealed in a vacuum at 130 °C for 8 h. The size of metal alloy foam was 1 cm by 4 cm and only 1 x 3 cm of the area was filled with the cathode material slurry, while the remaining area was used to attach the aluminum tab (Figure 3.6.1).

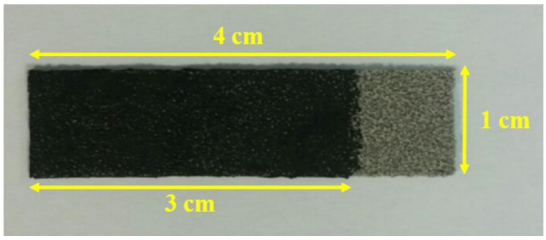

Figure 3.6.1 Optical image of a metal foam cathode using the 3D structured NiCr alloy metal foam of the bendable Li secondary battery.

The mass of the $LiFePO_4$/C loaded into the metal foam cathode was about 71 mg, and the active material density of the cells was about 0.8 g cm^{-3}. The electrochemical behavior was assessed by fabricating pouch cells in a dry box filled with pure Ar gas. The cells were prepared using lithium metal as the anode and celgard (polypropylene) as the separator. These were placed in a polymer-aluminum-polymer laminated pouch bag containing 1 M $LiPF_6$ in ethylene carbonate (EC) : diethyl carbonate (DEC) (1: 1 v/v) as the electrolyte. The lithium metal wrapped both sides of the metal foam electrode. The 4 mm-wide aluminum tab and copper tab connect the battery cycler system were attached respectively to, the NiCr alloy metal foam as the current collector of the positive electrode, and Li metal as the negative electrode [83, 90]. The charge and discharge cutoff voltage were set to 4.0 V and 2.5 V for the $LiFePO_4$/C cathode. Rate performance measures discharges at C-rates between 0.2 and 3, and constant charges at 0.2 C-rate [90]. Cycle-life performances were carried out at a 0.5 C-rate of both charge and discharge. Both tests were carried out using a WBCS 3000 battery cycler system at room temperature. The electrochemical impedance spectroscopy (EIS) of the cells was carried out using a CHI608A electrochemical analyzer at room temperature. The AC signal was applied with an amplitude of 5 mV. After the cells were discharged using the potentiostatic method at 2.5 V, the frequency ranged from 100 kHz to 0.01 Hz [33, 90].

Figures 3.6.2(a) and (b) show scanning electron microscope (SEM, JEOL JSM-5600) images of three-dimensional (3D) structured NiCr alloy metal foam as the current collector of the positive electrode. The thickness of the NiCr alloy metal foam was around 500 mm (Figure 3.6.2(c)). In addition, Figure 3.6.2(d) shows SEM (ZEISS, MERLIN Compact) using a back-scattered electrons (BSE) detector image after loading and drying the cathode slurry in NiCr alloy metal foam. The NiCr alloy metal foam as the current collector improves the electrochemical properties of Li secondary batteries due to its high surface area for a redox reaction, good electrical conductivity, and short diffusion length of the Li-ion [33, 37, 90, 91]. Moreover, thick metal foam cathodes with a high areal capacity and high electrochemical performances can be manufactured by NiCr metal foam because of good adhesion of the metal frames due to their rough surfaces [33, 37, 90].

The NiCr alloy metal foam is suitable for use in the current collector of a positive electrode because the Cr that is alloyed with the Ni foam improves the resistance against corrosion [34]. Figure 3.6.3 shows the charge/discharge curve using Ni foam current collector of positive electrode. First charge curve indicates theoretical specific capacity of $LiFePO_4/C$, in which the first discharge decreases rapidly due to the nickel corrosion around 4 V [34]. Eventually, the battery is not charged from the third charge. Therefore, Ni foam cannot be used as the current collector of positive electrode but it can be used for negative electrode [92, 93]. In addition, the NiCr alloy metal foam has excellent flexibility and can be repeatedly bent without fracture nor capacity fading.

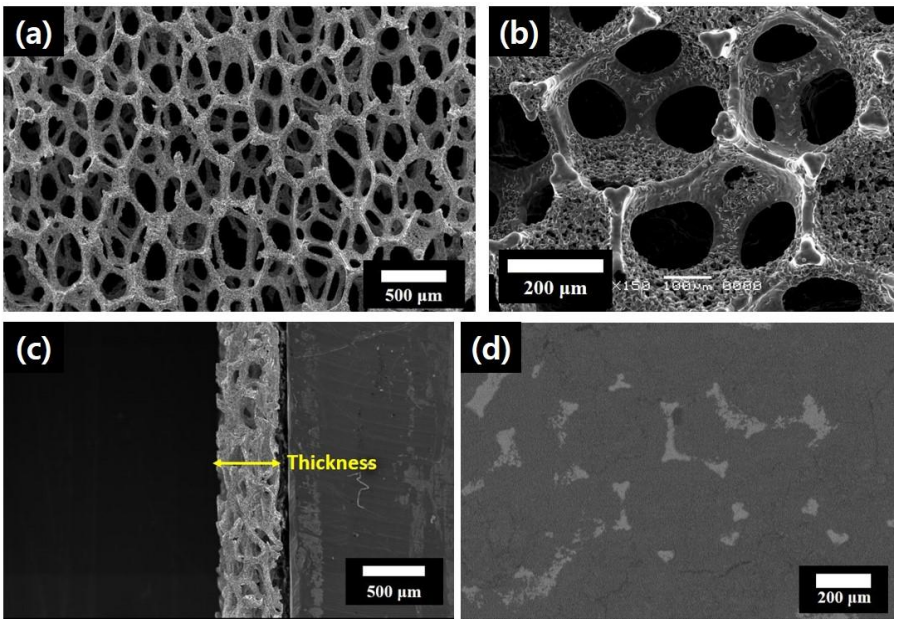

Figure 3.6.2 SEM images of the 3D NiCr alloy metal foam of the positive electrode in bendable batteries (a) x 35 and (b) x 100 magnifications. In addition, (c) cross section with 500 µm-thickness of current collector and (d) after loading and drying the cathode slurry in metal foam cathode.

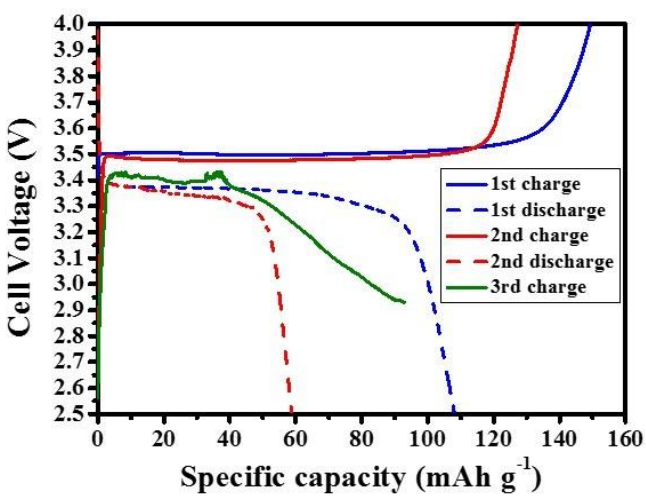

Figure 3.6.3 Charge/discharge cycles of $LiFePO_4$-based cell using Ni foam current collector at 0.2 C.

Figure 3.6.4 shows the assembled, bendable pouch LIB with the metal foam cathode in the bent state (R=12.5 mm). Figure 3.6.5 shows the rate performance of the flat and the bent pouch cells at various discharge current rates from 0.2 to 3 C. The rate performances of the LIBs with these two batteries are almost the same since neither failure nor delamination occurred. The specific discharge capacities are 150, 145, 135, 125, 116, 112, and 100 mAh g^{-1} at 0.2, 0.5, 1, 1.5, 2, 2.5, and 3C, respectively. In addition, our bendable pouch cells exhibited a high areal capacity of 3.5 mAh cm^{-2} at a C-rate of 0.2, which is significantly higher areal capacity. [94-96]. Figure 3.6.6 shows the Nyquist plots and the equivalent circuit obtained from the batteries for a full discharge at 2.5 V. The Nyquist plots also showed equivalent shapes for the cells in both the flat and bent positions since there was no damage. Moreover, the charge transfer resistance was about 6 Ω, which is much lower than that of the electrode used with the foil-type current collector (about 110 Ω) [33]. The metal foam current collector has a larger surface area for the Li redox reaction than the foil-type current collector since the metal frame exists inside of the positive electrode [33, 34]. The inset in Figure 3.6.6 shows the equivalent circuit used to analyze the AC impedance spectra. R_b, R_{ct}, Z_w, and C_{dl} represent the bulk resistance, the charge transfers resistance of the Li-ion at the electrolyte/$LiFePO_4$ interface, the Warburg impedance related to the diffusion behavior of the Li ions in the cathode active material and the capacitance double layer, respectively [89]. Yang et al. [33] and Yao et al. [34] also demonstrated the use of a similar equivalent circuit with a 3D structured foam-type current collector. In addition, the pouch cells in the flat and bent state do not show any f capacity fading during 10 cycles at a C-rate of 0.5, as shown in Figure 3.6.7. The 12.5 mm bent radius is thinner than the width of a person's wrist, which means it can be used in any wearable device intended for a radius smaller than a wrist.

Figure 3.6.8 shows the cycle-life performance of the electrode while it is flat for 20 cycles, and after 100, 200, and 300 times bending with R=12.5 mm, respectively, from cycle 21 to 30, cycle 31 to 40, and cycle 41 to 50. The results indicate there was no capacity fading related to the side reaction (fracture of the metal foam cathode or exfoliation between the active material and metal frame). Moreover, the pouch cells show a high capacity retention rate (94 %) after 50 cycles and a high areal capacity (around 3.2 mA cm^{-2}) at 0.5 C-rate. Figure 3.6.9 shows the Nyquist plots of the electrodes of flat and after bending 100 and 300 times at OCV. The plots maintain their shapes after bending many times, indicating that when bent over 300 times, the samples can still be used since there is no fracture nor delamination between the active material and the metal frames. Figure 3.6.10(a) shows a photograph of the bendable pouch cell using the metal foam as a current collector connected to a green LED in the bent state after bending 300 times. The brightness of the green LED was remained constant. Figure 3.6.10(b) shows the surface of the metal foam cathode after bending 300 times. There was a small crack on the surface of metal foam cathode, but no fracture nor delamination occurred.

Figure 3.6.4 Mechanical bent state of the flexible pouch LIBs consist of positive electrode of the 3D structured metal foam and negative electrode of the lithium foil with a bent radius of 12.5 mm.

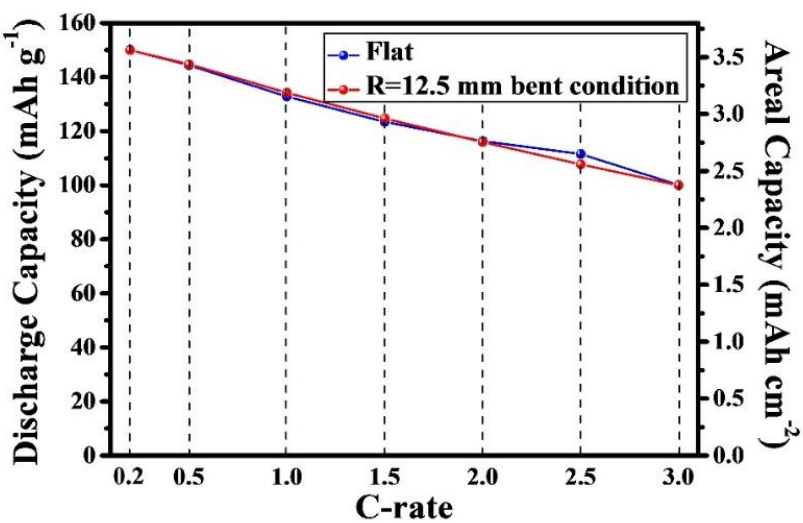

Figure 3.6.5 Comparison of the rate performance of the flat and bent state at various current rates.

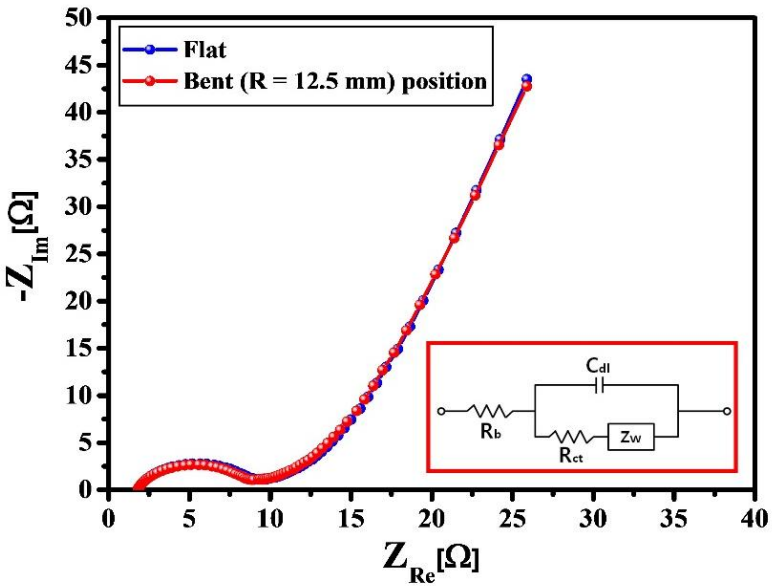

Figure 3.6.6 Nyquist plots of AC impedance spectroscopy at open circuit voltage (OCV) 3.43 V

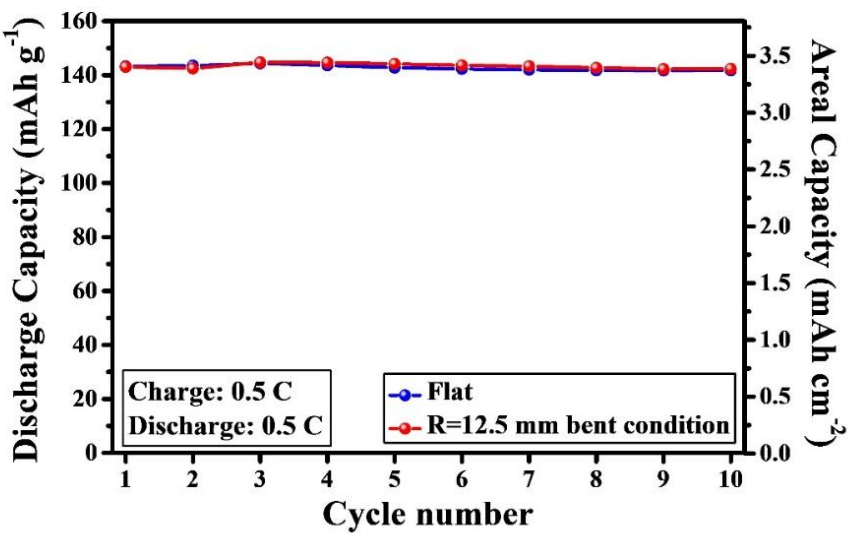

Figure 3.6.7 Discharge specific capacity (mAh g^{-1}) and areal capacity (mAh cm^{-2}) of the bendable pouch cell cycled at 0.5C.

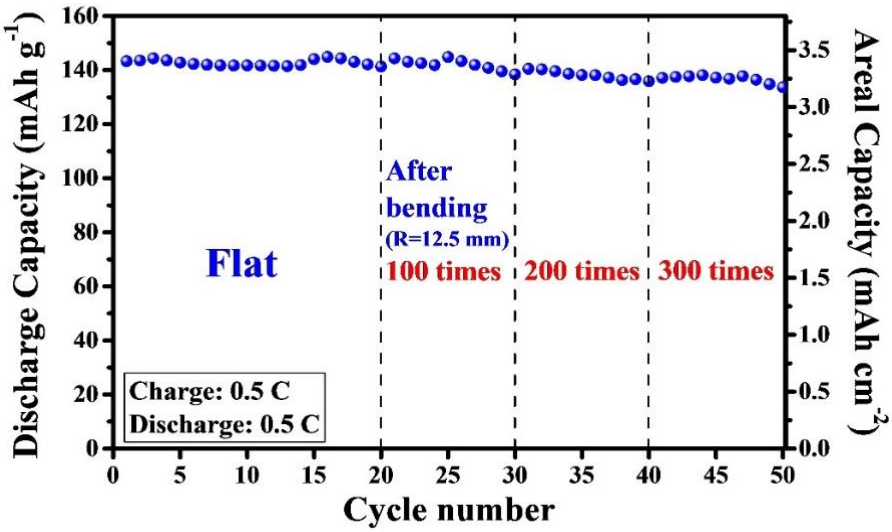

Figure 3.6.8 Discharge specific capacity (mAh g^{-1}) and areal capacity (mAh cm^{-2}) of the bendable pouch cell cycled at 0.5C with flat, after bending 100, 200 and 300 times.

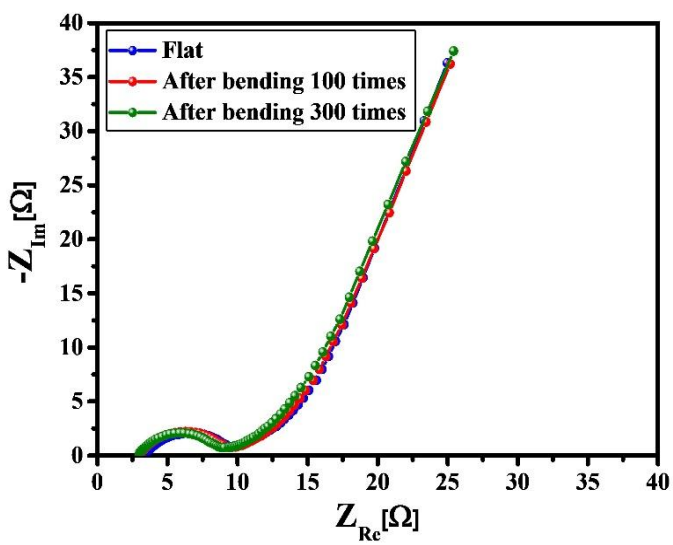

Figure 3.6.9 Nyquist plots of AC impedance spectroscopy with flat, after bending 100 and 300 times.

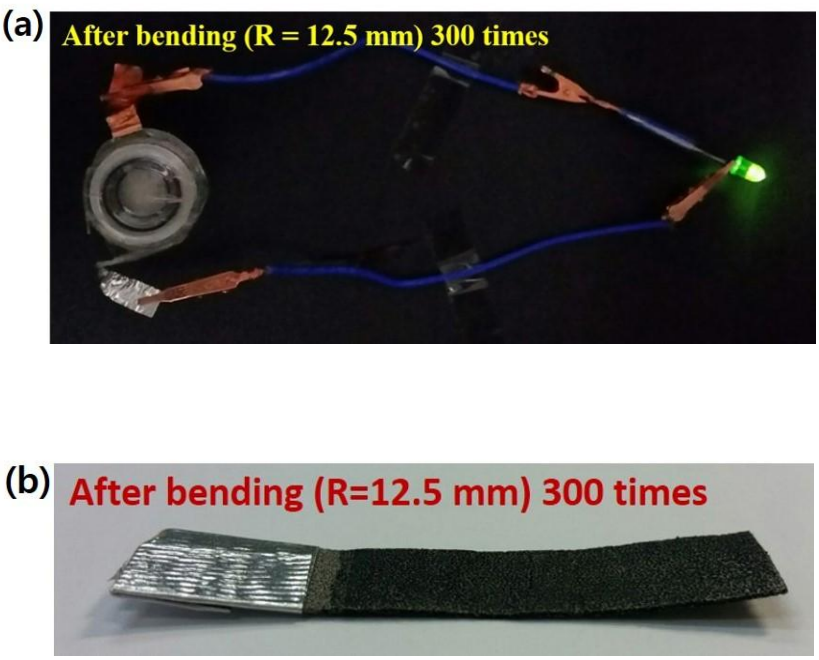

Figure 3.6.10 (a) Photograph of the flexible pouch LIB turning on a green LED after bending 300 times. **(b)** Photograph of the surface of the metal foam cathode after bending 300 times.

Figure 3.6.11 shows the discharge curve of cells in a flat and bent (R=12.5 mm and 2.5 mm) states at a C-rate of 0.5. Bending to a radius of 2.5 mm is almost the same as folding in half. The inset of Figure 3.6.11 shows a photograph of bendable cells in the bent state (R=2.5mm), indicating a good flexibility. A comparison of the discharge curves indicates that there was almost no loss in capacity and no voltage drop in the plateau region related to side reactions. The plateau is attributed to the coexistence of the two phases ($LiFePO_4$ and $FePO_4$), with no change in the voltage. A deviation from the plateau changed the composition from the two phases to single phase, causing the voltage to rapidly increase or decrease [11]. The pouch cell was mechanically bent and then kept in a flat state or bent state (12.5 and 2.5 mm) with 10, 20, and 30 charge/discharge cycles at a C-rate of 0.5 (Figure 3.6.12). The bendable cell did not loss its capacity after bending to a radius of 2.5 mm. In addition, the capacity retention rate was considerably higher at about 96 %, and there was virtually no reduction in capacity. In general, folding the pouch cells in half can lead to a fracture of the metal foam electrode or exfoliation between the active material and current collector [69]. Exfoliation or fracturing can lead to an increase in the contact resistance, which is the main reason for the decrease in the cell capacity due to a loss of electrical contact between the particles [69]. However, as shown in the Nyquist plots for our fabricated bendable cells (Figure 3.6.13), there were no differences in the impedance related to the bent states. Figure 3.6.14 shows an optical image of the bendable pouch cell connected to a green LED in the bent (R=2.5 mm) state.

Figures 3.6.15(a)-(c) show the voltage retention test of the bendable pouch cell connected to a digital multi-meter without bending and after bending (R=2.5 mm) for 50 and 200 times. The voltage of the pouch cell remained constant (3.433 V) after bending several times to a bend radius of 2.5 mm. Furthermore, Figure 3.6.16 shows

the cycle-life performance of the electrode while it is bent state for 10 cycles, and after 50, 100, and 200 times bending with R=2.5 mm, respectively, from cycle 11 to 20, cycle 21 to 30, and cycle 31 to 40. The discharge capacity gradually decreased as the electrochemical cycles increased. Therefore, the capacity retention rate exhibits around 86%, which is lower than that for the bent cell at a radius of 12.5 mm. However, the over-potential in discharge curve was almost constant, as shown in Figure 3.6.17. Due to the metal foam electrode was gradually fracture and exfoliation. The areal capacity of the initial bent state was 3.34 mAh cm^{-2}, and this was reduced to 3.08 mAh cm^{-2} after bending 200 times. Moreover, even after the strain due to being bent to a radius of 2.5 mm, we could not observe any decrease in the brightness nor in the cell voltage. Thus, we have achieved high electrochemical performance bendable cells using a 3D structured metal foam-type current collector.

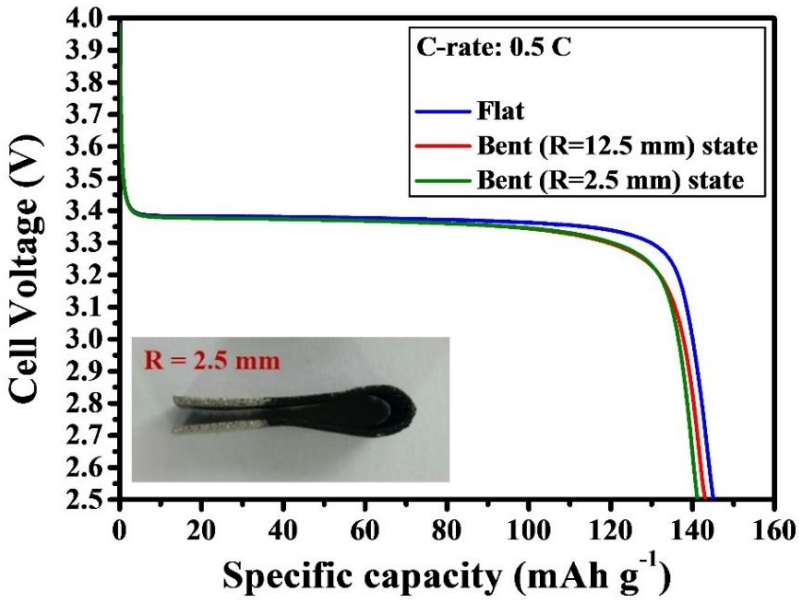

Figure 3.6.11 Comparison of the discharge curves at current rate of 0.5C with metal foam cathodes of flat and bent state cells (R = 12.5 mm and 2.5 mm), respectively.

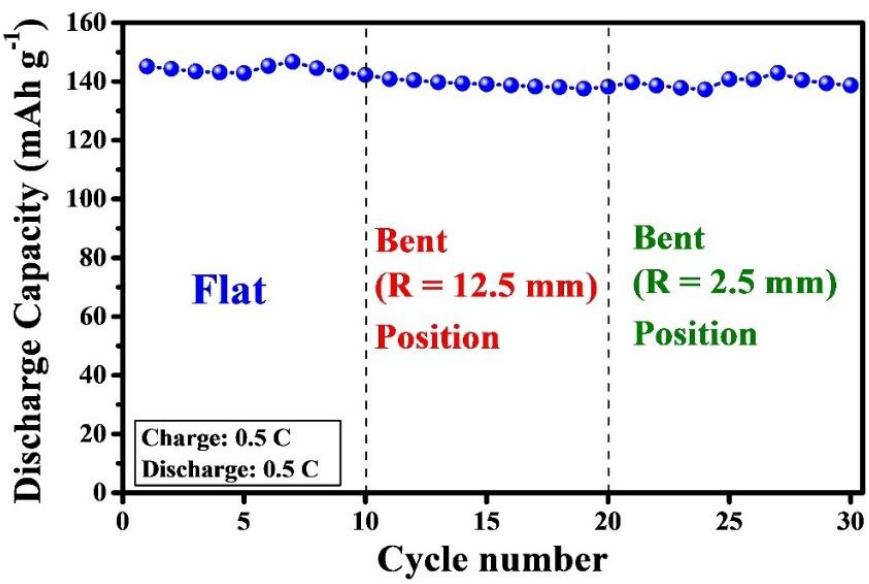

Figure 3.6.12 Discharge specific capacity (mAh g^{-1}) cycled at 0.5C with flat and bent state pouch cells (R = 12.5 mm and 2.5 mm).

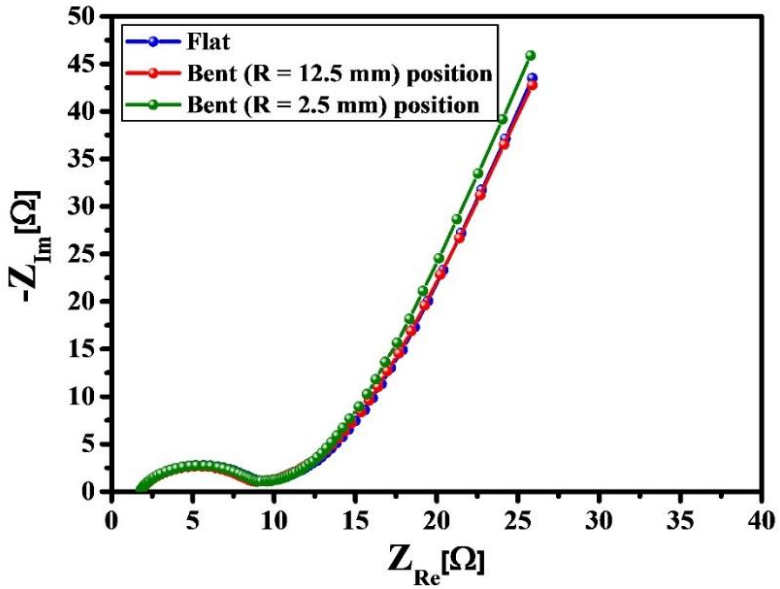

Figure 3.6.13 Nyquist plots of AC impedance spectroscopy (R = 12.5 mm and 2.5 mm).

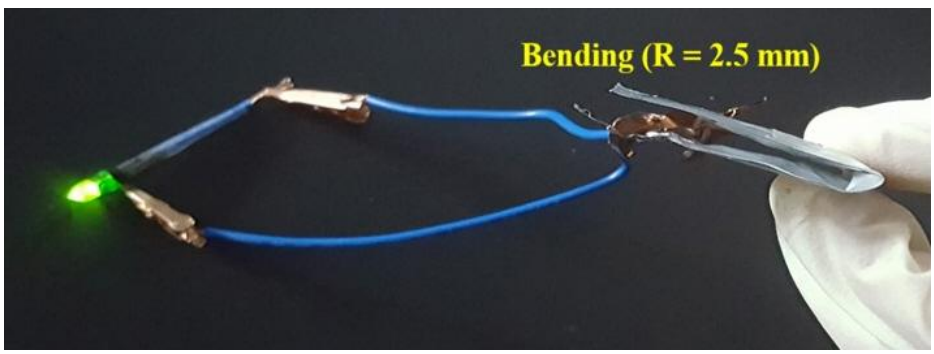

Figure 3.6.14 Demonstration of the turning on a green LED, by means of bendable pouch cell in the bent state (R = 2.5 mm).

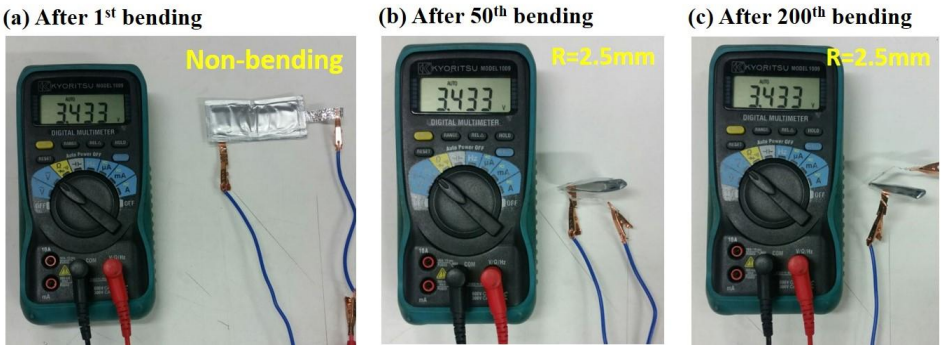

Figure 3.6.15 Voltage retention test of the bendable pouch cell connected to a digital multi-meter (a) when flat, (b) after bending 50 times, and (c) 200 times to a bending radius of 2.5 mm.

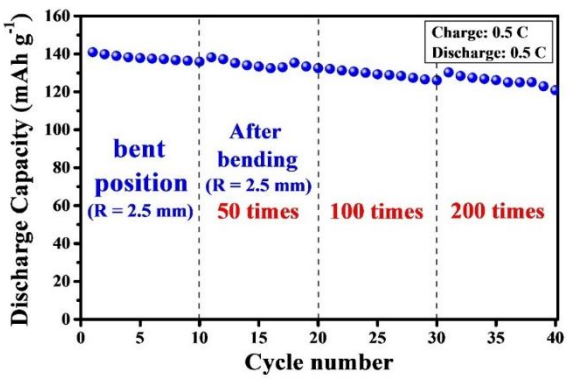

Figure 3.6.16 Discharge specific capacity (mAh g^{-1}) cycled at 0.5C after bending 200 times.

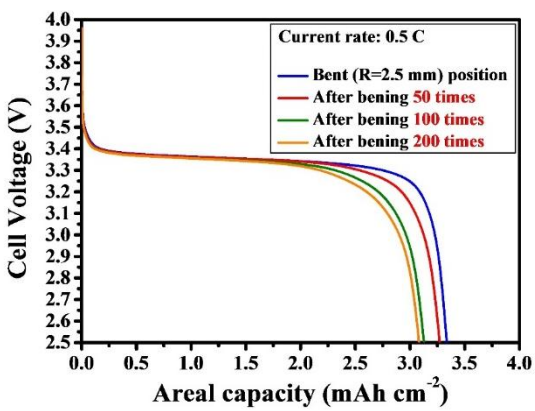

Figure 3.6.17 Comparison of the discharge curves after bending 200 times (R=2.5 mm) at 0.5C.

CHAPTER 4

Conclusion

When preparing positive electrodes using $LiFePO_4$, the morphology of the current collector and the conductive carbon content are important variables, because the electronic conductivity of $LiFePO_4$ is highly susceptible to the electrochemical performance of Li-ion batteries. Increase in carbon black loadings enhanced the electrochemical performances due to faster redox reaction and lower charge transfer resistance. In the case of metal foam cathode of 450 μm-pore size and 1000 μm-thickness, the difference of discharge specific capacity between 5 and 20 wt. %-carbon black was about 16 mAh g^{-1} at 2 mA cm^{-2}; however, at 8 mA cm^{-2} it was about 50 mAh g^{-1}. Cycle-life performance also showed high capacity retention rate, due to enhanced electrical contact between the particles and reduced resistance within the metal foam cathodes. Nyquist plots of AC impedance showed that there was no significant difference in bulk resistance. However, lower charge transfer resistance and lower diffusion limitation of Li-ion were observed for the electrode. However, increase in carbon black loading reduces the energy density of the cells. For example, metal foam cathode of 5 wt. %-carbon black exhibited the highest areal capacity (10.3 mAh cm^{-1}) at 2 mA cm^{-2}, due to the higher mass loadings of active material. In order to produce high-energy batteries, metal foam cathode of lower carbon black content offers better efficiency. Consequently, the amount of conductive carbon should be varied according to the intended use.

The electrode thickness and mass loading of active materials are significant factors for achieving high power and high specific energy for Li secondary batteries. At low

current density, there was no significant difference in discharge capacity for the cells. This is because the Li-ion sufficiently diffused from surface of metal foam cathode into the metal foam cathode. However, at high current density, thick electrodes exhibit higher cell capacity (mAh) and specific capacity (mAh g^{-1}) compared to thin electrodes. This is due to the increase in the amount of active materials and longer time of Li redox reaction. Therefore, to manufacture a high-energy (capacity) battery that uses a low current density, thick electrode offers more efficiency. This is due to the decreased mass of inactive materials, such as the current collector and separator. However, to manufacture a high-power battery that uses a high current density, it is preferable to stack thin metal foam cathode.

The results of the press intensity experiment indicated that the metal foam cathodes with the higher press intensity demonstrated lower electrochemical performance. It was noted that the cell capacity and kinetic performance of the 50% pressed electrode decreased significantly. This is because the electrochemical reaction mostly occurred on the surface of metal foam cathode due to decrease in the area of redox reaction. For instance, at discharge current density of 2 mA cm^{-2}, the difference of specific capacity between no pressed electrode and the 50% pressed electrode was about 20 mAh g^{-1}; however, at 8 mA cm^{-2} it was about 90 mAh g^{-1}. The study indicated that pre-firing process metal cathodes resulted in a higher electrochemical performance than metal foam cathodes fabricated by pressing after annealing process. This can be attributed to a larger redox reaction area and the formation of third pores into which the electrolyte can permeate in metal foam cathodes.

As shown in the results examining the effect of the proportion of metal frame in the metal foam electrode, an increase in the proportion of metal frame and a smaller cell size in metal foam enhanced the electrochemical performance due to increased

rate of redox reaction and lower charge transfer resistance. However, since the amount of active material decreases, the cell capacity decreased at a low current rate. Consequently, the active materials density, electrode porosity, and proportion of the metal frame need to be adjusted in order to fabricate batteries suitable for each application.

We have demonstrated a process to manufacture bendable pouch Li secondary batteries with a high electrochemical performance and excellent flexibility by using a NiCr alloy metal foam. Nyquist plots and discharge curves indicated that the resistance and specific capacities remained the same at a C-rate of 0.5 in the flat and bent position (radii of 12.5 and 2.5 mm) due to the lack of damage. The charge transfer resistance was about 6 Ω, which is much lower than that of a foil- type current collector. More importantly, our bendable batteries have a high areal capacity of 3.5 mAh cm^{-2} at a C-rate of 0.2, and they could maintain their capacity after bending several times to bending radii of 12.5 and 2.5 mm. In addition, the cycle- life performance also indicated a high capacity retention rate of above 90%. This article provides bendable Li secondary batteries with high areal capacity, stable cycle-life behavior, and high electrochemical performances using a NiCr alloy metal foam. The high areal capacity, high energy density, stable cycle-life behavior, and flexibility of bendable Li secondary batteries are most important factors for future wearable and portable electronic devices.

Bibliography

[1] R.S. Liu, L. Zhang, X. Sun, H. Liu, J. Zhang, Electrochemical Technologies for Energy Storage and conversion, Wiley-VCH, Germany, Volume 1 (2012).

[2] M. Ge, J. Rong, X. Fang, C. Zhou, *nano lett.*, 12, 2318 (2012).

[3] B. Scrosati, *nature*, 373, 557 (1995).

[4] W. Lu, A. Jansen, D. Dees, P. Nelson, N.R. Veselka, G. Henriksen, *J. Power Sources*, 196, 1537 (2011).

[5] Y.S. Chen, K.H. Chang, C.C. Hu, T.T. Cheng, *Electrochim. Acta*, 55, 6433 (2010).

[6] C.K. Park, Z. Zhang, Z. Xu, A. Kakirde, K. Kang, C. Chai, G. Au, L. Cristo, *J. Power Sources*, 165, 892 (2007).

[7] W.J. Zhang, *J. power source*, 196, 2962 (2011).

[8] C. Sun, S. Rajasekhara, J.B. Goodenough, F. Zhou, *J. Am. Chem. Soc.*, 133, 2132 (2011).

[9] A. Yamada, S. C. Chung, K. Hinokuma, *J. Electrochem. Soc.*,148 (3), A224 (2001).

[10] M.S. Islam, D.J. Driscoll, C.A.J. Fisher, P.R. Slater, *Chem. Mater*., 17, 5085 (2005).

[11] C.V. Ramana, A. Mauger, F. Gendron, C.M. Julien, K. Zaghib, *J. power sources*, 187, 555 (2009).

[12] J.M. Tarascon, M. Armand, *nature*, 414, 359 (2001).

[13] L. X. Yuan, Z.H. Wang, W.X. Zhang, X.L. Hu, J.T. Chen, Y.H. Huang, J.B. Goodenough, *Energy Environ. Sc*i., 4, 269 (2011).

[14] M. Takahashi, H. Ohtsuka, K. Akuto, Y. Sakurai, *J. Electrochem. Soc*., 152 (5), A899 (2005).

[15] J. Wang, X. Sun, *Energy Environ. Sci*., 5, 5163 (2012).

[16] Y.H. Ding, H.M. Ren, Y.Y. Huang, F.H. Chang, P. Zhang, *Mater. Res. Bull*., 48, 3713 (2013).

[17] G. Liang, L. Wang, X. Ou, X. Zhao, S. Xu, *J. power sources*, 184, 538 (2008).

[18] P. P. Prosini, D. Zane, M. Pasquali, *Electrochim. Acta*, 46, 3517 (2011).

[19] N. Ravet, Y. Chouinard, J. F. Magnan, S. Besner, M. Gauthier, M. Armand, *J. Power Sources*, 97-98, 503 (2001).

[20] L.H. Hu, F.Y. Wu, C.T. Lin, A.N. Khlobystov, L.J. Li, *Nat. Commun*., 4, 1 (2013).

[21] C.C. Yang, Y.C. Chen, Y.C. Liao, *Mater. Res. Bull*., 47, 2616 (2012).

[22] F. Croce, A. D' Epifanio, J. Hassoun, A. Deptula, T. Olczac, B. Scrosati, *Electrochem. Solid-State Lett.*, 5 (3), A47 (2002).

[23] Y.S. Hu, Y.G. Guo, R. Dominko, M. Gaberscek, J. Jamnik, J. Maier, *Adv. Mater*., 19, 1963 (2007).

[24] J.F. Ni, H.H. Zhou, J.T. Chen, X.X. Zhang, *Mater. Lett*., 59, 2361 (2005).

[25] D. Wang, H. Li, S. Shi, X. Huang, L. Chen, *Electrochim. Acta*, 50, 2955 (2005).

[26] D.W. Han, Y.M. Kang, R.Z. Yin, M.S. Song, H.S. Kwon, *Electrochem. Commun*., 11, 137 (2009).

[27] M. Wagemaker, B.L. Ellis, D. Lu#tzenkirchen-Hecht, F.M. Mulder, L.F. Nazar, *Chem. Mater*., 20 (20), 6313 (2008).

[28] S.Y. Chung, J.T. Bloking, Y.M. Chiang, *Nat. Mater*., 1, 123 (2002).

[29] F. Yu, J.J. Zhang, Y.F. Yang, G.Z. Song, *J. Mater. Chem*., 19, 9121 (2009).

[30] X.L. Wu, L.Y. Jiang, F.F. Cao, Y.G. Guo, L.J. Wan, *Adv. Mater.*, 21, 2710 (2009).

[31] M. Zhao, S. Kariuki, H.D. Dewald, F.R. Lemke, R.J. Staniewicz, E.J. Plichta, and R.A. Marsh, *J. Electrochem. Soc.,* 147, 2874 (2000).

[32] S.S. Zhang, and T.R. Jow, *J. Power Sources,* 109, 458 (2002).

[33] G.F. Yang, K.Y. Song, S.K. Joo, *J. Mater. Chem. A*, 2, 19648 (2014).

[34] M. Yao, K. Okuno, T. Iwaki, M. Kato, S. Tanase, K. Emura, T. Sakai, *J. Power Sources*, 173, 545 (2007).

[35] G.F. Yang, S.K. Joo, *Electrochim. Acta*, 170, 263 (2015).

[36] Q. Wang, D. Wang, B. Wang, *Int. J. Electrochem. Sci*., 7, 8753 (2012).

[37] G.F. Yang, K.Y. Song, S.K. Joo, *RSC Adv*., 5, 16702 (2015).

[38] H. Zhang, X. Yu, P.V. Braun, *Nat. Nanotechnol*., 6, 277 (2011).

[39] L. Hu, F. L. Mantia, H. Wu, X. Xie, J. McDonough, M. pasta, Y. Cui, *Adv. Energy Mater.*, 1, 1012 (2011).

[40] W. Chen, S. Maloney, W. Wang, *Electrochim. Acta*, 176, 96 (2015).

[41] W. Yang, G. Cheng, C. Dong, Q. Bai, X. Chen, Z. Peng, Z. Zhang, *J. Mater. Chem. A*, 2, 20022 (2014).

[42] M. Yao, K. Okuno, T. Iwaki, S. Tanase, K. Harada, M. Kato, K. Emura, T. Sakai, *J. Power Sources*, 171, 1033 (2007).

[43] M. Yao, K. Okuno, T. Iwaki, M. Kato, K. Harada, J.J. Park, S. Tanase, T. Sakai, *J. Electrochem. Soc*., 154 (7), A709 (2007).

[44] H. Fukunaga, M. Kishimi, N. Matsumoto, T. Ozaki, T. Sakai, T. Tanaka, T. Kishimoto, *J. Electrochem. Soc*., 152 (5), A905 (2005).

[45] M. Yao, K. Okuno, T. Iwaki, M. Kato, K. Harada, J.J. Park, S. Tanase, T. Sakai, *Electrochem. Solid-State Lett*., 10 (3), A56 (2007).

[46] S. Yoon, S. Lee, S. Kim, K.W. Park, D. Cho, Y. Jeong, *J. Power Sources*, 279, 495 (2015).

[47] R. Tajima, T. Miwa, T. Oguni, A. Hitotsuyanagi, H. Miyake, H. Katagiri, Y. Goto, Y. Saito, J. Goto, M. Kaneyasu, M. Hiroki, M. Takahashi, S. Yamazaki, *Journal of the SID*, 22/5, 237 (2015).

[48] S.D. Kim, K. Rana, J.H. Ahn, *J. Mater. Chem. A*, 4, 19197 (2016).

[49] L. Li, Z.P. Wu, H. Sun, D. Chen, J. Gao, S. Suresh, P. Chow, C.V. Singh, Nikhil Koratkar, *ACS Nano*, 9, 11342 (2015).

[50] H. Nishide, K. Oyaizu, 319, 737 (2008).

[51] M. Yousaf, H.T.H. Shi, Y. Wang, Y. Chen, Z. Ma, A. Cao, H.E. Naguib, R.P.S. Han, *Adv. Energy. Mater.*, 6, 1600490 (2016).

[52] Y. Hu, X. Sun, *J. Mater. Chem. A*, 2, 10712 (2014).

[53] M.S. Balogun, Z. Wu, Y. Luo, W. Qiu, X. Fan, B. Long, M. Huang, P. Liu, Y. Tong, *J. Power Sources*, 308, 7 (2016).

[54] Q.C. Liu, L. Li, J.J. Xu, Z.W. Chang, D. Xu, Y.B. Yin, X.Y. Yang, T. Liu, Y.S. Jiang, J.M. Yan, X.B. Zhang, *Adv. Mater.,* 27, 8095 (2015).

[55] S.H. Lee, P. Liu, C.E. Tracy, D.K. Benson, *Electrochem. Solid State Lett.*, 2 (9), 425 (1999).

[56] L. Hu, H. Wu, F.L. Mantia, Y. Yang, Y. Cui, *ACS Nano*, 4, 5843 (2010).

[57] M. Koo, K.I. Park, S.H. Lee, M. Suh, D.Y. Jeon, J.W. Choi, K. Kang, K.J. Lee, *nano lett.*, 12, 4810 (2012).

[58] M. Kammoun, S. Bergb, H. Ardebili, *Nanoscale*, 7, 17516 (2015).

[59] M.S. Wu, J.T. Lee, P.C.J. Chiang, J.C. Lin, *J. Mater. Sci*., 42, 259 (2007).

[60] Q. Li, H. Ardebili, *J. Power Sources*, 303, 17 (2016).

[61] S.W. Song, K.C. Lee, H.Y. Park, *J. Power Sources*, 328, 311 (2016).

[62] D. Wei, S. Haque, P. Andrew, J. Kivioja, T. Ryhänen, A. Pesquera, A. Centeno, B. Alonso, A. Chuvilin, A. Zurutuzab, *J. Mater. Chem. A*, 1, 3177 (2013).

[63] J. Glenneberg, F. Andre, I. Bardenhagen, F. Langer, J. Schwenzel, R. Kun, *J. Power Sources*, 324, 722 (2016).

[64] N. Li, Z. Chen, W. Ren, F. Li, H.M. Cheng, *PNAS*, 109, 17360 (2012).

[65] A. Ramadoss, K.Y. Yoon, M.J. Kwak, S.I. Kim, S.T. Ryu, J.H. Jang, *J. Power Sources*, 337, 159 (2017).

[66] J. He, Y. Chen, W. Lv, K. Wen, P. Li, F. Qi, Z. Wang, W. Zhang, Y. Li, W. Qin, W. He, *J. Power Sources*, 327, 474 (2016).

[67] Y. Meng, H. Wu, Y. Zhang, Z. Wei, *J. Mater. Chem. A*, 2, 10842 (2014).

[68] L. Noerochim, J.Z. Wang, S.L. Chou, D. Wexler, H.K. Liu, *Carbon*, 50, 1289 (2012).

[69] A.M. Gaikwad, B.V. Khau, G. Davies, B. Hertzberg, D.A. Steingart, A.C. Arias, *Adv. Energy. Mater.*, 5, 1401389 (2015).

[70] H. Lee, J.K. Yoo, J.H. Park, J.H. Kim, K. Kang, Y.S. Jung, *Adv. Energy. Mater.*, 2, 976 (2012).

[71] X. Zhu, X. Wu, T.N.L. Doan, Y. Tian, H. Zhao, P. Chen, *J. Power Sources*, 326, 498 (2016).

[72] J.Q. Huang, H.J. Peng, X.Y. Liu, J.Q. Nie, X.B. Cheng, Q. Zhang, F. We, *J. Mater. Chem. A*, 2, 10869 (2014).

[73] A. Goyal, A.L.M. Reddy, P.M. Ajayan, *Small*, 7, 1709 (2011).

[74] Z. Chen, J.W.F. To, C. Wang, Z. Lu, N. Liu, A. Chortos, L. Pan, F. Wei, Y. Cui, Z. Bao, *Adv. Energy. Mater.*, 4, 1400207 (2014).

[75] Y. Zhang, Y. Wang, L. Wang, C.M. Lo, Y. Zhao, Y. Jiao, G. Zheng, H. Peng, *J. Mater. Chem. A*, 4, 9002 (2016).

[76] H. Qu, O. Semenikhin, M. Skorobogatiy, *Smart Mater. Struct.*, 24, 025012 (2015).

[77] Q.C. Liu, J.J. Xu, D. Xu, X.B. Zhang, *Nat. Commun.*, 6, 7892 (2015).

[78] Y. Liu, S. Gorgutsa, Clara Santato, M. Skorobogatiy, *J. Electrochem. Soc.,* 159 (4), A349 (2012).

[79] J.S. Kim, Y.H. Lee, I. Lee, T.S. Kim, M.H. Ryou, J.W. Choi, *J. Mater. Chem. A*, 2, 10862 (2014).

[80] L. Jabbour, M. Destro, C. Gerbaldi, D. Chaussy, N. Penazzi, D. Beneventi, *J. Mater. Chem.,* 22, 3227 (2012).

[81] Y. Huang, Z. Lin, M. Zheng, T. Wang, J. Yang, F. Yuan, X. Lu, L. Liu, D. Sun, *J. Power Sources*, 307, 649 (2016).

[82] L. Jabbour, C. Gerbaldi, D. Chaussy, E. Zeno, S. Bodoardod, D. Beneventi, *J. Mater. Chem.,* 20, 7344 (2010).

[83] S.E. Trask, K.Z. Pupek, J.A. Gilbert, M. Klett, B.J. Polzin, A.N. Jansen, D.P. Abraham, *J. Electrochem. Soc.*, 163 (3), A345 (2016).

[84] W.J. Zhang, *J. Electrochem. Soc*., 157 (10), A1040 (2010).

[85] W.L. Wang, E.M. Jin, H.B. Gu, *Trans. Electr. Electron. Mater*., 13 (3), 121 (2012).

[86] L. Fransson, T. Eriksson, K. Edström, T. Gustafsson, J.O. Thomas, *J. Power Sources*, 101, 1 (2001).

[87] H. Zheng, J. Li, X. Song, G. Liu, V.S. Battaglia, *Electrochim. Acta*, 71, 258 (2012).

[88] D.Y.W. Yu, C. Fietzek, W. Weydanz, K. Donoue, T. Inoue, H. Kurokawa, S. Fujitani, *J. Electrochem. Soc*., 154 (4), A253 (2007).

[89] L. Li, X. Tang, H. Liu, Y. Qu, Z. Lu, *Electrochim. Acta*, 56, 995 (2010).

[90] K.Y. Song, G.S. Jang, J. Tao, J.H. Lee, S.K. Joo, *J. Electrochem. Soc.,* 163 (14), A2981 (2016).

[91] S. Chen, Y. Xin, Y. Zhou, F. Zhang, Y. Ma, H. Zhou, L. Qi, *J. Mater. Chem. A*, 3, 13377 (2015).

[92] S.S. Chi, Y. Liu, W.L. Song, L.Z. Fan, Q. Zhang, *Adv. Funct. Mater.*, 27, 1700348 (2017).

[93] A. Goyal, A.L.M. Reddy, P.M. Ajayan, *Small*, 7, 1709 (2011).

[94] M. Koo, K.I. Park, S.H. Lee, M. Suh, D.Y. Jeon, J.W. Choi, K. Kang, K.J. Lee, *nano lett.*, 12, 4810 (2012).

[95] A.M. Gaikwad, B.V. Khau, G. Davies, B. Hertzberg, D.A. Steingart, A.C. Arias, *Adv. Energy. Mater.*, 5, 1401389 (2015).

[96] Z. Chen, J.W.F. To, C. Wang, Z. Lu, N. Liu, A. Chortos, L. Pan, F. Wei, Y. Cui, Z. Bao, *Adv. Energy. Mater.*, 4, 1400207 (2014).

[97] K. Y. Song, G. S. Jang, J. Tao, J. H. Lee, and S. K. Joo, *J. Nanosci. Nanotechnol.*, 18 (2), 992 (2018).

[98] K. Y. Song, and S. K. Joo, *Mater. Res. Bull.*, 94, 328 (2017).

요약 (국문 초록)

리튬 이차 전지의 메탈 폼 양극 최적화에 관한 연구

송 경 엽
서울대학교 공과대학 재료공학부

리튬 이차 전지는 다른 이차 전지에 비해 에너지 밀도와 작동 전압이 가장 높기 때문에 휴대용 장치나 전기 자동차 등에 가장 적합한 전지이다.

현재 상용화 되고 있는 전지는 활물질에 전자를 내어주고 받아주는 역할을 하는 집전체인 금속 포일 위에 활물질을 약 100 μm 이하의 두께로 코팅함으로써 제작한다. 그러나 고용량 배터리 제작을 위하여 수백 μm 이상의 두께로 활물질을 코팅하면 활물질과 포일 간에 박리가 쉽게 발생하고, 전지 내부의 저항이 높아지는 등 배터리의 효율을 급격히 감소하게 된다. 즉, 활물질이 얇은 두께로 코팅 된 전극의 면적을 넓혀야 하므로 용량과 관계없는 대량의 분리막과 집전체가 필요하게 되어 결국 전지의 무게와 부피가 증가하게 된다.

본 연구에서는 이 문제를 해결하기 위해 금속 포일형 집전체 대신 3 차원 구조의 기공을 가지는 발포 금속을 적용하였다. 발포 금속 집전체는 금속 포일 집전체와 달리 전극의 표면과 내부에도 금속 프레임이 존재하기 때문에 전지의 내부 저항을 줄임과 동시에 리튬 이온의 확산 거리를 짧게 함으로써 전기화학 특성을 향상시킬 수 있다. 더욱이, 금속 프레임의 표면이 거칠고 3 차원 구조로 되어 있어 전극을

두껍게 제작하여도 활물질과 금속 간에 분리가 발생하지 않아 수명 특성 또 한 향상시킬 수 있다.

전극의 내부 저항을 감소시키고 전자 전도도를 향상시키기 위해 첨가하는 카본 블랙의 함량에 따른 전기 화학 특성을 비교 분석한 결과, 카본 블랙의 함량이 증가할수록 전하 전달 저항이 급격히 낮아져 더 우수한 질량당 용량 (mAh g^{-1})을 나타내었다. 그러나 활물질 질량당 용량이 아닌 전지 전체 용량 (mAh) 을 보면 카본 블랙의 함량이 적은 것이 더 높은 용량을 나타내는데, 이는 카본 블랙의 함량이 적어진 만큼 활물질의 양이 증가하였기 때문이다. 즉, 낮은 전류에서 사용하는 대용량 전지의 경우, 카본 블랙의 함량을 낮추는 것이 유리한 반면, 고출력 전지의 경우는 카본 블랙의 함량을 높이는 것이 유리하다는 것을 확인할 수 있다.

발포 금속 집전체를 이루고 있는 기공 사이즈에 따른 전기화학 특성을 비교하면 카본 블랙의 함량이 15 wt. % 일 때, 기공 사이즈가 가장 작은 450 μm 가 가장 우수한 용량과 낮은 과전압을 나타내었는데, 이는 기공 사이즈가 가장 작아 리튬의 확산 거리가 가장 짧고, 산화/환원 반응의 표면적이 가장 넓기 때문이다. 그러나 카본 블랙의 함량이 25 wt. % 로 증가하면 기공 사이즈 450 μm 와 3000 μm 가 비슷한 용량과 과전압을 나타내었는데, 이는 기공 사이즈가 큰 발포 금속일수록 카본 블랙의 영향이 커지기 때문이다. 이 실험의 결과로 기공 사이즈가 3000 μm 인 발포 금속에 15 wt. %를 채워 전지를 제작하는 것이 더 가볍고 고용량을 갖는 전지 제작이 가능하다는 것을 나타낸다.

다음은 전극 밀도에 따른 특성을 비교하였다. 먼저, 전극 열처리 후 프레스 정도에 따른 특성을 비교하면 프레스를 강하게 할수록 전류 증가에 따른 용량이 급격히 감소하는 결과를 보였다. 이는 유기 용매와

활물질, 카본 블랙, 바인더와 유기 용매를 혼합 한 슬러리를 메탈 폼 전극에 채워 넣은 후 열처리하면 유기 용매가 제거되면서 전극 내부로 전해액이 침투할 수 있는 제 3 기공을 형성하는데, 프레스를 하지 않거나 두께 감소가 약 20 % 이하로 프레스 하면 이 제 3 기공이 유지되어 전해액이 전극 내부로 침투가 가능하기 때문에 전극 내부에서도 리튬의 산화/환원 반응이 이루어져 높은 용량을 나타낸다. 반면, 열처리 후 두께 감소가 약 20 % 이상으로 프레스 하면 이 제 3 기공들이 없어지게 되고 전극 내부로 전해액이 침투하지 못해 전극의 표면에서만 반응이 이루어지기 때문에 전류가 높아질수록 용량이 급격히 감소하게 된다. 이와 함께, 메탈 폼 전극에 슬러리를 채우고 1 차 열처리 후, 적당한 두께의 프레스와 최종 열처리하여 전극을 제작하였다. 그 결과, 1 차 열처리 한 전극이 가장 우수한 전기화학 특성을 나타내었는데, 이는 활 물질의 양이 증가함과 동시에 전해액이 침투할 수 있는 제 3 기공이 유지되었기 때문이다. 이 실험의 결과로 메탈 폼을 사용하여 전지를 제작할 때, 사용 용도에 따라 제 3 기공의 형성 여부가 매우 중요하다는 것을 알 수 있다. 예를 들어, 낮은 전류에서 사용하는 전지의 경우는 열처리 후 두께 감소가 20~50% 정도까지 프레스하여도 활물질의 이론 용량만큼 사용이 가능하고 전극의 두께를 줄일 수 있기 때문에 유리한 반면, 높은 전류에서 사용하는 고출력 전지의 경우는 프레스를 하지 않거나 두께 감소가 20% 이하의 범위로 프레스 또는, 1 차 열처리를 통하여 제 3 기공이 유지되도록 해야 한다.

전극 구조에 따른 특성을 비교하면, 음극인 리튬 금속을 메탈 폼 양극의 양쪽에 배치한 것이 한쪽에만 배치한것보다 더 높은 용량을 나타내었는데, 이는 반응 표면적이 넓어지고, 리튬의 확산 거리가 짧아지기 때문이다. 또한, 낮은 전류에서 사용하는 경우 전극의 두께를 증가시키는 것이 유리한

반면, 높은 전류에서 사용하기 위해서는 얇은 전극을 여러 층 적층하는 것이 유리하다.

마지막으로, 최근 웨어러블 및 커브드 디바이스가 개발되면서 커브드 전지에 대한 수요가 높아지고 있기 때문에 본 연구에서는 3 차원 구조의 니켈-크롬 합금 발포 금속 집전체를 사용한 고용량 커브드 전지를 제작하였다. 실험 결과 곡률의 반지름이 12.5 mm 가 되도록 구부리거나 반으로 접어도 전지의 용량과 저항 등의 변화가 없었으며, 3.5 mAh g^{-1} 의 높은 단위 면적당 용량과 6-8 Ω 의 낮은 전하 전달 저항을 나타내었다. 이는, 고용량을 필요로 하는 휴대용 커브드 디바이스에 가장 적합한 전지가 될 것이다.

이상 본 연구에서 제시된 것과 같이 발포 금속 집전체의 기술과 구조는 현재 상용화 되고 있는 포일형 집전체에 비해 가볍고 고용량/고출력을 갖는 배터리 제작이 가능하기 때문에 상업적으로 가장 유망한 집전체가 될 것이다.

주요어: 리튬 이차 전지, 발포 금속 양극, 집전체, 대용량 전지, 고출력 전지, 커브드 전지

학 번: 2013-30938